REGIONAL GROUNDWATER FLOW AND WATER QUALITY IN THE VIRGIN RIVER BASIN AND SURROUNDING AREAS, UTAH AND ARIZONA

by Paul Inkenbrandt, Kevin Thomas, and J. Lucy Jordan

REGIONAL GROUNDWATER FLOW AND WATER QUALITY IN THE VIRGIN RIVER BASIN AND SURROUNDING AREAS, UTAH AND ARIZONA

by Paul Inkenbrandt, Kevin Thomas, and J. Lucy Jordan

Cover photo: *View of the Pine Valley Mountains and I-15 corridor from the top of the Hurricane Cliffs.*

CONTENTS

FIGURES

REGIONAL GROUNDWATER FLOW AND WATER QUALITY IN THE VIRGIN RIVER BASIN AND SURROUNDING AREAS, UTAH AND ARIZONA

by Paul Inkenbrandt, Kevin Thomas, and J. Lucy Jordan

ABSTRACT

The purpose of this study is to improve understanding of the regional groundwater system in the area of the Hurricane fault in Washington County and to design future investigations for that area. We aim to characterize the deep aquifer system and its connections to the overlying aquifers.

To achieve our objectives, we (1) examined over 3000 water-well logs and over 50 oil-well logs in the area, (2) created and examined several potentiometric-surface maps extending from northern Washington County to the Colorado River, identifying major hydrostratigraphic units in the area, and separating the units based on hydrostratigraphic boundaries, (3) examined and compiled groundwater quality data from various sources and created maps of chemical characteristics of the water in the study area, creating cluster analysis maps, (4) compared chemistries of water from various aquifers in the area, (5) designed and conducted gravity surveys along the Interstate Highway 15 (I-15) corridor, (6) examined remote sensing data for surface lineaments that may correspond to highly fractured, fault-related damage zones, and (7) determined three areas for potential exploratory/pilot/monitoring wells and designed a chemical sampling procedure to determine if water from monitoring wells has a source that is distinct from water derived from the Navajo Sandstone.

We conclude:

- Groundwater levels indicate that depth to water in the R and C aquifers may exceed 500 feet in the I-15 corridor area. A groundwater divide for the R and C aquifers likely exists south of the Utah-Arizona state line.

- Regional groundwater flow preferentially follows open fracture systems, which are likely parallel to extensional faults and Sevier fold trends in the area, having mean azimuths of approximately 6 and 22 degrees east of north, respectively.

- Fracture hydraulic conductivity is highest in the area nearest to the Hurricane fault and decreases with distance from the fault. The probable hydraulic conductivity ranges from 0.2 to 20 feet per day, and is a function of distance from the fault.

- Dissolution of evaporites, most of which are found in the Triassic units in the area, likely increases the concentration of TDS in groundwater.

- An 8-inch diameter well should be drilled into the footwall of the Hurricane fault near the town of Pintura. Groundwater samples from the well and an aquifer test conducted on the well could help characterize a potential source of water.

INTRODUCTION

Population will likely increase in Washington County, which will create additional demands for water supply. To provide water for the expected growth and development, the Washington County Water Conservancy District must have a diverse array of sources. The Utah Division of Water Rights considers the Navajo and Kayenta aquifers on the west side of the Hurricane fault as fully allocated. Further allocation of the area's primary surface-water source, the Virgin River, is unfeasible because it has flow variability and water-quality issues (Tetra Tech, 2004).

The Washington County Water Conservancy District (the District) approached the Utah Geological Survey (UGS) to search for previously unidentified additional sources of water related to regional groundwater flow systems. In this endeavor, the UGS investigated and defined the groundwater flow system in the Hurricane fault zone/Ash Creek area. We compiled well-log, water chemistry, and geologic information and provided recommendations to help the District make informed water-management decisions on where to place exploratory wells to study regional flow systems.

To examine deep, regional groundwater conditions, exploratory wells would likely exceed depths of 1200 feet in material that is susceptible to drilling-fluid circulation loss and borehole caving. Choosing appropriate exploratory sites is necessary for an efficient and effective study of regional groundwater flow because deep drilling techniques in fractured material are expensive and time intensive. We have compiled information on the hydraulic and geologic conditions of the area and recommended locations for exploratory wells that will provide information about the regional groundwater flow system.

Objectives

The main objectives of the study are to gain a better understanding of the regional groundwater system in the area of the Hurricane fault in Washington County, and to design future investigations that will improve understanding of that groundwater system. We characterized the deep aquifer system and how it is connected to the overlying aquifers.

Approach

This study involved identifying water chemistry sampling localities and potential sites for an exploratory drill hole. First, we compiled and examined existing data. Then we designed future projects that will provide information that the existing data lack. We completed the following steps to achieve our objectives:

1. We examined more than a thousand water-well logs in the area. We also examined over 50 oil-well logs in the area, some of which provided important water-quality and stratigraphic information.

2. We created and examined several potentiometric-surface maps extending from northern Washington County to the Colorado River. We first identified the major hydrostratigraphic units in the area, separating the units based on hydrologic properties and stratigraphic boundaries. We compiled water-level data from 3445 wells and identified the aquifer each well penetrated and then created potentiometric maps based on that information. We combined our compiled groundwater-level information with existing potentiometric-surface maps to create a final set of more detailed potentiometric surface maps.

3. We examined and compiled groundwater quality data from various sources and created maps of chemical characteristics of the water in the study area. We compiled information from the U.S. Bureau of Reclamation, the Utah Department of Environmental Quality, the U.S. Geological Survey and other studies (Everitt and Einert, 1994; Nelson and others, 2009). We created both a regional and an Upper and Central Virgin River basin cluster analysis map. We also compared chemistries of water from various aquifers in the area.

4. We designed and conducted gravity surveys along the I-15 corridor, which measure contrasts in the gravity field, which is a function of density of the underlying material. For the surveys, we chose areas that required a better understanding of the geology of the area and that transected faults. We focused on areas of unconsolidated basin fill, seeking areas of basin deepening to outline the trend of faults. We compiled estimates of the density of area rock units to better understand the structure.

5. We examined orthophotographs, detailed topographic information, geophysical surveys, and side-looking radar to help determine surface lineations that may correspond to highly fractured, fault-related damage zones. We delineated damage zones conducive to groundwater flow and the general density and trends of fractures in the area.

6. We determined three areas for potential exploratory/pilot/monitoring wells. We recommend the locations, design specifications, and drilling methods for monitoring wells in the areas of interest. We examined areas north of Toquerville, in the Hurricane fault zone, along the Virgin River in the area of the Pah Tempe Springs, and along the I-15 corridor south of Ash Creek Reservoir. If the District chooses to proceed with phase 2 of this study, the UGS would provide on-site geologists for later phases involving well drilling.

7. We designed a chemical sampling procedure to determine if water from monitoring wells has a source that is distinct from water derived from the Navajo Sandstone. We picked wells and springs to sample to help us determine possible sources that contribute to the water supplies.

Physiography

The area we examined encompasses all of the central and eastern Virgin River basin in Utah and the Shivwitts and Uinkaret plateaus in Arizona (figure 1). It straddles the transition zone between the Basin and Range and Colorado Plateau physiographic provinces. From north (Pine Valley Mountains and Markagunt Plateau) to south (Grand Canyon) the topography and stratigraphy gradually step down, creating the Grand Staircase. We focused our attention on the central and upper Virgin River basins, emphasizing the area surrounding the Hurricane fault along the I-15 corridor (figures 1 and 2).

Interstate Highway 15 is oriented roughly north-south through a narrow corridor bordered to the east by the Hurricane Cliffs and to the west by the Pine Valley Mountains (figure 2). Our specific area of interest is between New Harmony and Hurricane. The trace of the Hurricane fault is approximately parallel to I-15, marking the base of the Hurricane Cliffs. Ash Creek is also roughly parallel to I-15, flowing from Ash Creek Reservoir, past Toquerville Springs, and into the Virgin River near Hurricane.

Geologic Setting

Geology of the Grand Staircase Area

The greater study area includes the Grand Staircase, a regional physiographic feature that extends from the Markagunt Plateau to the Colorado River (figure 1) and includes geologic units spanning in age from Quaternary to Precambrian. Figure 3 shows an index of published 1:100,000-scale
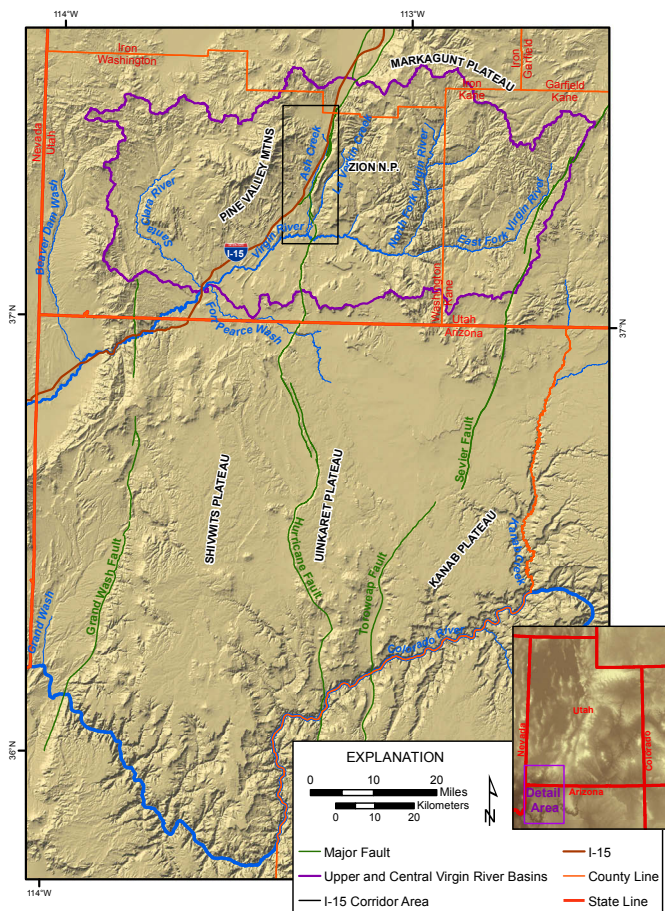
Figure 1. *The regional area examined for this study. The Virgin River basin and I-15 corridor areas are the progressively more localized areas of study. The Grand Staircase is east of the Hurricane Fault and north of the Colorado River.*

Figure 2. *Interstate 15 (I-15) corridor area.*

(30' x 60') geologic maps that cover the area. The larger north-south structure of the Grand Staircase is relatively simple, as the rock layers are relatively consistent in thickness and distribution, dipping gently to the north. Several large-displacement (greater than 100 ft), generally north-south trending normal faults offset the units in the Grand Staircase. These faults include the Grand Wash fault, the Hurricane fault, the Sevier fault, and the Toroweap fault (figure 1). The Hurricane fault displays significant displacement and extends from the Colorado River to north of the I-15 corridor area.

Geology of the I-15 Corridor Area

Biek and others (2009) produced a 1:100,000-scale (30' x 60') geologic map and associated report of the Washington County area. In addition, several 1:24,000-scale 7.5' geologic maps are available for the I-15 corridor area, including the New Harmony (Grant, 1995), Hurricane (Biek, 2003a), Pintura (Hurlow and Biek, 2003), Kolob Arch (Biek, 2007), and Harrisburg Junction (Biek, 2003b) quadrangles.

The I-15 corridor area (figures 1 and 2) includes several important geologic features. The Hurricane fault is a long, large-displacement normal fault, responsible for the offset observed at the Hurricane Cliffs, east of I-15 (figure 2). The Hurricane Cliffs expose some of the oldest rocks in the eastern Washington County area, which are at the core of the Kanarra anticline. West of the fault, the basin in the I-15 corridor area is filled by unconsolidated and semiconsolidated alluvial sediments, interspersed with and overlain by basalt flows found on both sides of the Hurricane fault. West of the I-15 area are the Pine Valley Mountains, made up of fractured, Tertiary-age quartz monzonite.

Hurricane Fault

The Hurricane fault is a 155-mile long, steeply dipping, active normal fault. The fault is made up of six fault sections (Lund and others, 2007; figure 4). The Ash Creek and Anderson Junction sections are within the primary area of interest and intersect at a complex structural boundary near Toquerville. In all sections, the Hurricane fault dips steeply west at about 65 to 85 degrees (Stewart and Taylor, 1996).
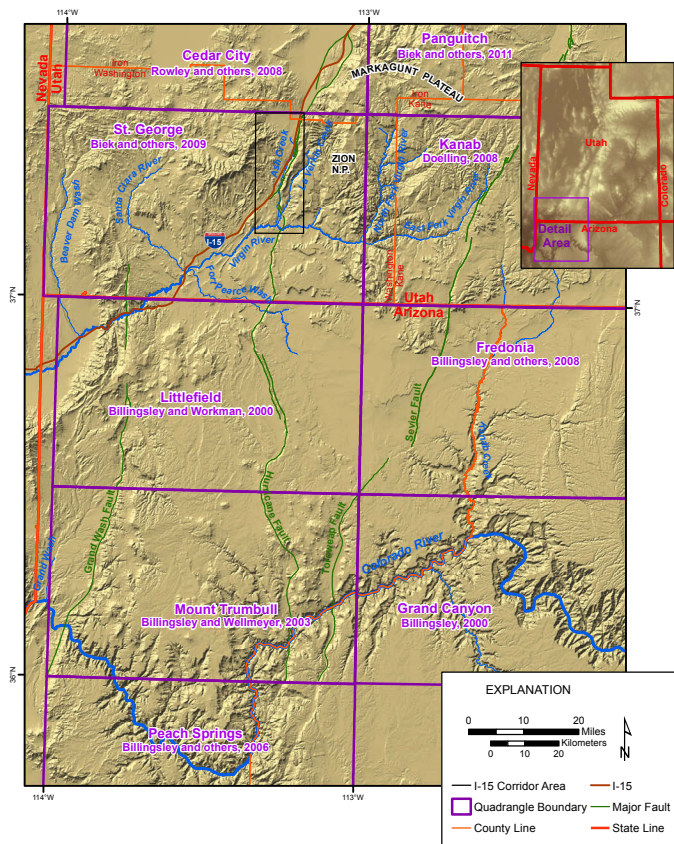
Figure 3. Index of 30' x 60' geologic quadrangle maps covering the greater study area.

Figure 4. Major sections of the Hurricane fault (modified from Lund and others, 2002).

The Hurricane fault exhibits normal, dip-slip movement (Lund and others, 2007; Biek and others, 2009), and the net displacement increases northward from the Colorado River. The fault has 800 to 1300 feet of net displacement near the Colorado River (Karlstrom and others, 2007) and about 3470 feet of net displacement near the transition from the Ash Creek section to the Anderson Junction section, near where the Hurricane fault intersects the Virgin River (Stewart and Taylor, 1996). Farther north, in the I-15 corridor area, the fault has approximately 7450 feet of net displacement (Stewart and Taylor, 1996). Vertical displacement (throw), unlike net displacement (slip) along the fault plane, is a measure of the purely vertical component of fault offset and does not include the horizontal component of movement. Anderson and Christenson (1989) determined the throw of the Hurricane fault at the latitudes of St. George and Toquerville to be 3600 and 4900 feet, respectively.

The sections of the Hurricane fault in Utah are older and have higher slip rates than the fault sections in Arizona (Lund and others, 2007; Biek and others, 2009). Biek and others (2009) hypothesized the northern sections of the fault have been active for the past 20 million years, while the sections of the fault on the Uinkaret and Shivwits Plateaus in Arizona have only been active for the past 3.6 million years (Billingsley and Workman, 2000). The average slip rate for the Anderson Junction section (figure 4) is 8 inches per 1000 years, whereas the estimated average slip rate for the Ash Creek section near Ash Creek Reservoir is 22 inches per 1000 years (Biek and others, 2009).

Folds

The Virgin anticline and the Kanarra anticline are two major Sevier-age (140–50 Ma) (Biek and others, 2009) anticlines in the primary area of interest (figure 5). The Virgin anticline is a 30-mile long, symmetrical, upright, open, northeast-trending fold (Biek and others, 2009). The limbs of the anticline dip from 25 to 35 degrees, exposing Permian, Triassic, and Jurassic strata (Biek and others, 2009). The three struc-
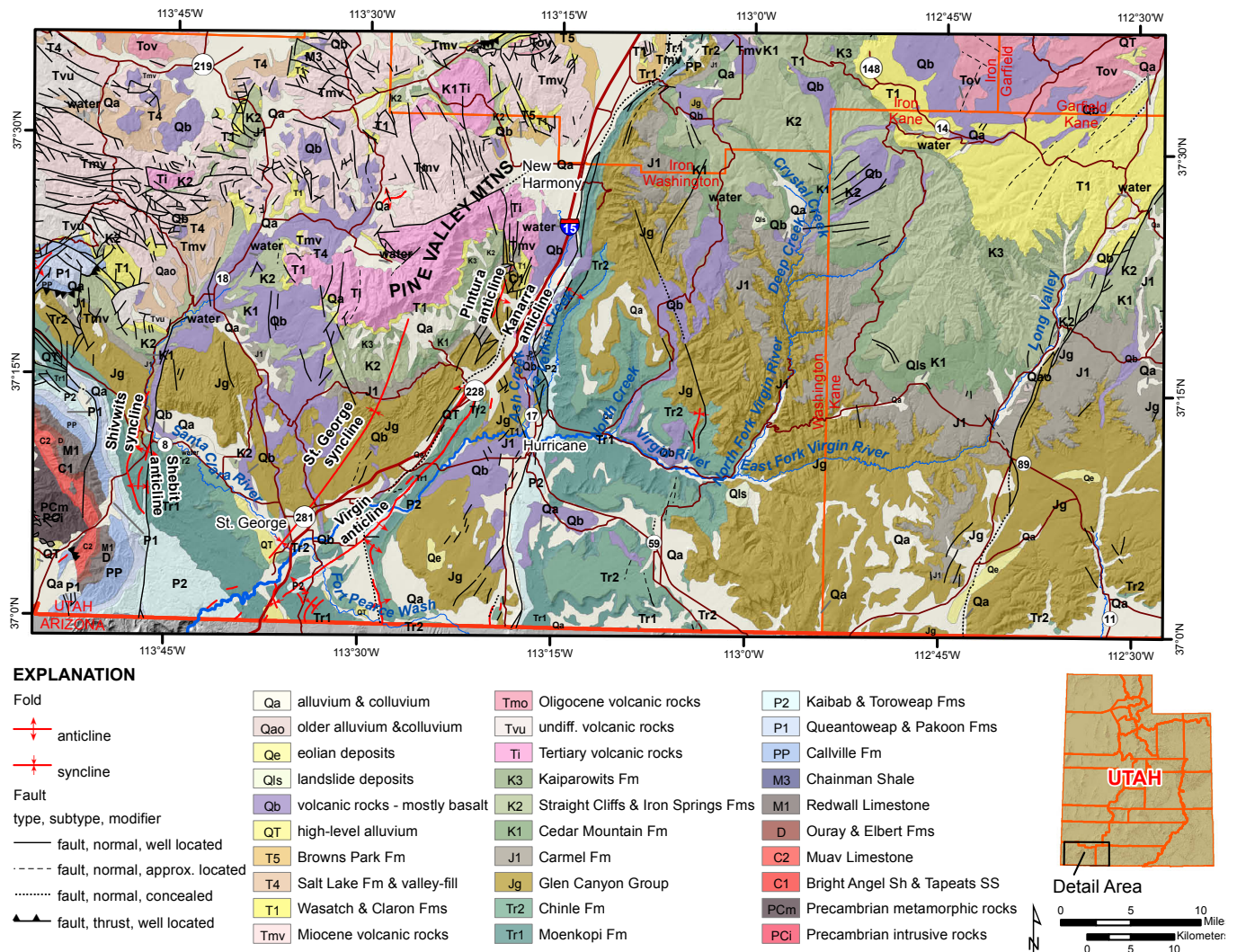
Figure 5. *Geology and major folds in the study area. Fold data modified from the St. George 30' x 60' geologic map (Biek and others, 2009). Geology from Hintze and others (2000).*

tural domes along the length of the Virgin anticline, from south to north are: Bloomington Dome, Washington Dome, and Harrisburg Dome.

The presence of smaller, subsidiary folds on the gently northeastward-plunging nose of the Virgin anticline suggests that the Virgin anticline is a separate structure from the genetically related, co-linear, Kanarra anticline on the footwall of the Hurricane fault (Biek and others, 2009). Significant differences in fold geometry also support that the Virgin and Kanarra anticlines are related to two different thrust faults (Biek and others, 2009). A syncline may be located in the subsurface between the folds (Stewart and Taylor, 1996). The Kanarra anticline coincides with the strike of the Ash Creek section of the Hurricane fault (figure 5), indicating that the Hurricane fault in this section may be a reactivated thrust fault along the western limb of the Kanarra anticline.

The Pintura anticline, located north of the Virgin anticline and west of the Kanarra anticline (figure 5), is also of Sevier age,

and was used to infer the time of deformation for the Virgin and Kanarra anticlines (Biek and others, 2009). In their geologic cross section, Biek and others (2009) depicted the Pintura anticline as a separate fold from the Kanarra anticline, but it could be the dismembered west limb of a structurally higher section of the Kanarra anticline, whose east limb was deformed by reverse drag of the Hurricane fault (Biek and others, 2009).

Hydrogeologic Setting

Previous Studies

Numerous hydrogeologic studies have been done in and around the study area. Many reports (Cordova and others, 1972; Cordova, 1978; Sandberg and Sultz, 1985; Hurlow, 1998; Heilweil and others, 2000) provide in-depth discussions of the basin-fill, Pine Valley, Navajo, and Kayenta aquifers. Cordova and others (1972) obtained preliminary information for both the consolidated and unconsolidated aquifers in the area and created a hydrologic budget. Cordova (1978) inves-

tigated groundwater conditions in the upper Virgin River and Kanab Creek basins to the east of the Hurricane fault. Sandberg and Sultz (1985) examined the water quality distribution along the Virgin River. Hurlow (1998) examined the geology of the Virgin River basin with consideration of groundwater conditions. Heilweil and others (2000) created a numerical groundwater flow model of the Navajo and Kayenta aquifers.

Everitt and Einert (1994) documented the influence of the Virgin River draining into sinkholes on the flow of Pah Tempe hot springs. Nelson and others (2009) thoroughly examined the hydrogeologic setting of the Pah Tempe hot springs, using both chemical data and physical observations. Christiansen (2009) presented groundwater hydrographs from U.S. Geological Survey (USGS) monitoring wells in the study area. Herbert (1995) completed a seepage study of the Virgin River from Ash Creek to Harrisburg Dome, and concluded that the Virgin River is a gaining stream along most of the stretch that they examined and not a losing stream along any of it. Rowley and Dixon (2010) investigated the feasibility of constructing a reservoir near Anderson Junction and recommended several sites for production wells. Rowley and Dixon (2010) recommended drilling production wells that intersect normal faults to take advantage of the higher permeability of fractured/damage zones near faults.

Hydrostratigraphy

Several aquifer units are in the area. Descriptions of aquifers by Alpine (2010) in northern Arizona provided the primary descriptions for hydrostratigraphic units in Utah. Aquifers in the Utah portion of the field are comprised of unconsolidated alluvium, fractured igneous rock, and Mesozoic sedimentary rocks. Alpine (2010) denotes the existence of several perched zones in the northern Arizona aquifers, specifically the Redwall/Muav (R), Coconino/Permian (C), and Triassic aquifers (figure 6). The perched aquifer zones in Triassic formations can be 1000 feet or more above the larger underlying C and R aquifer systems. Groundwater in northern Arizona flows horizontally down gradient, discharging at springs, as well as migrating deeper into lower aquifers through penetrating fracture systems (Alpine, 2010).

Basin-fill aquifers: Unconsolidated sediment is scattered throughout the study area in alluvial basins. These basins usually make satisfactory aquifers; however, the basin fill is not the focus of this study. Hurlow (1998) and Heilweil and others (2000) described the distribution of basin-fill sediment in the Washington County area and summarized the transmissivities of the basin fill.

Pine Valley aquifer: The Pine Valley Mountains are made up of the fractured Pine Valley Monzonite, which Hurlow (1998) mentions as a viable aquifer unit. The Pine Valley Monzonite is prominent in the I-15 corridor north of La Ver-

kin. Groundwater flow from the Pine Valley Monzonite may contribute to springs like the Toquerville Springs.

Navajo and Kayenta aquifers: The Navajo Sandstone aquifer is the most used aquifer in Washington County (Heilweil and others, 2000). The thick, well-exposed Navajo Sandstone has uniform grain size and is capable of receiving and storing large amounts of water (Heilweil and others, 2000). Within the study area, the Navajo Sandstone is an important aquifer only on the west side (hanging wall) of the Hurricane fault. Extensive fracture zones in the sandstone enhance groundwater recharge and flow, and normal faults compartmentalize the Navajo into discrete blocks (Hurlow, 1998).

The Kayenta Formation, which underlies the Navajo Sandstone (figure 7), is also a common source for groundwater (Clyde, 1987). The Kayenta aquifer is generally less transmissive than the Navajo aquifer (Heilweil and others, 2000).

Groundwater in the Navajo and Kayenta aquifers moves from the base of the Pine Valley Mountains southward to southeastward (Heilweil and others, 2000). Tertiary deposits and unconsolidated basin fill also provide groundwater to some wells (Hurlow, 1998; Biek, 2007).

The Navajo and Kayenta aquifers are bounded on the east by the Hurricane fault, which completely offsets the Jurassic formations. Immediately east of the Hurricane fault are older Permian units.

Triassic aquifers: Triassic strata in the field area include the Chinle Formation and the Moenkopi Formation (figure 7). The members of these formations mostly act as confining units. However, the Shinarump Conglomerate member of the Chinle, and the upper red and Virgin Limestone members of the Moenkopi are aquifers (figure 7). The Rock Canyon Conglomerate may also be an aquifer.

The Petrified Forest Member and the Shinarump Conglomerate Member make up the Triassic Chinle Formation (figure 7). The Petrified Forest Member is dominantly mudstone, claystone, and siltstone. This member also contains some sandstones and nodular limestones. Swelling, sealing bentonite clay layers are common in this member of the Chinle (Biek and others, 2009), which likely acts as a confining layer.

Underlying the Petrified Forest Member is the Shinarump Conglomerate Member (figure 7). The Shinarump Conglomerate Member is a medium to coarse-grained sandstone, pebbly sandstone, and pebbly conglomerate (Biek and others, 2009). It contains uncommon, local beds of smectite claystone and silty sandstone (Biek and others, 2009). This unit is an aquifer and several private wells pump water from it, and can contain relatively fresh water (Cordova, 1981), having a mean total dissolved solids (TDS) concentration of 900 mg/L.

Figure 6. *Stratigraphy and hydrostratigraphic subdivisions of northwestern Arizona, near the Grand Canyon (modified from Alpine, 2010).*

TIME STRAT. UNIT	FORMATION			SYMBOL	THICKNESS feet (m)	LITHOLOGY	Aquifer Potential	Aquifer System
Quaternary	Surficial deposits			Q	0–150+ (0–45+)			Basin fill and fractured igneous aquifer system
	Pintura flows			Qbp	0–1140 (0–350)	0.81–0.89 Ma (see appendix)		
Miocene / Lower	Pine Valley latite			Tvp	~100 (~30)	K-feldspar megacrysts		
	Quartz monzonite (Pine Valley Mtns.)			Tip	450+ (135+)	20.32–20.66 Ma		
	Megabreccia			Tm	~150 (~45)	fault-bounded, brecciated Tertiary volcanic rocks		
Oligocene	Brian Head Formation (?)			Tbh?	~30 (~9)			
Eocene	Claron Formation	upper		Tcu	520 (160)			
		lower		Tcl	1090 (330)	intruded by Pine Valley Mtns. quartz monzonite porphyry		
Paleocene	Canaan Peak Formation			TKcp	0–119 (0–36)	quartzite and volcanic clasts		
Cretaceous / Upper	Iron Springs Formation			Kis	3200+ (975+)	soft-sediment deformation / cross-bedding		Cretaceous aquifer system
Jurassic / Middle	Carmel Formation	Paria River Member		Jcp	360–680 (110–210)			Jurassic aquifer system
		Crystal Creek Mbr.		Jcx	100–190 (30–60)			
		Co-op Creek Ls. Mbr.		Jcco	300–450 (90–135)			
	Temple Cap Formation			Jts	10–50 (3–15)	gypsum		
Jurassic / Lower	Navajo Sandstone			Jn	~2300 (~700)	high-angle cross beds / transition zone	Navajo and Kayenta Aquifers : Major aquifers of Washington Co.	
	Kayenta Formation	Main body		Jk	~455+ (~140+)			
		Springdale Sandstone Mbr.		Jks	~100 (~30)			
	Moenave Formation	Whitmore Point Member		Jmw	~60 (~18)		a few low yield wells	
		Dinosaur Canyon Mbr.		Jmd	~200 (~60)			
Triassic / Upper	Chinle Formation	Petrified Forest Mbr.		Ͳ̵cp	~400 (~120)	swelling, brightly colored clays	confining unit	Triassic aquifer system
		Shinarump Cgl. Mbr.		Ͳ̵cs	~120 (~37)		a few low yield wells	
Triassic / Middle	Moenkopi Formation	upper red member		Ͳ̵mu	~200 (~60)		a few low yield wells	
Triassic / Lower		Shnabkaib Member		Ͳ̵ms	~350 (~110)	"bacon-striped" gypsum	confining unit; gypsiferous beds	
		middle red member		Ͳ̵mm	~200 (~60)			
		Virgin Limestone Mbr.		Ͳ̵mv	120–270 (37–82)	3 limestone ledges	a few low yield wells	
		lower red member		Ͳ̵ml	250–315 (75–95)		leaky confining unit	
		Timpoweap Member		Ͳ̵mt	50–180 (15–55)			
		Rock Canyon Cgl. Mbr.		Ͳ̵mr	0–100 (0–30)		a few low yield wells	
Permian / Lower	Kaibab Formation	Harrisburg Member		Pkh	120–180 (37–55)	gypsum / white chert / "black-banded"	karstic and fractured rock may provide some water; gypsiferous beds may influence groundwater quality	C aquifer system
		Fossil Mountain Mbr.		Pkf	240–280 (73–85)			
	Toroweap Formation	Woods Ranch Mbr.		Ptw	120–250 (37–76)			
		Brady Canyon & Seligman Mbrs.		Ptbs	250–285 (76–87)			
	Queantoweap Sandstone	upper member		Pqu	1300–1630 (400–500)	forms stairstep topography	fairly pourous and permeable; fines to the south; little information on quality and quantity available	
		lower member		Pql	120–800 (37–245)		may act as a leaky confining layer in some areas. Analogous to Hermit Shale to the south	
	Pakoon Formation			Pp	250+ (75+)		karstic and fractured rock may provide some water	
Pennsylvanian	Callville Limestone			PⱣPc	285 (85)		karstic and fractured rock may provide some water	R aquifer system
Mississippian	Redwall Limestone			Mr	1220 (370)	Thunder Springs Mbr	karstic and fractured rock may provide some water; water quality generally poor to saline	
	Chainman Shale			Msc	160 (50)	Msc absent in Beaver Dam Mountains	confines where present	
Devonian	Devonian, undivided			Du	570+ (175+)			

Figure 7. Stratigraphic column and hydrostratigraphy of Pintura, Utah, area (modified from Hurlow and Biek, 2003).

The Moenkopi Formation is a thick unit throughout the upper and central Virgin River basin. It contains seven members, most of which act as confining units (figure 7). The members, from youngest to oldest, include:

1. Upper red member – dominantly siltstone, mudstone, and fine-grained sandstone that contains numerous gypsum stringers. A fine-grained sandstone forms the base of the member. This member thickens to the southwest, from 200–280 feet at Zion National Park to 400–600 feet near St. George (Biek and others, 2009). This may be a water-producing member that is hydrologically connected to the Shinarump Conglomerate Member of the Chinle.

2. Shnabkaib Member – a gypsiferous mudstone and siltstone. Like the upper red member, the Shnabkaib Member thickens southwestward, from 350–500 feet east of the Hurricane Cliffs, to 800–1000 feet west of St. George (Biek and others, 2009). Because of the predominance of gypsum in this unit, it is likely a confining layer, and it may influence the water chemistry of adjacent aquifers.

3. Middle red member – comprised of siltstone, mudstone, and fine-grained sandstone interbedded with several thick gypsum beds near the base (Biek and others, 2009). Like the Shnabkaib, the gypsum and fine-grained materials in this unit make it a confining layer.

4. Virgin Limestone Member – comprised of limestone and silty limestone, this unit generally thickens westward (Biek and others, 2009). A few low-producing, private wells are open to this member, but it has limited potential as an aquifer.

5. Lower red member – a slope-forming mudstone, siltstone, and fine-grained sandstone (Biek and others, 2009). Its use as an aquifer is not well documented, and the unit may produce small amounts of water at some locations.

6. Timpoweap Member – a limestone having some intermittent sandy parts (Biek and others, 2009). Some drillers have reported this unit as a water producer, but, based on a thickness of 50 to 180 feet, the Timpoweap Member could likely only supply small, private wells.

7. Rock Canyon Conglomerate Member – This unit is up to 200 feet thick in local channels west of St. George, and is composed of clast-supported pebble conglomerate and a 3- to 10-foot thick sedimentary breccia (Biek and others, 2009). Although there is little information available to document this unit's potential as an aquifer, this unit, where present, would likely be a sufficient aquifer for smaller wells.

C aquifer: The C aquifer derives its name from the Permian Coconino Formation, and is also referred to as the Coconino aquifer (McGavock and others, 1986). In Arizona, the C aquifer includes the Kaibab Limestone, the Toroweap Formation, and the Coconino Sandstone (figure 6). In Arizona, th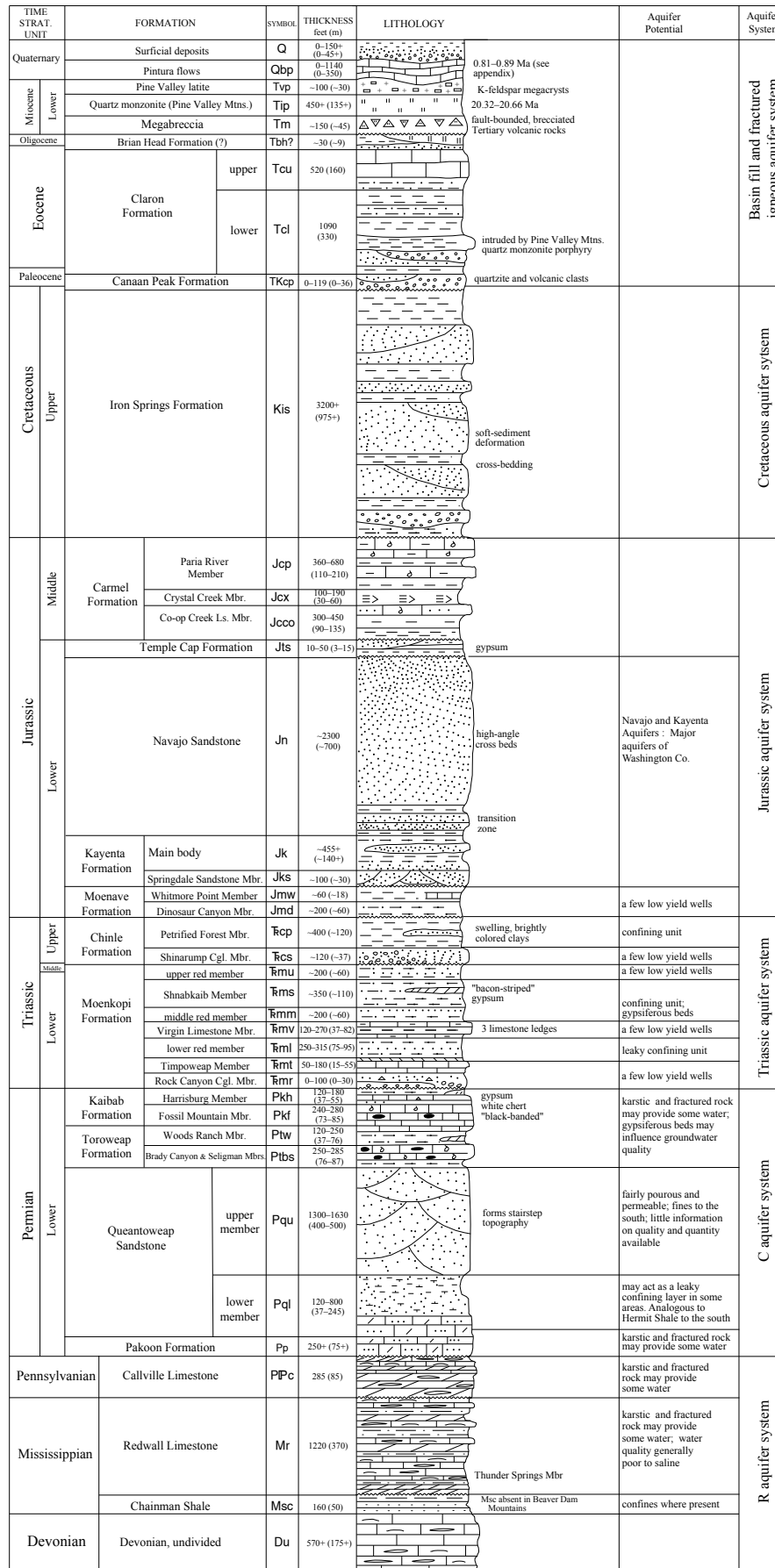e impermeable Hermit Shale underlies the C aquifer. In the Washington County area, the Queantoweap Sandstone is equivalent to the Coconino Formation, Hermit Shale, and Esplanade Sandstone in Arizona (figure 7). Although the Hermit Shale is an effective confining unit in Arizona (Alpine, 2010), an analogous, significant confining unit for the C aquifer is not present or hard to discern in the Washington County stratigraphy.

The Permian Kaibab Formation is a limestone made up of the Harrisburg and Fossil Mountain Members. In the I-15 corridor area, it is exposed along the Hurricane Cliffs in the footwall of the Hurricane fault. Near the fractured zones of the Hurricane fault, the Kaibab may provide a source of water (Dutson, 2005). The Kaibab Formation gradually thickens to the west. In Arizona, the Kaibab Formation is composed of cyclic beds of carbonate and siliciclastic sediments mixed with diagenetic chert and dolomite (Ross, 2005). Huntoon (1970) noted that joint spacing in the Fossil Mountain Member in Arizona ranges from 3.9 to 7.9 feet. Joint spacing in the Harrisburg Member ranges from 0.16 to 2 feet (Huntoon, 1970). Laboratory analyses of unfractured cherty limestone and unfractured sandy limestone of the Kaibab Formation indicate effective permeabilities of 0 and 1.1×10^{-4} feet per day, respectively (Huntoon, 1970).

The Woods Ranch, Brady Canyon, and Seligman Members comprise the Permian-age Toroweap Formation (Biek and others, 2009). The Woods Ranch Member is a laminated to thinly bedded dolomite and is the youngest member of the Toroweap (figure 7). In the Virgin River Gorge, this member contains gypsum beds 20 to 50 feet thick. However, farther north in the Hurricane Cliffs, the gypsum is less prevalent (Biek and others, 2009). The Brady Canyon Member of the Toroweap underlies the Woods Ranch Member and is a fossiliferous limestone (figure 7). The Seligman Member of the Toroweap is slope-forming thin-bedded sandstone that thickens westward from 30 feet near the Hurricane Cliffs to about 100 feet southwest of St. George (Biek and others, 2009). The fine-grained, gypsiferous Seligman Member of the Toroweap Formation is relatively impermeable and has lower fracture density than overlying and underlying units (Dutson, 2005).

The Toroweap Formation contains several breccia features, in both Utah and Arizona (Loughlin, 1983; Alpine, 2010). Alpine (2010) attributes the breccia formation observed in Arizona to collapse of karst features in the underlying Mississippian Redwall Limestone. Alpine (2010) commented that, in Arizona, the brecciated areas are conduits for water flow from areas above the Toroweap to lower units such as the Redwall Limestone. In the Utah portion of the study area, there are no verifiable reports of breccia pipes. Although there are many collapse features in the Washington

County area, Biek and others (2009) attribute them to dissolution of interbedded gypsum, and not karst collapse as observed to the south.

In Arizona, joint spacing in the Toroweap ranges from 2 inches to 3 feet in redbeds to 8 feet in limestone beds. The Toroweap has a complex hydrogeologic setting composed of multiple groundwater flow pathways enhanced through karst development (Huntoon, 1970). Springs are common in the Toroweap Formation where clastic layers inhibit vertical groundwater migration. Laboratory analyses of unfractured Toroweap limestone indicate that the limestone is impermeable, further evidence that secondary porosity through fracturing and karst development is the most important groundwater flow pathway. The depositional setting of the Toroweap in the vicinity of Grand Canyon was a fluctuating shallow marine environment, leading to the dramatic changes in lithofacies (Turner, 1990).

Underlying the Seligman Member is the thick, eolian Queantoweap Sandstone, which has significant primary porosity supplemented by secondary porosity in fractured areas near faults. The Permian Queantoweap Sandstone is fine- to medium-grained sandstone that forms the majority of the Hurricane Cliffs near Pintura. The upper half is stratigraphically equivalent to the Coconino Sandstone and Hermit Shale in Arizona, and the lower half is equivalent to the Esplanade Sandstone of the Supai Group in Arizona. Underlying the Queantoweap Sandstone is dolomitic limestone of the Pakoon Formation. The permeability of the Pakoon Formation is likely mostly from fractures that have undergone some level of solution weathering. The Queantoweap Sandstone and other Permian units below it may be conduits for regional flow from the east and the north (Nelson and others, 2009).

In their stratigraphic column, Biek and others (2009) show a silty unit near the base of the Queantoweap, which may act as a leaky confining layer between the Queantoweap and the underlying Permian Pakoon Formation (figure 7). Also, the Pakoon Formation contains a gypsiferous interval near its upper contact that also may hydrologically separate the Pakoon from the Queantoweap. However, this gypsum layer is not prevalent everywhere, and has not been observed in the Hurricane Cliffs. Near the Hurricane fault, the Pakoon is highly fractured (Biek and others, 2009).

Between the Grand Canyon and the I-15 corridor, the Pennsylvanian and Permian rocks undergo significant facies changes and are therefore referred to by different names (Giardina, 1979; figure 8). In the Washington County area, the Queantoweap Sandstone is stratigraphically equivalent to the Hermit Shale (Biek and others, 2009), and the Pennsylvanian Callville Limestone and Permian Pakoon Formation are stratigraphically equivalent to the Supai Group of the Grand Canyon area (figure 8). The differences in the

units are due to a facies change from deep-water, fine-grained facies in the south (Grand Canyon) to shallow-water clastic/carbonate facies in the north (Pintura). The base of the Callville Limestone may act as a confining layer in the Washington County area for the R aquifer because it has several fine-grained intervals. The Pakoon Formation is a vuggy, fractured dolomite in the Washington County area, and it is likely hydraulically connected to the Pennsylvanian and Mississippian units underlying it. Finer, lenticular shaley beds at the base of the Queantoweap Sandstone likely act as a confining unit that separates the Permian and older carbonates from the Queantoweap and younger formations.

R aquifer: The R aquifer is primarily composed of the Redwall Limestone and various underlying Devonian and Cambrian carbonate rocks, including the Cambrian Muav Limestone (figure 6). The Cambrian Bright Angel Shale marks the bottom of the R aquifer. In the Grand Canyon region, the Pennsylvanian and Permian Supai Group and the Permian Hermit Shale separate the R aquifer from the C aquifer (Alpine, 2010).

Based on oil well logs, the Redwall Limestone is 615 to 1000 feet thick in the area of the I-15 corridor and St. George, thinning to the southeast and thickening to the northwest (Langenheim, 1963; Biek and others, 2009; Hintze and Kowallis, 2009). The Redwall Limestone represents a shallow carbonate shelf that extended throughout Utah and Arizona during Mississippian time. However, normal faults having significant vertical offset divide the Mississippian carbonates into smaller, hydrologically separate packages.

Normal faults compartmentalize the R aquifer (and other regional aquifers) in the Grand Staircase area. Crossey and others (2006) define these compartments as the Far Western (FW) region, the Hurricane-Toroweap (HT) region, and the North Eastern (NE) region. The R aquifer is laterally continuous and connected along the footwall of the Hurricane fault, hydrologically bounded to the west by the Hurricane fault and to the east by the Sevier and Toroweap faults. This compartment is the HT compartment of Crossey and others (2006). The cliffs of the Grand Canyon create the southern hydrologic boundary of the HT compartment, although Huntoon (1981) provides evidence of groundwater flow beneath the Colorado River in the NE compartment of the R aquifer. The northern extent of the HT compartment of the R aquifer is unknown, but it likely extends to the north of the Markagunt Plateau.

Many workers (Ross, 2005; Crossey and others, 2006) have defined the R aquifer as karstic, where the dominant porosity and permeability appear to be secondary, created from fractures (Gettings and Bultman, 2005) and dissolution (Ross, 2005). In Arizona, fracture orientations correlate to breccia pipes that extend upward as much as 3300 feet from the Redwall Limestone (Ross, 2005). The breccia pipes
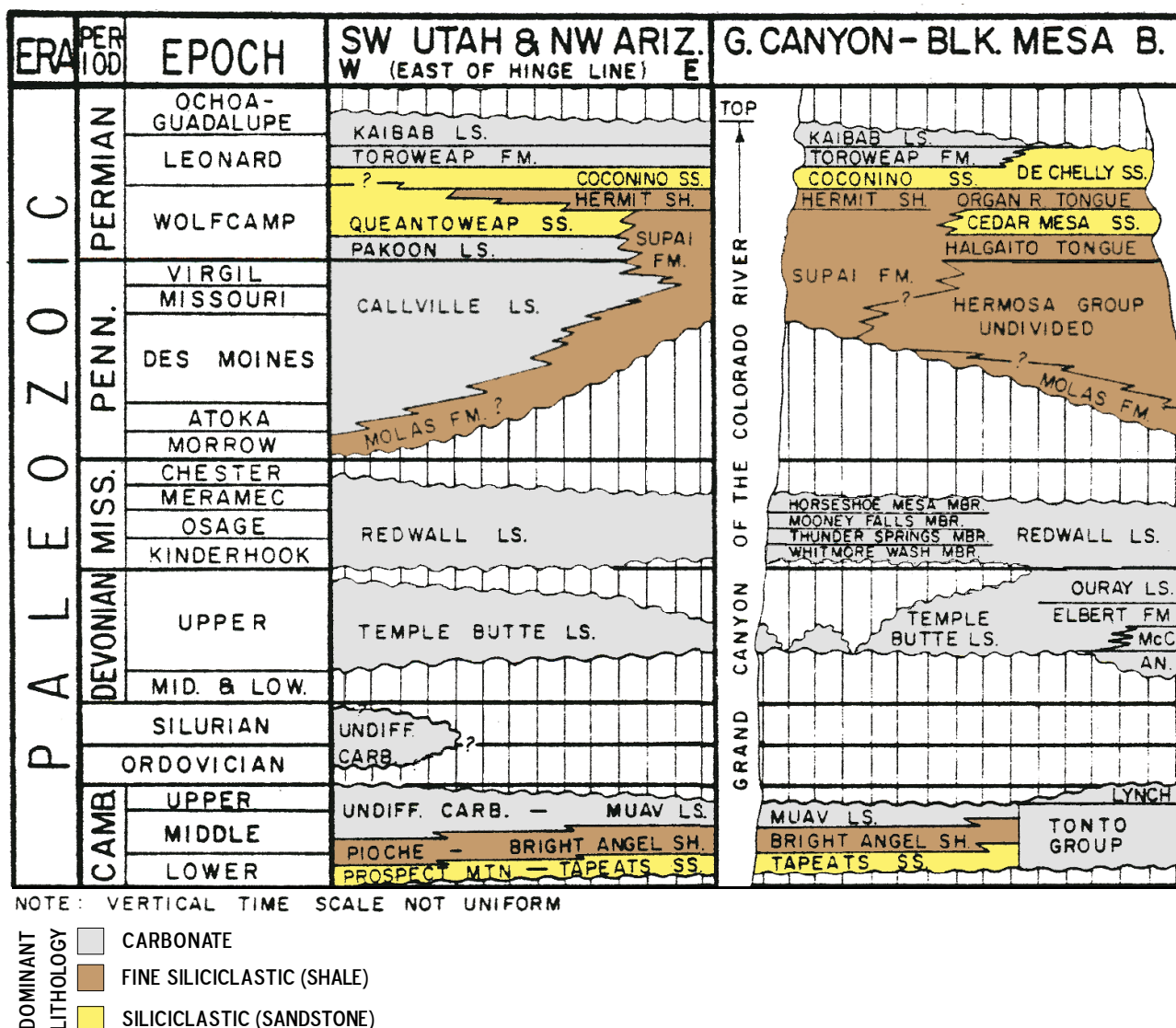
Figure 8. *Statigraphic relationships between southwestern Utah and northwestern Arizona (modified from Giardina, 1979).*

likely formed when overlying strata collapsed into solution caverns of the Mississippian Redwall Limestone (Ross, 2005; Alpine, 2010). In Arizona, breccia pipes can allow hydrologic connection between the ground surface and the R aquifer (Ross, 2005; Alpine, 2010).

Fractures and Faulting

Enhanced permeability in fault zones may enable the interaction of deeper regional groundwater with younger, shallower groundwater. Fault gouge probably restricts transverse flow through faults in the Navajo Sandstone aquifer, but fracturing in the damage zone adjacent to the gouge zones likely results in high permeability along fault planes (Hurlow, 1998). Nelson and others (2009) concluded that the fractured area adjacent to the Hurricane fault, as in

other area normal faults, is conducive to flow. The density of fractures in the damage zone decreases away from the fault. A majority of flow is concentrated in a small number of fractures with larger (> 0.35 in) apertures (Nelson and others, 2009).

Sevier-age deformation and subsequent extensional deformation created two sets of fractures in the area of study. Dutson (2005) described fractures where the Virgin River intersects the Hurricane fault, and noted that fracture frequency does not decrease, as expected, at greater distances from the fault. Biek and others (2009) hypothesized that the Ash Creek segment of the Hurricane fault is localized along deformation of the Kanarra fold, and may even be a reactivated Sevier-age thrust fault.

POTENTIOMETRIC SURFACE AND UNIT IDENTIFICATION

Introduction

Understanding the direction of horizontal groundwater flow requires knowledge of the potentiometric surface, which represents the distribution of hydraulic head within an aquifer (Poehls and Smith, 2009). Comparing the relative positions of potentiometric surfaces in separate aquifers can provide insight into how those aquifers are connected and the vertical hydraulic gradient between them. To organize groundwater-level data into various hydrogeologic units, we used hundreds of water and oil well drillers' logs (lithologic and geophysical) to construct a hydrogeologic cross section and structure contour maps to more easily delineate units.

We compared existing potentiometric surface maps to our maps to ensure that results were logical. Scientists at the U.S. Geological Survey (USGS) have created potentiometric surface maps of the basin-fill, Navajo, and Kayenta aquifers within the Virgin River basin. The USGS created a general potentiometric-surface map of the Jurassic Navajo aquifer in the central Virgin River basin (Cordova, 1978, plate 3) and a map of an areally limited and discontinuous potentiometric surface of the Jurassic Navajo aquifer in the eastern (upper) Virgin River basin (Cordova, 1981, plate 1). Heilweil and Freethey (1992) used numerical modeling to generate hypothetical potentiometric-surface lines in the upper (eastern) Virgin River basin. Heilweil and others (2000, plate 2) completed a comprehensive potentiometric-surface map of the basin-fill, Navajo, and Kayenta aquifers in the central Virgin River basin. Alpine (2010) presented a general diagram of groundwater flow paths, divides and potentiometric-surface contours (figure 9) for the R aquifer in the area of northwestern Arizona.

Methods

Constructing potentiometric-surface contours required depth-to-water measurements from wells, well and spring surface elevations, and geologic source data. We assumed water levels were relatively stable over time and that the potentiometric surfaces may be approximated by linear interpolation between data points in areas where well data are unavailable, and where no major faults or folds were crossed. Land-surface elevation data of the various measuring points are required to derive the elevation of the potentiometric surface (absolute measurement) from the depth to water (relative measurement). We assumed that the spring and sink surface elevations approximate the regional elevation of the potentiometric surface. We assigned each spring and well to aquifers described above to separate the water-level elevations (and later the chemistry data) into different aquifers.

Data Compilation

The area of well and spring data compilation includes wells and springs south of Cedar Valley, north of the Colorado River, west of the eastern extent of the Virgin River basin, and east of the western border of Utah (figure 10). The large area was necessary to check for potential groundwater flow to the Colorado River, primarily along the major north-south normal faults in the region (figure 1), and to include more measurement points from the R and C aquifers.

We compiled a variety of data sources, including (1) the Utah Division of Water Rights (DWR) (2011), (2) the USGS National Water Information System (NWIS), (3) the high-resolution National Hydrography Dataset (NHDplus) (U.S. Environmental Protection Agency, 2011), (4) the Utah Division of Drinking Water (DDW) (2011), (5) the Utah Division of Oil, Gas, and Mining (2011) oil well dataset, (6) the Arizona Well Registry (Arizona Department of Water Resources, 2011a), and (7) the Arizona Ground Water Site Inventory (GWSI) (Arizona Department of Water Resources, 2011b).

We obtained the Water Rights Points of Diversion (WR POD) spatial database from the DWR (2011). The WRPOD database includes location and well construction information for all wells with water rights in Utah. We only used wells with well identification numbers (WIN) because wells without them cannot be associated with the water-level table that DWR provides. We assigned land-surface elevations to these wells, but no measured elevation values were available for comparison. The depth-to-groundwater-level data maintained by the DWR are usually the values recorded by the well driller, sometimes before the well is complete or developed. Because of these factors, the water levels in the WRPOD database are generally less reliable than the USGS data.

We also compiled all USGS groundwater-level measurements available in the NWIS database (U.S. Geological Survey, 2011). All data noted as being influenced by nearby waters or pumping in the NWIS database were removed.

Spring locations came from a variety of sources. The NHDplus database provided location information for most of the springs in the area of interest. We selected springs from only the Lower Colorado region of the NHDplus database (U.S. Environmental Protection Agency, 2011). Upon request, the DDW (2011) provided locations of Utah municipal springs and wells and chemistry data for those sites (see the Groundwater Quality Characterization section of this report). The USGS NWIS database also listed several spring locations.

The Utah Division of Oil, Gas, and Mining (2011) provided the information about locations and construction of oil wells in Utah. However, drillers rarely use reliable methods to measure the depth to water. Downhole geophysical logs sometimes

EXPLANATION

— 4,000 – – ? Potentiometric contour of the Redwall-Muav aquifer —Shows altitude at which water would have stood in a tightly cased well penetrating the Redwall-Muav aquifer prior to about 1990, in feet above sea level. Contour interval 100-400 feet. Dashed where approximately located, queried where uncertain.

-------?--?- Redwall-Muav aquifer groundwater divide —Queried where uncertain

⟶ Direction of groundwater movement

● (3,000) Well —Text is well name; number is static water level in feet above sea level

Figure 9. *Potentiometric surface and groundwater flow map of the Redwall-Muav aquifer in northwestern Arizona (modified from Alpine, 2010).*

indicate the presence of water, but some rock units could be mistaken for a water level, and the driller usually only saves the saturated portion of the log because many of the geophysical tools only work when submerged in liquid. Also, oil wells are often open to several hydrogeologic units. The lack of information limits the availability of water data from oil wells.

Well locations and information for wells in Arizona came from two sources—the Arizona Well Registry and the GWSI (Arizona Department of Water Resources, 2011b). The Arizona Well Registry stores well information in the AZ-55 database. Most of the wells in this database have drilling information, including lithologic descriptions from well drillers. Some of the GWSI wells have information regarding the aquifers supplying the screened intervals and most have accurate water level data.

Where our compilation resulted in duplicate wells or springs, we used the most recent water level data available. Data points within 30 feet of each other were assumed to be duplicates and the older point was removed, unless clear evidence (such as different depth information) existed that allowed for distinction between the two points.

Elevations

The National Elevation Dataset (NED) 10-meter horizontal resolution digital elevation models (DEM) provide the elevation data for all surface elevations, to ensure consistent geodetic datums and elevation values. The vertical accuracy of the NED data is 8 feet (Gesch, 2007). The relative vertical accuracy for closely spaced data within the larger NED dataset is 2.6 feet (Gesch, 2007). The USGS continuously updates the NED dataset as they collect data.
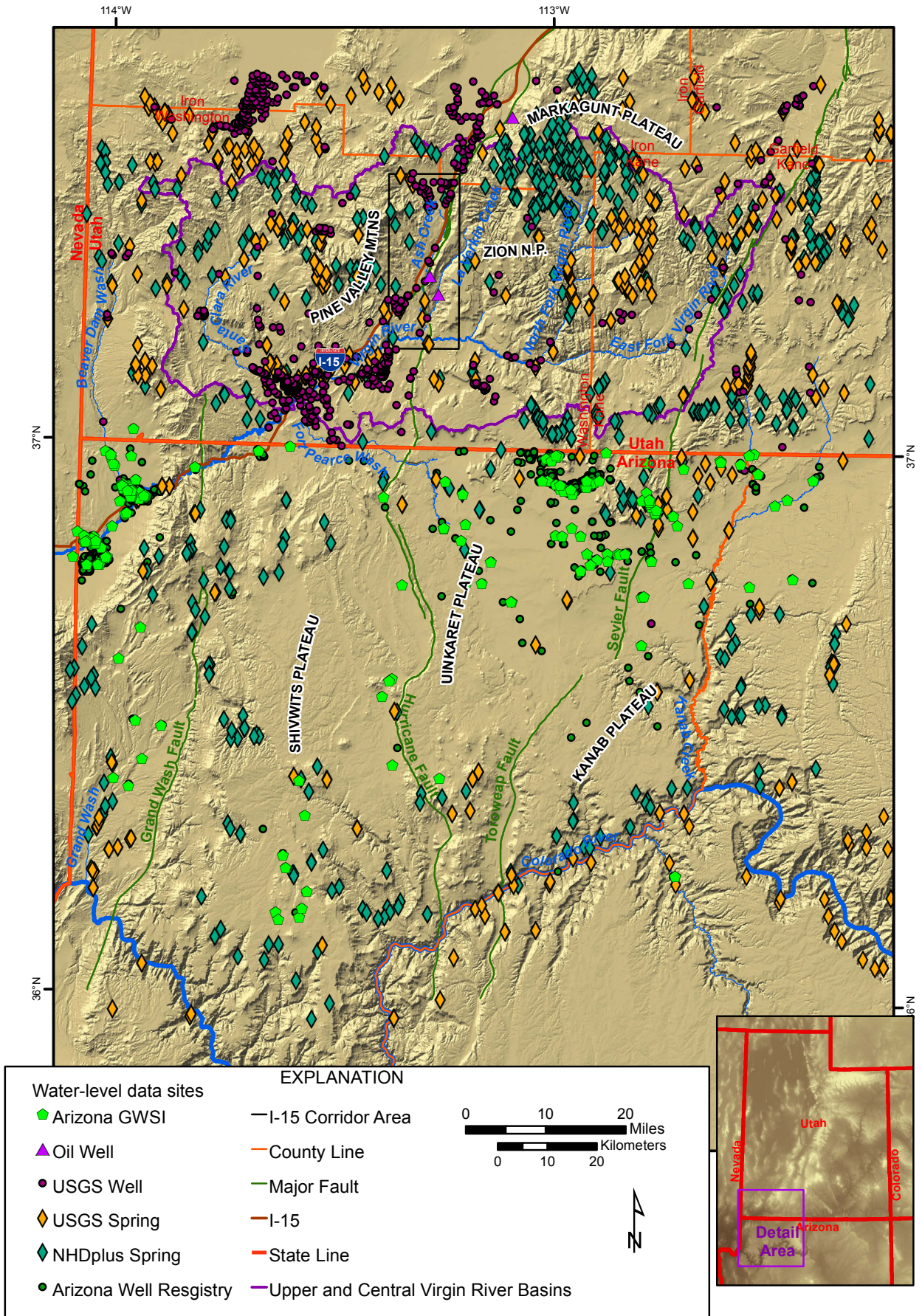
Figure 10. *Sites compiled from various agencies of groundwater level measurements.*

Although the USGS NWIS database provides elevation data for each point, the USGS applied a variety of measurement techniques and vertical and horizontal geodetic datums to determine those elevations. Most of the elevations from the NWIS database in the areas of interest are based on USGS 1:24,000-scale topographic maps, which are slightly less accurate than the 10-meter resolution DEMS (Gesch, 2007). We checked DEM elevations against the station elevations of the wells measured by the USGS from the NWIS database. Where wells had differences between the NWIS and DEM elevations of greater than 50 feet, we adjusted the well location based on their NWIS-designated cadastral location value, and assigned new DEM elevations based on their new locations. After we corrected locations and assigned new DEM elevations for the new well locations, we eliminated wells having elevation differences between the original DEM elevation and the DEM elevation at the new location greater than 40 feet. Wells with questionable locations were also eliminated from our compilation (database).

For all springs we assumed that the elevation of the ground surface where the spring point plots on a map is the representative elevation of the spring (and the potentiometric surface) at that point; however, the water level may be lower (i.e., a spring box is in place) or higher (i.e., the spring is an artesian flowing spring, whose potentiometric head is higher than the land surface). We checked the location of each spring using USGS 1:24,000-scale topographic maps and high-resolution aerial photographs and adjusted locations as needed.

Structure Contours

To construct structure contours of the top of key stratigraphic units, we used methods adapted from Ross (2005) in the area to the southeast of the area of interest. Using ArcGIS (ESRI, 2010), we traced outcrop contacts from 30' x 60' geologic maps and assigned elevations to the vertices of those contact trace elevations based on 10-meter horizontal resolution digital elevation models (DEMS). The outcrops we traced surround large portions of the units of interest. We then supplemented the surface data by including oil well location and stratigraphy data from the Utah Division of Oil, Gas, and Mining (2011), and assigned the oil wells land-surface elevations using the 10-meter DEMs, and converted the depth-below-surface of formation contacts to elevations. We also digitized and projected geologic cross sections from the St. George (Biek and others, 2009), Cedar City (Rowley and others, 2006), and Littlefield (Billingsley and Workman, 2000) 30' x 60' geologic maps, and the Kolob Arch (Biek, 2007), Hurricane (Biek, 2003a), Harrisburg Junction (Biek, 2003b), Divide (Hayden, 2004), and Pintura (Hurlow and Biek, 2003) 1:24,000-scale geologic maps. We converted the digitized lines into evenly spaced points having three-dimensional coordinates. We interpolated between the outcrop, oil well, and cross-section data points to create surfaces (raster files) having units of elevation above mean sea level. We

contoured the resulting surfaces using the ArcGIS (ESRI, 2010) contour tool and removed extraneous contours. We assumed that the stratigraphic boundaries are distinct over the region of interpolation and did not interpolate across faults having offsets more than a couple of hundred feet (e.g., the Hurricane fault).

Unit Identification

We identified the aquifer(s) from which each well obtained its water based on well drillers' lithologic logs, geologic cross sections, and our structure contour maps, and then compiled our aquifer-to-well assignments into a geospatial database. Due to the ambiguous nature of well logs, our database likely includes some misidentified wells and springs. Also, well drillers' records are not always reliable sources of information and can be less so where complex heterogeneities (faults, folds, facies changes) exist. We removed wells and springs lacking positive identification of hydrogeologic unit(s).

USGS and UGS 30' x 60' digital geologic map polygons provided the geologic information for the springs. Using the spatial join feature in ArcGIS (ESRI, 2010), we assigned a geologic unit to each spring based on which geologic unit is mapped at the spring location. This assumes that the geologic unit from which the spring issues is the source unit, which is commonly not the case, as some springs issue from alluvium or colluvium covering the source unit. Where only a small areal extent of alluvium or colluvium was present, we assumed that the underlying bedrock unit was the source of the spring.

Identifying the source hydrogeologic units for the wells was more complicated. Some of the USGS wells have unit identifications assigned in the NWIS database. Most of the DWR wells have well drillers' logs, but we interpreted each log in terms of its hydrogeologic source. For wells that do not contain stratigraphic information, but have well depth, we used geologic maps and isopach lines to determine the unit from which the wells extract water. We used 30' x 60' geologic quadrangles (figure 3), their respective cross sections, and all available well drillers' logs to identify screened units in Arizona and Utah.

Creating Contours

After we attributed elevations and probable source lithologies to the groundwater-level values, we were then able to interpolate and contour the groundwater-level values. First we separated the groundwater elevations into their respective assigned source aquifers. Then we separated values from the footwall and values from the hanging wall of the Hurricane fault. We then used the Natural Neighbor technique in ArcGIS (ESRI, 2010) to interpolate the groundwater elevations, which resulted in a grid-like surface of continuous elevation data known as an elevation raster. The automated contouring tool in ArcGIS (ESRI, 2010) created contours from the ras-

ter. We then checked the automatically created contours and modified them as necessary to reflect the nature of potentiometric surfaces and the elevations of the groundwater at the measurement sites.

Oil Well Log Examination

In the interest of discovering groundwater-level data and to help create our hydrogeologic sections, we examined several oil well logs. The American Petroleum Institute (API) number is a common way to identify oil wells, but other names are also common.

Pintura: The Pintura wells are located approximately 3 miles west of Pintura, along southern Ash Creek (figures 2 and 11). Cary (1963; use his figure 2 as a supplement) correlated stratigraphy between the Pan American Martin-Pintura well (API 4305310879) and the Sun Pintura Unit 1 well (API 4305311164) in the Pintura anticline. The Martin-Pintura well record indicated water from the Moenkopi Formation (3400 to 3423 feet) and the Mississippian and Devonian formations

(8921 to 9501 feet). In the Sun Pintura Unit 1 well, the driller noted important water sands at 2247 to 2272, 2550 to 2618, 2332 to 2347 feet, and 5300 to 5496 feet below ground surface. The driller identified the sandstone as parts of the Chinle, Moenkopi, and Queantoweap Formations. Significant loss of returns and circulation at the Redwall Limestone and Devonian dolomites could be indicative of karst and/or fracture systems.

Conde: For the Federal 1-25 Conde well site (API 43053 30024), Reber (2003) noted water at a depth of 420 feet. Reber (2003) said that the water-bearing zone of interest is the semi-consolidated Tertiary alluvial fan material, underlying alternating layers of fractured basalt and unconsolidated alluvial fill. Reber (2003) claimed that the Claron Formation is at a depth of 800 feet. The driller's log likely misidentifies the formation names but properly identifies the geologic material, while Reber (2003) cautiously (and likely correctly) identifies the hydrogeology of the site. The driller's log leaves out the Navajo Sandstone and skips to the units beneath it. Reber (2003), however, provided a more accurate representation of the geology of the well in his A–A' cross section.
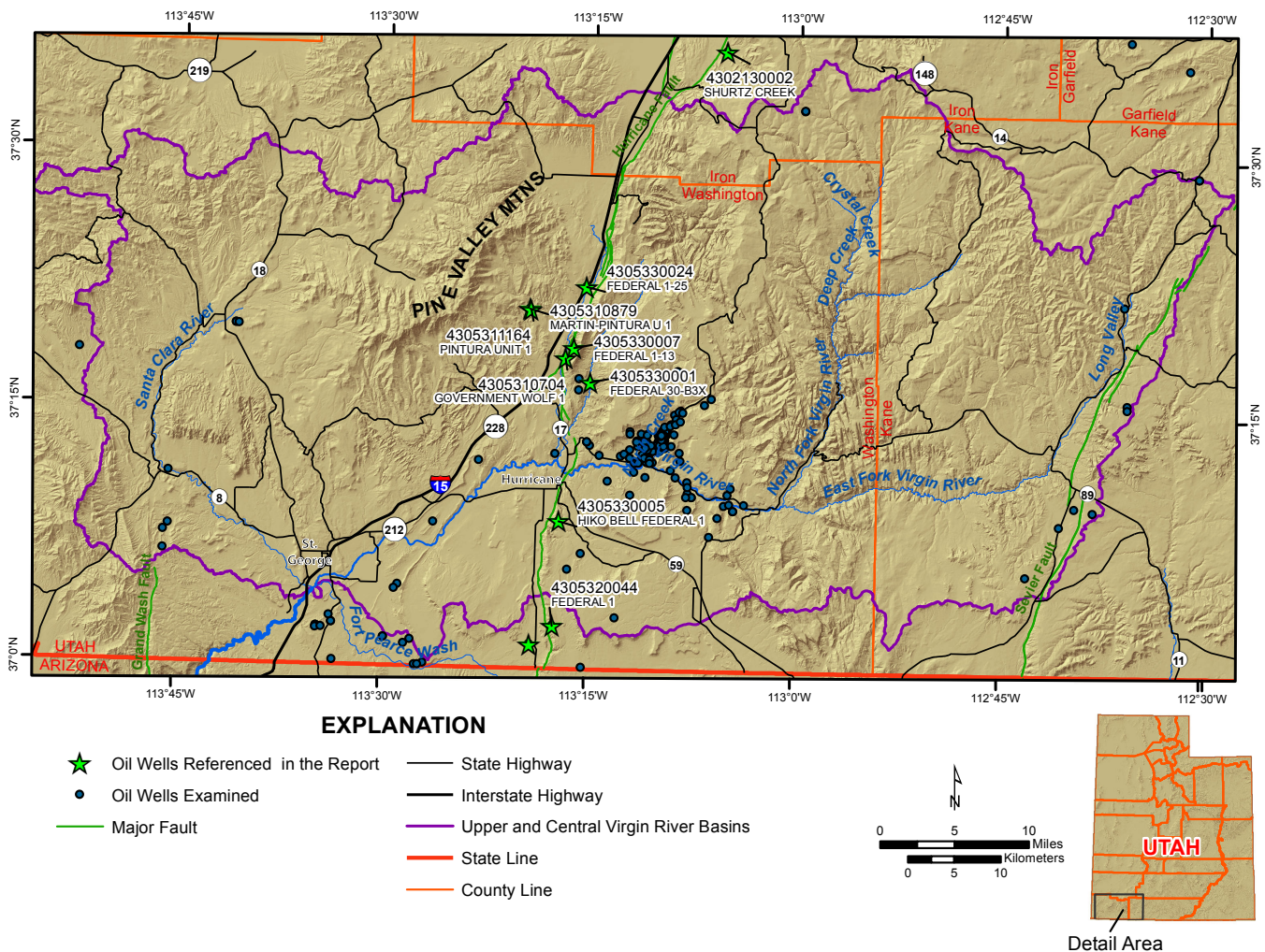

Figure 11. *Location of examined oil wells.*

Shurtz Creek: The Shurtz Creek well (API 4302130002) is located on the footwall of the Hurricane fault, just south of Cedar City (figure 11). The well has a total depth of 5996 feet. The driller noted Redwall Limestone at 5070 feet, Callville Formation at 4664 feet, Coconino Sandstone (likely Queantoweap Sandstone) at 2477 feet, Kaibab Formation at 746 feet, and the Toroweap Formation at 540 feet. The driller's record indicates water mist at 1543 feet and water pumped at 5100 feet. Water samples indicate that water at this depth likely contains around 4500 mg/L TDS, which is Class III (<10,000 and >3000 mg/L TDS) water according to the Utah Division of Water Quality (2011).

Devereux: The Devereux Corporation Federal 1 well (API 4305320044) is located on top of the Hurricane Cliffs, approximately 9 miles south of the town of Hurricane (figure 11). The well driller noted Coconino Sandstone at 996 feet below ground surface, Pakoon Dolomite at 2030 feet, and Redwall Limestone at 3130 feet. The driller reported some relatively fresh water at 2736 to 2754 feet below ground surface (in the Pakoon Dolomite) and a lot of relatively fresh water at 3292 to 3325 feet below ground surface (in the Redwall Limestone). The resistivity log plots groundwater level at 1214 feet.

Knowles-Skyline: The Intex S Penn USL Knowles-Skyline 1 well (API 4305310602) is west of the Devereux well, 9 miles south of Hurricane, in the hanging wall of the Hurricane fault (figure 11). The well driller's record reports the groundwater level at 940 feet below ground surface, the Toroweap Formation at 905 feet, Coconino Sandstone (Queantoweap Sandstone) at 1425 feet, and Pakoon Dolomite at 2745 feet. The record shows "important water sands" at 270 to 295 feet, 975 to 980 feet, 1225 to 1235 feet, and 2750 to 2940 feet below ground surface. Unfortunately, no information on water quality is provided.

Hiko Bell: The Hiko Bell Federal 1 well (API 4305330005) is 2 miles south of Hurricane, in the footwall of the Hurricane fault (figure 11). The driller's log reports Coconino Sandstone (Queantoweap Sandstone) at 1240 feet, Pakoon Dolomite at 2340 feet, Callville Limestone at 3320 feet, Mississippian-age rocks at 3490, Redwall Limestone at 3850 feet, and Cambrian rocks at 5090 feet below ground surface. The driller reported fresh water at 1240 to 2300 and 3510 feet below ground surface.

Buttes Federal: The Buttes Federal 30-B3X well (API 4305330001) was drilled along La Verkin Creek, north of Toquerville Springs, in the footwall of the Hurricane fault (figure 11). The well driller report lists Toroweap Formation at 552 feet, Coconino Sandstone at 1057 feet, Hermit Shale at 1230 feet, Queantoweap Sandstone at 1500 feet, Supai Group at 2280 feet, Callville Limestone at 3230 feet, Madison Limestone at 4203 feet, Redwall Limestone at 4500 feet, Devonian strata at 4688 feet, and Cambrian rocks at 5240 feet below ground surface. However, the Coconio Sandstone, Su-

pai Group, and Madison Limestone are generally formation names applied to units in Arizona, so the unit identification by the driller may be unreliable for this well.

Groundwater sample records are available at several depths for the Buttes Federal well. Because the driller collected these samples during the drilling process, they are likely contaminated by drilling fluids and may be unrepresentative of the reported sample depths. Although the sampling methodology is questionable, the data are the best available information we have and we use them as a general indicator of water quality in deep aquifers. Based on the water quality samples, the total dissolved solids are likely higher than acceptable levels for drinking water. The data indicate Class III water is present from 1000 to about 3000 feet below surface in the Queantoweap, (i.e., the C aquifer) and groundwater quality decreases with depth. Sodium and chloride ions account for most of the total dissolved solids.

Pease Willard: The Pease Willard Federal 1-13 well (API 4305330007) is located on the footwall of the Hurricane fault at the base of the Hurricane Cliffs, south of Pintura (figure 11). The well driller reported "slightly brackish" water at 523 to 540 and 579 to 612 feet below surface. The oil well log shows Pakoon Dolomite at the surface, Callville Limestone at 360 feet below surface, and Redwall Limestone below 1460 feet. The reported depths would put the slightly brackish water in the Pennsylvanian Callville Limestone.

McCulloch Government Wolf 1: The McCulloch Government Wolf 1 well (API 4305310704) is approximately 2 miles northeast of Anderson Junction (figure 11). Hurlow and Biek (2003) interpreted the well as being in the footwall of the Hurricane fault, but crossing several damage zones of the fault. Hurlow and Biek (2003) noted that the driller reported the Hurricane fault at 375 feet, the Redwall Limestone at 792 feet, Devonian formations at 1742 feet, another fault strand at 3375 feet, and Cambrian strata at 5315 feet below ground surface.

The driller sampled water quality for this well during drilling and the USGS reports the results in the NWIS database. The driller's record reports "very fresh" water at 400 to 1600 feet and "salty" water 4960 to 5002 feet below ground surface. The USGS measured the depth to water in this well as 765 feet below surface while the driller was drilling the well. The driller noted that the water likely emits through fractured carbonates, most likely the Callville and/or the Redwall Limestone.

In a letter to the mayor of Toquerville dated February 26, 1992, geologist S. B. Montgomery reported that the McCulloch Oil Corporation encountered water in the Pakoon Formation from 1200 to 1750 feet below ground surface while drilling the McCulloch Government Wolf 1 well (figure 11). Montgomery (1992) claimed that the most probable recharge area for the groundwater in the Pakoon Formation is the Kolob Terrace and the Markagunt Plateau.

Although the well was abandoned, the driller did not completely fill it with cement grout. However, the driller's record notes that grout was forced into the perforated intervals of the well casing in areas where the well was producing water. The driller also installed a significant surface plug.

Results and Discussion

Although the oil well drillers' logs provided little information in regards to groundwater elevation, there were some groundwater elevations available from water well drillers' logs and spring elevations. We have a few more points for groundwater levels in the C aquifer and very little information for the R aquifer.

Trends of Hydrogeologic Units

Our examination of geologic unit and groundwater elevations resulted in (1) a series of potentiometric-surface maps for the basin-fill aquifer (figure 12), Triassic aquifers (figure 13), C aquifer (figure 14), and R aquifer (figure 15); (2) structure contour maps for the Chinle Formation (figure 16), Kaibab

Figure 12. Potentiometric surface of the basin-fill aquifer in the I-15 corridor area.

Formation (figure 17), Queantoweap Sandstone (figure 18), and Redwall Limestone (figure 19); and (3) a conceptual hydrostratigraphic cross section of the footwall of the Hurricane fault (figure 20). Potentiometric-surface maps provide the elevation of the groundwater level, which in turn allows for an estimate of depth to groundwater. Structure contour maps provide the approximate elevation of the geologic formation tops, which allows for determining the approximate depth to water-bearing formations.

Basin-fill units: Several disconnected basin-fill units exist throughout the field area. The most important areas to mention for this study are the New Harmony basin and I-15 corridor. The basin-fill sediments include both unconsolidated Quaternary units and older consolidated Tertiary units. Heilweil and others (2000) described the potentiometric surface in the New Harmony basin. Based on available groundwater-level data from wells in the I-15 corridor, groundwater moves from the New Harmony basin and the Pine Valley Mountains and follows the corridor south (figure 12). In the I-15 corridor, groundwater is likely flowing through a combination of basin-fill material, fractured basalt, and Navajo Sandstone. Evidence for this connection is that adjacent wells in differing units show water levels within 10 feet of each other. Groundwater may be moving into the basin-fill sediments in the I-15 corridor via the fractured carbonates in the footwall of the Hurricane fault to the east (Hurlow, 1998).

Cretaceous units: Previous workers (Cordova and others, 1972; Cordova, 1981; Hurlow, 1998; Heilweil and others, 2000) made little mention of the Iron Springs Formation and similar Cretaceous-age units, mainly because there are few areas where these units are viable aquifers. Cretaceous strata surround the flanks of the Pine Valley Mountains and are contained on the Markagunt Plateau. Groundwater levels in these units are generally perched and higher than the stratigraphically underlying units.

Jurassic units: Heilweil and others (2000) created an accurate and detailed potentiometric-surface map of the hanging wall of the Hurricane fault. There may be some flow from/to the Jurassic in the area of the I-15 corridor, where the Jurassic formations are below the ground surface (Hurlow, 1998).

Little is known of potentiometric surfaces in the Jurassic formations in the footwall of the Hurricane fault, primarily because the Jurassic units sit much higher on the footwall than on the hanging wall. The Jurassic units are highly dissected by streams on the footwall and therefore outcrops are discontinuous. Groundwater flows from the northeast to the southwest, roughly following the surface topography and flow of the Virgin River.

Gates (1965) examined several springs, test holes, and wells near the east entrance of Zion National Park, and noted that the Navajo Sandstone contains several small, perched areas of
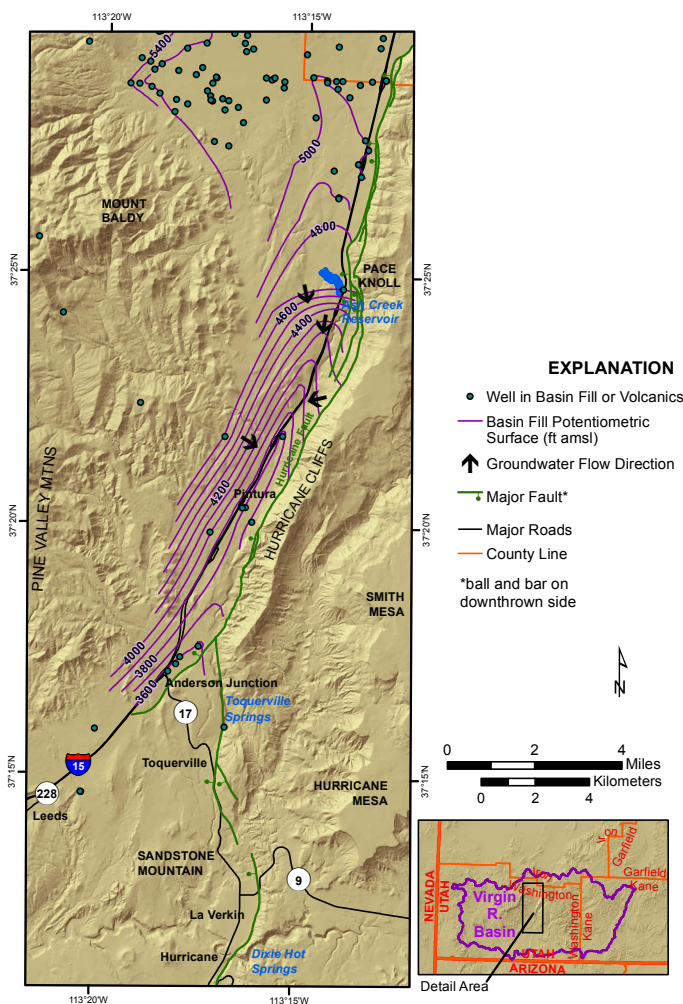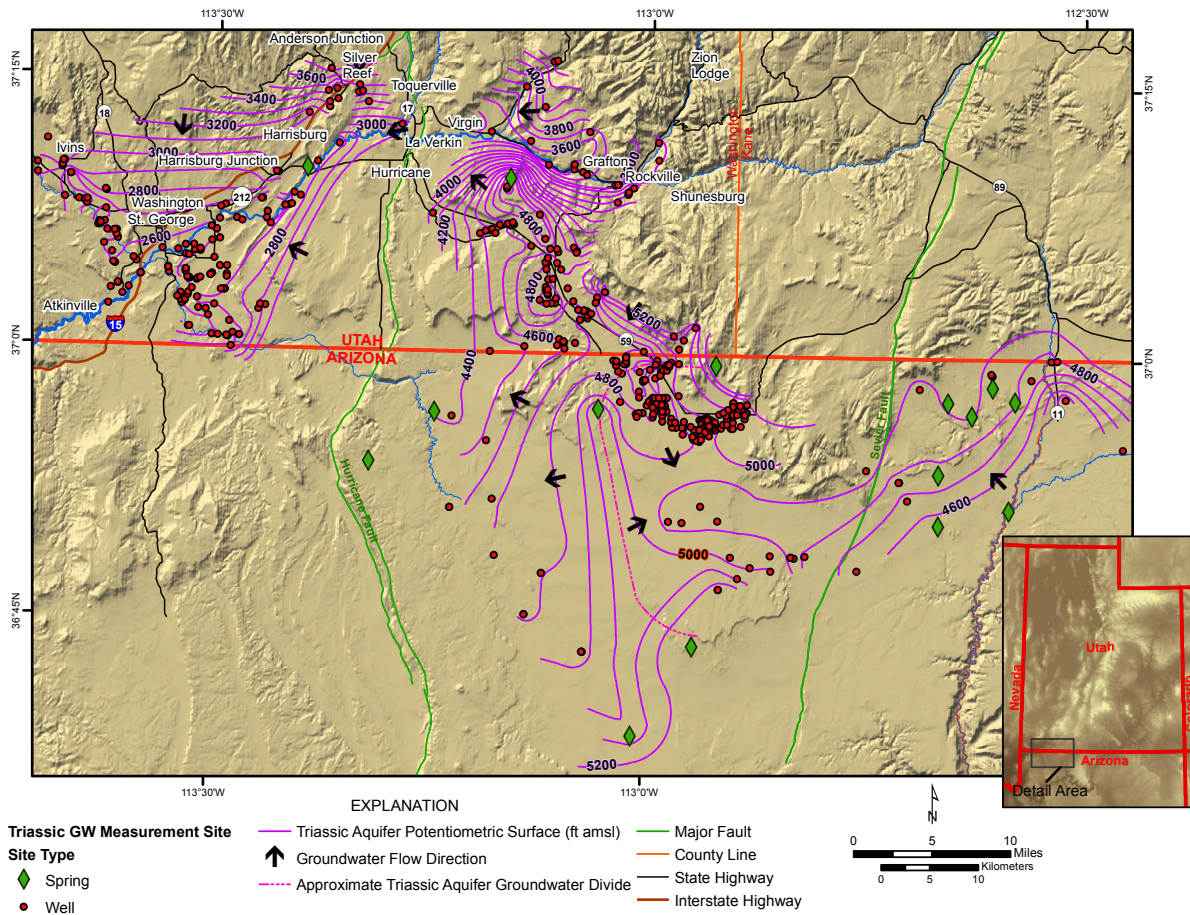
Figure 13. *Approximate potentiometric surface map for the Triassic aquifers.*

saturation, created by local precipitation collecting on top of discontinuous fine-grained intervals. Gates (1965) noted that one well near the east entrance had a static water level of 4830 feet above mean sea level (865 feet below ground surface).

Christensen and others (2005) examined the seepage from the Navajo Sandstone into the Virgin River. They determined that total water discharge from the Navajo Sandstone ranges seasonally from 50 to 91 cubic feet per second, which comprises a majority of the base flows for the East and North Forks of the Virgin River.

Triassic units: The groundwater divide in the Triassic aquifers is approximately midway between the Hurricane and Sevier faults, south of the Utah-Arizona state line (figure 13). West of the divide, the groundwater in the Triassic units flows toward the Virgin River. These units are discontinuous south of the Utah-Arizona state line on the hanging-wall side of the Hurricane fault. Paleozoic rocks are exposed by folds and erosion in the footwall of the Hurricane fault in the study area, indicating that the overlying Triassic units are fairly discontinuous across the fault as well (figure 16). The Virgin anticline

also splits the Triassic units in the area east of St. George in the hanging wall of the Hurricane fault (figure 16). The fine-grained nature and gypsum mineralization of the Moenkopi Formation likely seal the Hurricane fault from groundwater flow where these units are present. Flow between the Triassic units of the footwall and hanging wall of the Hurricane fault is likely negligible because they are separated by several thousands of feet of throw along the fault.

C aquifer: In the southern part of the area, near the Colorado River, the potentiometric surface of the C aquifer (figure 14) is higher than, and likely perched above, the R aquifer potentiometric surface (figure 15). Many workers (Huntoon, 1970; Ross, 2005; Alpine, 2010) distinguish the C and R aquifers to the south, near the Colorado River. However, in the north, near the I-15 corridor, the facies and lithology are different from the Supai Group to the south, and fractures from the Hurricane fault and Sevier folds may provide hydrologic connection between the two aquifers. The C and R aquifer systems are likely hydraulically connected Paleozoic sandstone and limestone. However, groundwater-level elevation data for both the C and R aquifer are sparse and do not
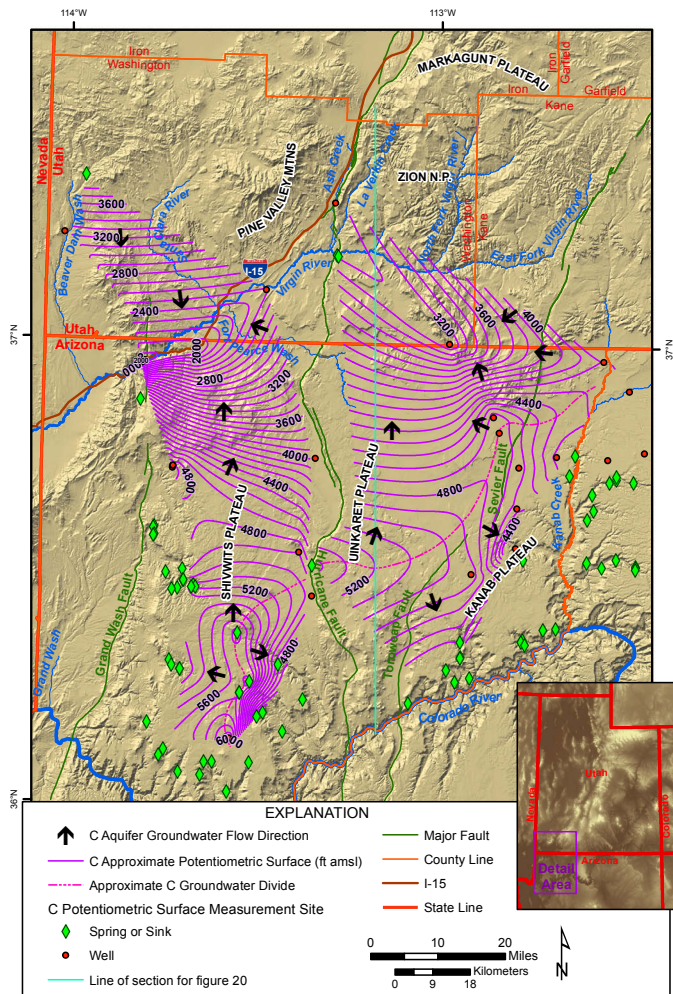
Figure 14. Potentiometric surface map for the C aquifer.

Figure 15. Potentiometric surface map for the R aquifer.

provide adequate evidence in the I-15 corridor area to support the connection.

The Kaibab Formation (figure 17) and Queantoweap Sandstone (figure 18) of the C aquifer are closest to the surface in Utah in the footwall of the Hurricane fault nearest to the fault. On the hanging wall, high points are near the crest of the Virgin anticline and to the southeast, near the Utah-Arizona state line (figures 15 and 16).

R (Redwall/Muav) aquifer: This cavernous and fractured limestone aquifer likely covers a massive areal extent, but is deep in most parts of Utah (figure 19). Based on several descriptions from oil well drillers and two water quality analyses, the quality of water from this aquifer can range from potable to saline in the Utah region. There are some very minor oil shows in several oil wells that penetrate this formation in Utah. High total dissolved solids are likely present in the R aquifer in southwestern Utah. This unit is a good candidate for fault-enhanced fluid flow. Due to its high mechanical competency, fault-induced fractures propagate more readily in this material than in more ductile units such as shale. This unit is

present in the subsurface on both sides of the Hurricane fault and is thick and fairly continuous (figure 19), increasing the probability of hydraulic connectivity to adjacent units where not obstructed by fault gouge and clay smear. Offset on the Hurricane fault is significant enough to make the R carbonate sequences discontinuous across the fault, but there still may be minor hydraulic connection through the fractures.

The potentiometric-surface map of the R aquifer (figure 15) is based on limited groundwater level information on either side of the Hurricane fault zone. For the displayed potentiometric-surface contours, we assume the cavernous and highly fractured Redwall and Muav limestones are well connected. We also assume that the McCulloch oil well has a representative groundwater level, as the USGS notes that the McCulloch well was completed in the C aquifer, and the USGS recorded the groundwater level during well drilling.

Potentiometric-surface lines (figure 15) indicate that groundwater flow in this aquifer roughly follows topography. Even at its great depth, there appears to be a groundwater divide in northern Arizona, north of the Grand Canyon. Based on
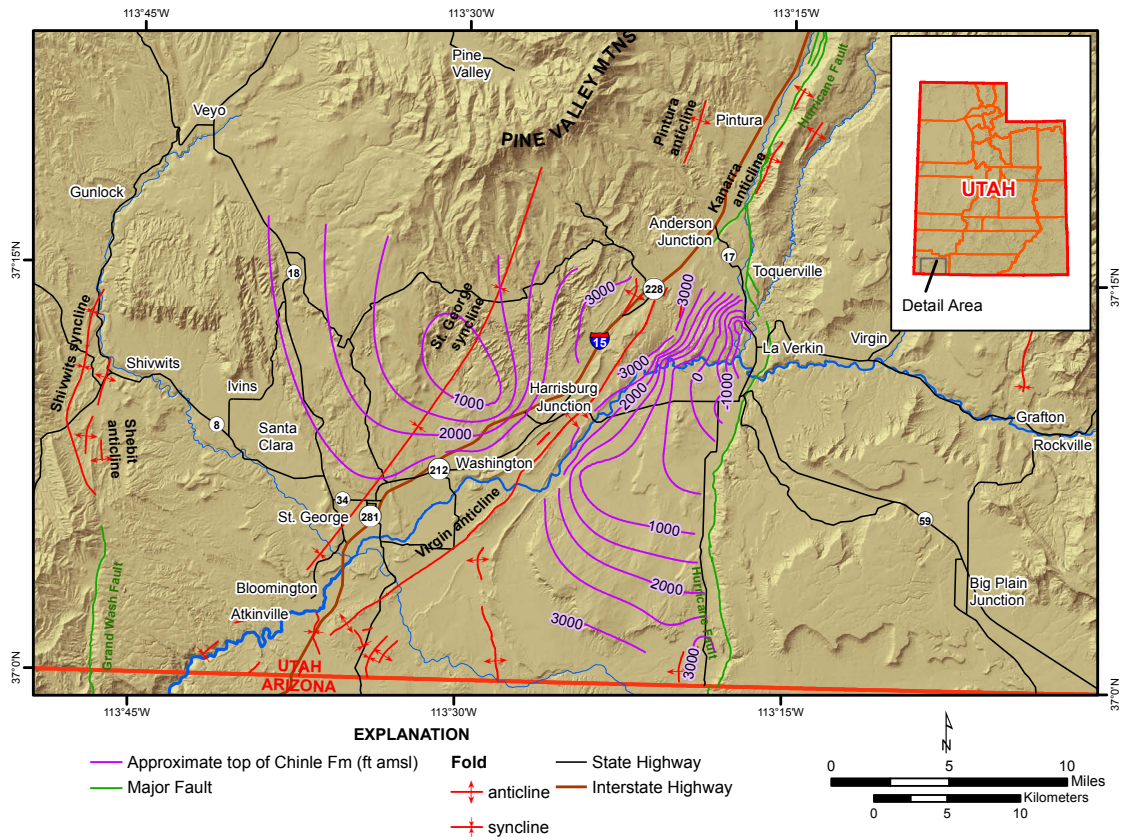
Figure 16. *Approximate structure contours for the top of the Triassic Chinle Formation.*
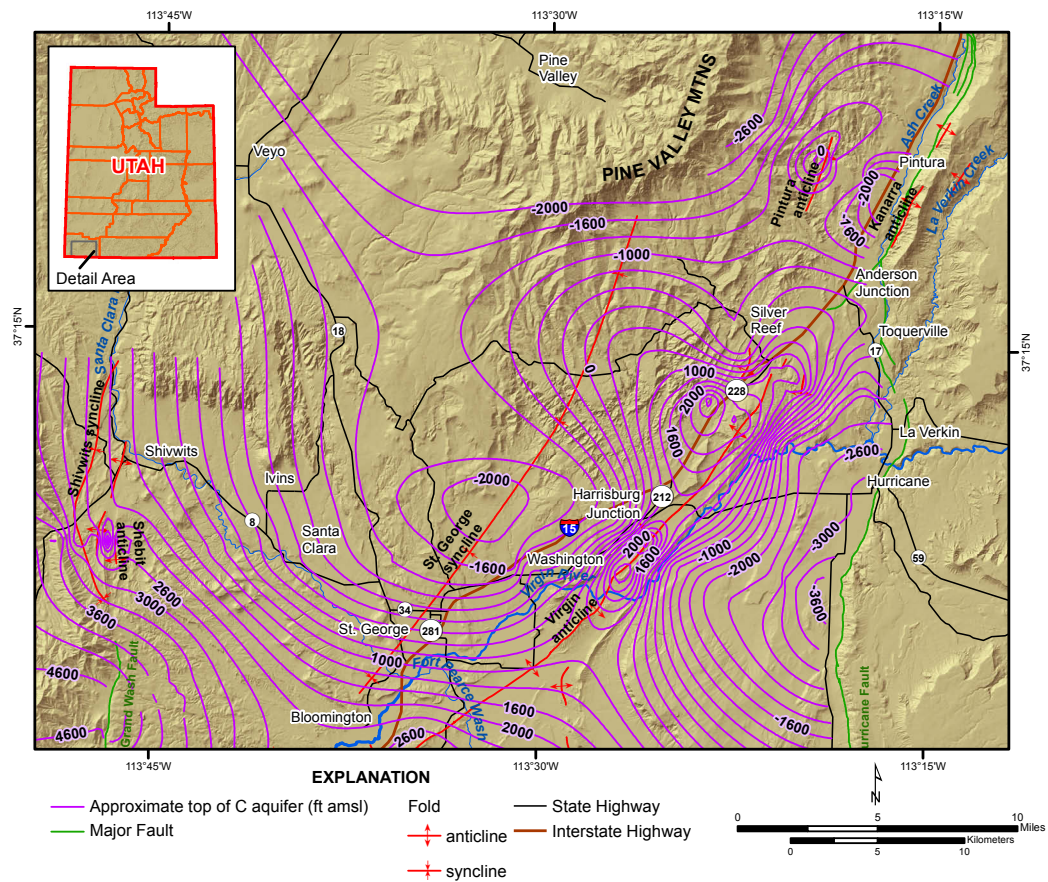
Figure 17. *Approximate structure contours for the top of the Permian Kaibab Formation, which marks the top of the C aquifer.*
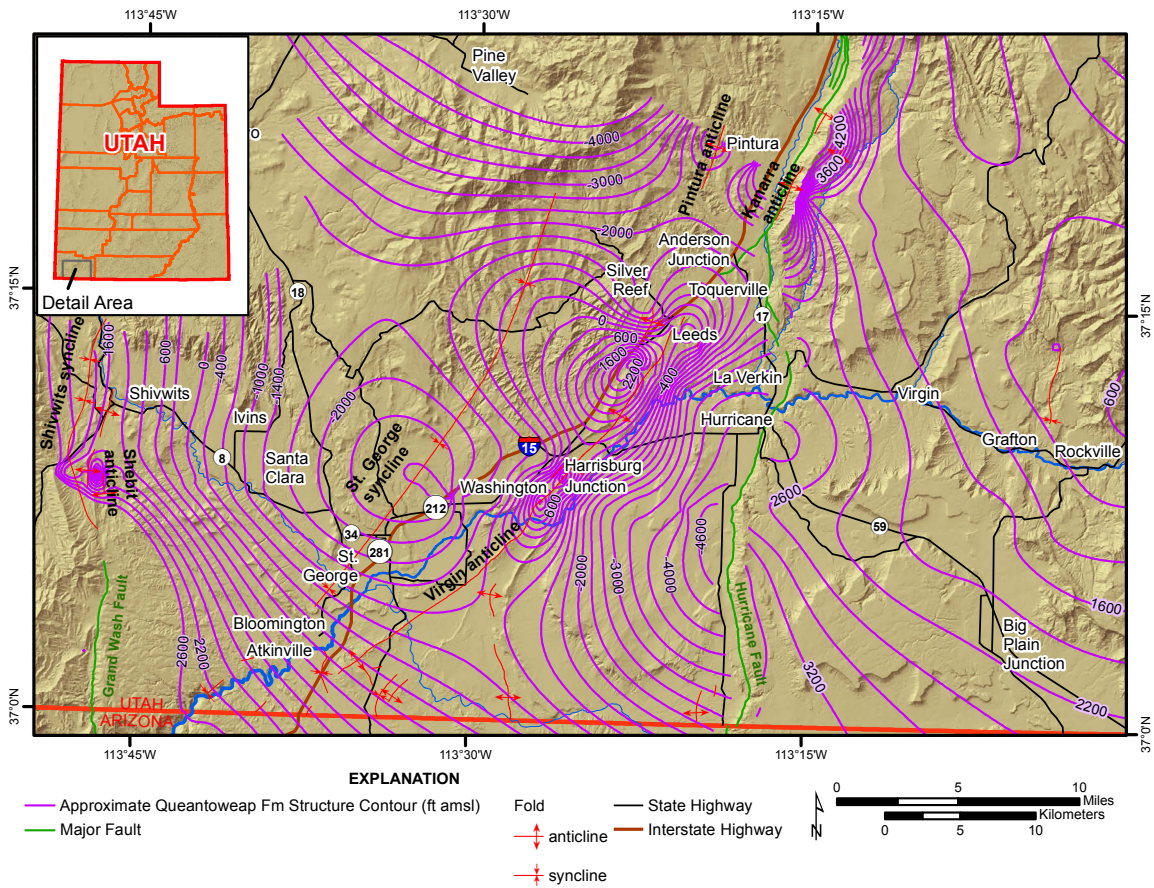
Figure 18. *Approximate structure contours of the top of the Permian Queantoweap Sandstone.*

Figure 19. *Approximate structure contours for the top of the Mississippian Redwall Limestone, which marks the top of the R aquifer in this area.*

Figure 20. *Hydrostratigraphic cross section of the footwall of the Hurricane fault, showing the approximate tops of major aquifer systems and the potentiometric surface of the C aquifer. See figure 14 for the line of cross section.*

available groundwater levels in the west, along the Virgin River, near the Utah-Arizona state line, there is a relatively low potentiom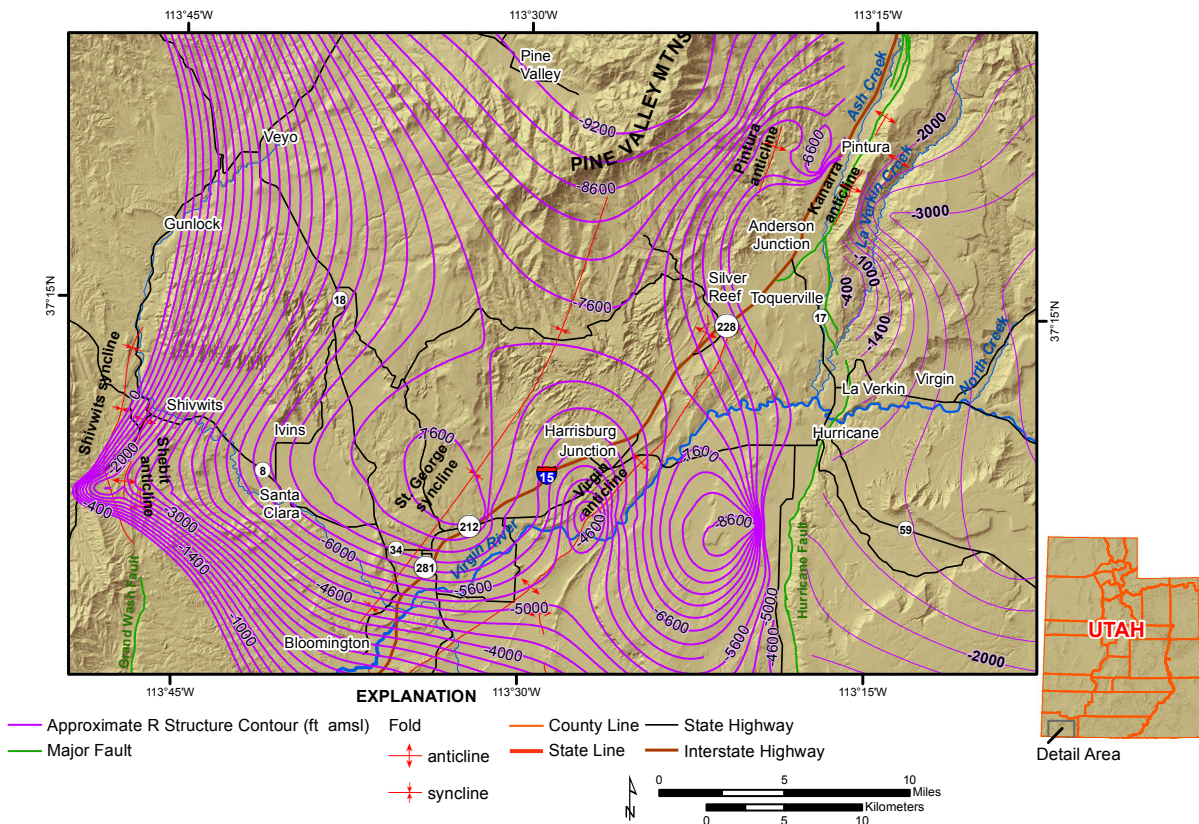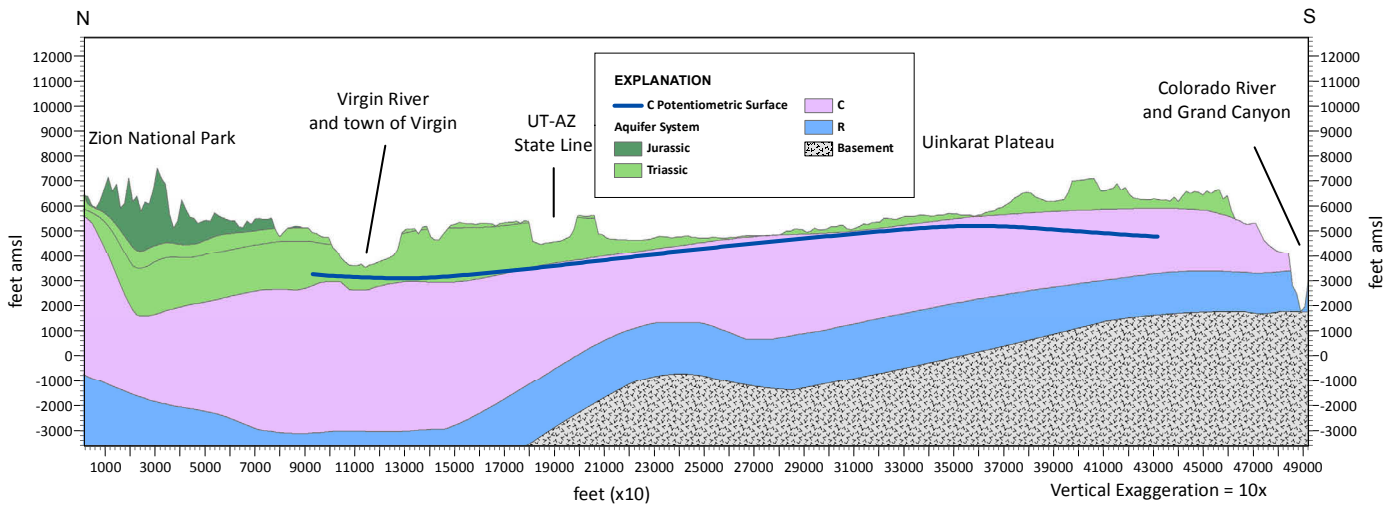etric surface near the Virgin River. The low point in potentiometric surface could indicate a zone of discharge from the R aquifer into overlying hydrologic units. Evidence for this includes the high temperature and total dissolved solid zones identified by Heilweil and others (2000). Fracturing associated with the Virgin anticline and extensional faults in the area could enhance discharge from this unit. The water-level elevation from the McCulloch Government Wolf 1 well (API 4305310704) of 3060 feet above mean sea level is also good evidence that groundwater levels increase to the north of the Virgin River (figure 15).

I-15 Corridor Area

In the aquifers where data are available and sufficient for near-fault interpretation, potentiometric-surface lines bend and become parallel to the Hurricane fault (figure 12; Heilweil and others, 2000, figure 20a and plate 2), which may indicate that the fault does not act as a barrier, because the lines are not perpendicular to the fault strike. However, the bends in the lines are west of the fault, inferred, and minor.

Large spring flows found east of the Kanab Plateau on the north side of the Colorado River may suggest that the groundwater recharge area for these springs is expansive enough to intersect the Virgin River basin. Regionally, however, flow in the C (figure 14) and R (figure 15) aquifers does not appear to move from the I-15 corridor towards the Grand Canyon. No significant springs issue from the R aquifer along the Hurricane fault (figure 15). Neither Johnson and Sanderson (1968) nor Grand Canyon Wildlands Council, Inc. (2001) show very large springs issuing from the north rim of the Grand Canyon in the Hurricane-Timpoweap (HT) block (Ross, 2005). Alpine (2010) presents a potential divide in the HT block for the R aquifer (figure 9). Furthermore, flow

to the Grand Canyon from the I-15 corridor region would be opposite of the dominant direction of dip of the geologic units in the area. Thus, there is no evidence that the Virgin River basin provides intrabasinal groundwater flow to the Grand Canyon.

Regarding flow along the damage zone of the Hurricane fault, the fault is extremely complex, having many bends and separate segments (Lund and others, 2007). Although the Hurricane fault, due to its displacement and length, is likely a good candidate for aquifer connectivity and recharge by infiltration to deep hydrogeologic units (Gettings and Bultman, 2006), it seems improbable that the damage zone is highly connected over the entire approximately 80-mile distance between the I-15 corridor and the Grand Canyon west of Mt. Trumbull, where the Hurricane fault intersects the wall of the Grand Canyon north rim. Minor and Hudson (2006) described impediments, such as mineralization and igneous intrusions, that preclude such extensive flow along faults.

Wells of Interest

The Reber (2003) recommendations for well drilling and development near the Conde oil well are in general agreement with interpretations of water-bearing units outlined by Hurlow (1998) and Biek and others (2009). If Reber is correct, and the source aquifer units are older consolidated alluvial deposits, then the aquifer may not be conducive to production, due to a relatively low transmissivity (Hurlow, 1998). However, greater transmissivity may have been induced by deformation from Basin and Range extensional faulting. Due to faulting, igneous intrusion, and volcanism, the area of the Conde well is geologically very complex, meaning that the "yellow sand" encountered by the driller could even be Navajo Sandstone, as is common in the subsurface just south of the well (Hurlow, 1998). If drilling at

the Conde site, one would likely need to drill through a significant thickness of basalt in which loss of circulation of drilling fluids may be an issue. Based on the potentiometric surface created using information from surrounding wells, the depth to water is likely shallower than the value that the well driller cited. In summary, the Conde site is likely a good site to find water, but a well at this site would likely be tapping into an existing, common source for groundwater (the Quaternary basin-fill aquifer), as outlined by Hurlow (1998).

The Government Wolf 1 well (API 4305310704) appears to have produced small quantities of potable drinking water from the C and R aquifers. Based on the well driller's abandonment notes, this well would not be a good candidate for refurbishment. The driller reported that the well produced approximately 500 gallons per hour during drilling in the C aquifer. This may be an insufficient quantity of water for a municipal source. Also, pumping water from a depth of 400 feet (or greater) could incur significant pumping costs.

Based on water chemistry samples from the Federal 30-B3X well (API 4305330001), salinity increases with depth. The potable and brine water interface appears to be near 2000 feet below land surface. The potable water derived from this well is most likely from the Queantoweap Sandstone (figure 18), indicating that the Queantoweap Sandstone is a potential aquifer near the Federal 30-B3X well.

GRAVITY SURVEY

Introduction

Gravity interpretations and modeling provide insight into the structure and distribution of geologic formations or earth materials in the subsurface. The hanging wall of the Hurricane fault in the I-15 corridor region is a highly geologically complex area. Gravity measurements help verify and clarify existing geological interpretations of the I-15 corridor area, and in turn, allow us to better understand the hydrogeologic conditions of the area.

Regional gravity studies can help identify large-scale features, while smaller, higher resolution surveys, such as the one conducted for this study, help add important details. Cook and Hardman (1967) conducted a regional gravity survey along the Hurricane fault in the study area. The Pan American Center for Earth and Environmental Studies (PACES) database includes the data Cook and Hardman (1967) collected. Biek and others' (2009) interpretations that the Virgin and Kanarra anticlines are two separate Laramide structures likely separated by a syncline clarified the Cook and Hardman (1967) interpretation that the Virgin and the Kanarra anticlines are the same Laramide fold, offset and divided by the Hurricane fault.

Blank and Kucks (1989) compiled and contoured aeromagnetic and gravity data for a large area that includes the area of this study. They made no specific interpretations of the structures we examined for this study.

Methods

We conducted a gravity survey along the I-15 corridor to better understand the subsurface geology of the area. Using ArcGIS (ESRI, 2011), we located a series of gridded, semi-evenly spaced data-collection points (figure 21) on aerial photographs. When establishing the point locations, we attempted to maintain a square, grid-like pattern, while also locating the points along existing trails and roads to facilitate data acquisition.

We collected and processed the gravity data following standard methods (for example, Telford and others, 1976). In addition to subsurface variations in density that reflect geologic structure, raw gravity measurements include the effects of earth tides,
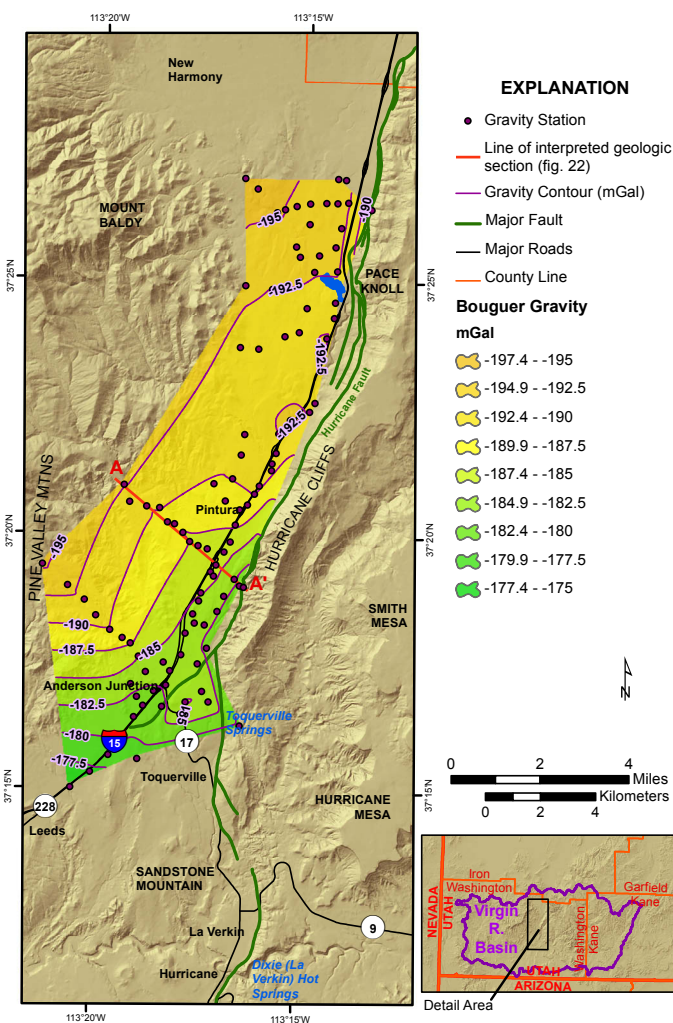
Figure 21. *Gravity measurement stations and the resulting gravity interpolation from the data collected for this study.*

latitude, elevation, topography, and instrument drift (e.g., Telford and others, 1976; Milsom, 1996; Parasnis, 1997). Corrections for the non-geologic components of gravity measurements are well established and the corrected gravity value is referred to as the Bouguer gravity anomaly, expressed in units of milligals. The Bouguer anomaly reflects variations in gravity relative to a standard reference plane, typically sea level. Appendix A contains the gravity data (table A1) and equations used in calculating the necessary corrections.

We compiled gravity information from the PACES database, and used the data that we collected to supplement and enhance the resolution of the existing PACES data. Plotting the gravity values as a function of the y-direction coordinates indicates that there is a 1.3 mGal decrease per mile in the direction of north. This regional trend estimate is similar to the 1.5 mGal per mile trend mentioned by Cook and Hardman (1986). We did not adjust for the regional trend and present only the Bouguer gravity interpolations.

We interpolated the gravity values of the combined data using ArcGIS (ESRI, 2010) and then contoured the resulting interpolation. We trimmed the edges of the contoured area to eliminate edge boundary effects of the interpolation and examined the contours for consistency. We compared our contours to existing contour sets to check for differences in trends or outliers. We also used these same methods to interpolate and contour only the data we collected (figure 21). Our data have a higher point density, which results in a higher resolution interpolation.

The GM-SYS software modeled a cross section through the area south of Pintura (figures 21 and 22). The GM-SYS software calculates the Bouguer gravity anomaly of a geologic model and compares it to the observed values, which allows the construction of a model that accurately depicts the observed Bouguer anomaly. We used the cross section from the Pintura 1:24,000-scale geologic quadrangle map (Hurlow and Biek, 2003) as the foundation of our interpretation. Then we adjusted the various layer thicknesses and densities to match the measured gravity signal.

Results and Discussion

The resulting gravity interpolation (figure 23) clearly displays the major geologic features in the region, especially the Hurricane fault and the Virgin anticline. There is a clear depression in the gravity data south of Ash Creek Reservoir in the I-15 corridor, which likely represents local accumulations of low-density basin fill in the hanging wall of the Hurricane fault due to fault displacement. Another interesting anomaly is east of Anderson Junction, just west of the main strand of the Hurricane fault (figure 21). A splay of the Hurricane fault near the boundary of the Ash Creek and Anderson Junction segments of the fault is probably creating differential offset in that location.
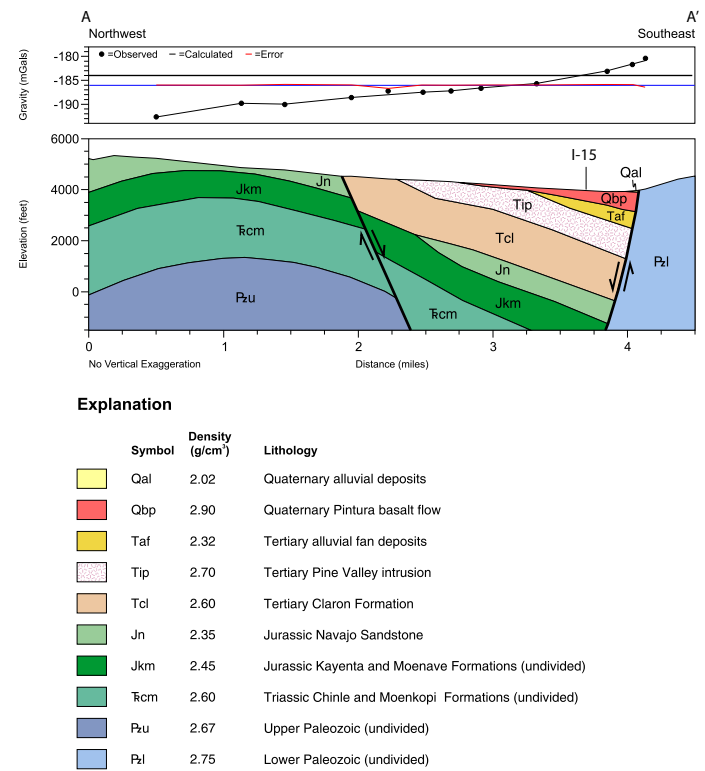
Figure 22. Modeled geologic cross section of the Pintura area. Figure 19 displays the location of this section in map view.

The regional gravity interpolation (figure 23) does not provide enough information to distinguish the Virgin and Kanarra anticlines as two separate folds. However, there is a low-density area to the east of the Virgin anticline, which may represent a syncline or a density gradient created from offset of stratigraphic units by the Hurricane fault.

The gravity-based geologic model also displays the major geologic features along the I-15 corridor in the Pintura area (figure 21). The model depicts the Pintura anticline, the Hurricane fault, and a smaller subsidiary fault. The gravity model confirms cross-section A–A' from Biek and Hurlow (2003), except our model suggests a much thinner Navajo Sandstone beneath the I-15 corridor.

Interpretations of the gravity data provide some insight into the I-15 corridor groundwater system. Interpolation of the data collected during this study indicates a relatively large accumulation of basin-fill sediment south of Ash Creek, which could provide a satisfactory amount of groundwater. The detailed gravity map also supports Biek and others' (2009) interpretations of the fault splays east of Anderson Junction, which could influence groundwater flow. The modeled cross section helps verify the suspected dip and location of the fault, to better constrain the drilling depth required to penetrate the Hurricane fault damage zone.
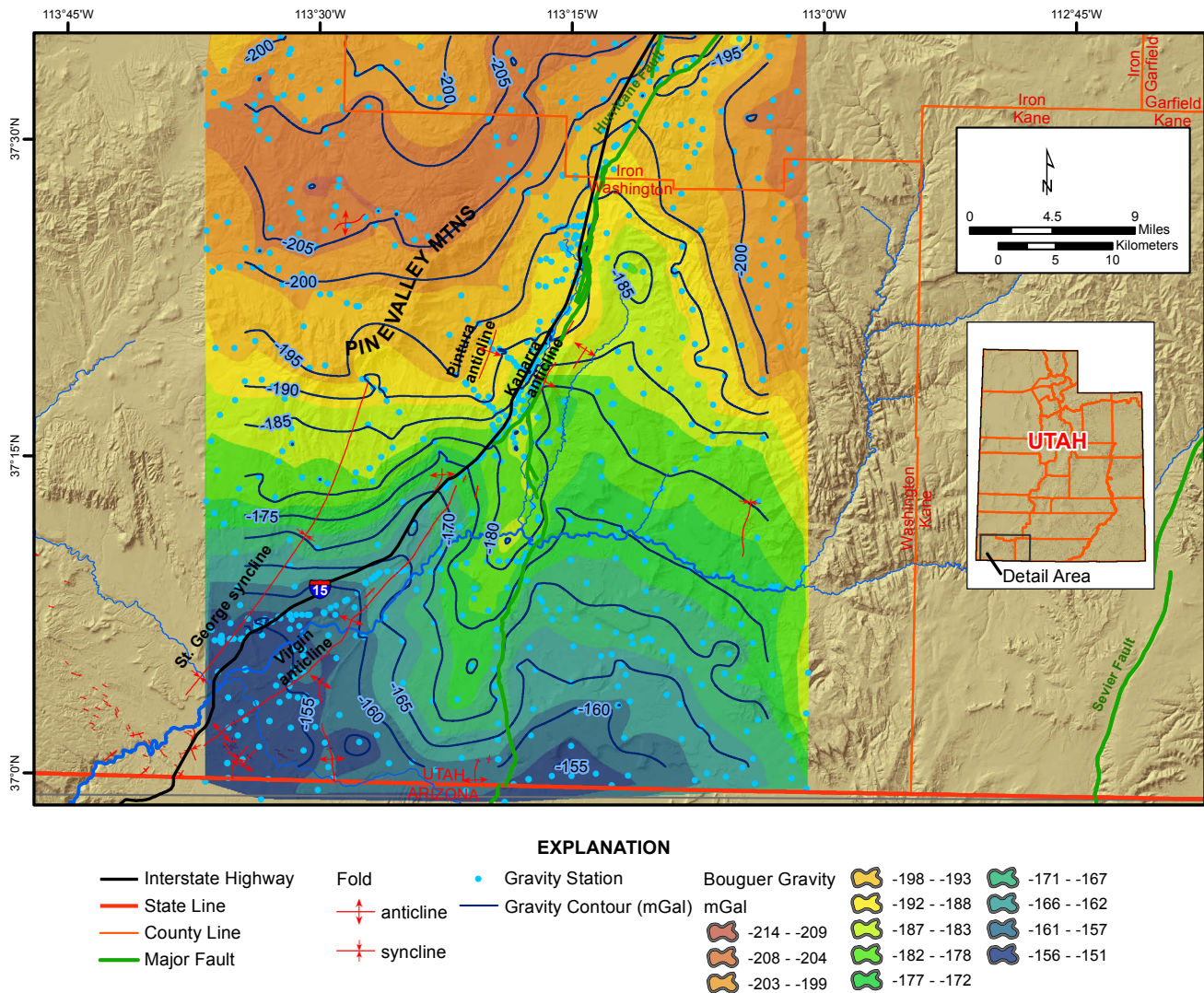
Figure 23. *Bouguer gravity interpolation of PACES data combined with data from this study.*

FRACTURE PATTERNS AND STRUCTURAL CONSIDERATIONS

Introduction

The two main factors controlling groundwater flow in the area of the Hurricane fault are geologic structures, such as faults and folds, and fractures related to those structures.

Fractures

Knowledge of where water travels and how it infiltrates is key to understanding groundwater resources. Hurlow (1998) examined fracture orientation and density of the Navajo Sandstone. Although the Navajo is not the major unit of interest for this study, fracture density and orientation within this surface unit can be indicative of the greater regional stress regime, as some fractures are through-going to other geologic units. One can assume that deeper units have undergone similar stresses,

and therefore, similar deformation (Gettings and Bultman, 2005).

Gettings and Bultman (2005) conducted a penetrative fracture mapping study south of Washington County, in northwestern Arizona. They analyzed various remote sensing data sets using computer vision technology. Computer vision automatically detects areas of maximum gradient in images and matches lines to them. Using computer vision to detect lineaments is advantageous because it limits bias and allows for repeatability of results (Gettings and Bultman, 2005). We attempted to apply a similar remote-sensing-based methodology to better understand groundwater flow.

Approximation of Damage Zone Fracture Density

Several authors (Scholz and Cowie, 1990; Shipton and Cowie, 2001; Bernard and others, 2002; Faulkner and others, 2011; Savage and Brodsky, 2011) have noted an empirical power

law relationship of fault displacement and damage zone fracture density:

$$d = c \, r^{-n} \qquad (1)$$

where:

d =   fracture density

c =   fault constant

r =   distance from fault

n =   decay exponent

The fault constant and decay exponent have been constrained as a function of fault displacement through the examination of thousands of fault measurements, including many measurements from large extensional faults in Utah (Shipton and Cowie, 2001; Savage and Brodsky, 2011).

We can apply the power law to the dimensions of the Hurricane fault to estimate the extent of its damage zone and distribution of fracture density around the fault and its strands. This estimation technique is necessary because many areas along the Hurricane fault are covered by alluvium or inaccessible, making the distribution of fractures difficult to estimate. Dutson (2005) measured fracture distribution at a well-exposed location, where the Virgin River intersects the Hurricane fault. We compared results of our fracture distribution estimate to Dutson's (2005) work to judge the validity of the estimates.

Structure and Fluid Flow

Caine and others (1996) documented the basic structure of faults, delineating the host rock from a fractured damage zone and an impermeable core. Several authors (Braathen and others, 2009; Bastesen and others, 2009; Bastesen and Braathen, 2010) studied how bends and fault windows can create holes in fault cores, allowing for water to cross otherwise impermeable extensional fault boundaries. Bastesen and Braathen (2010) also noted that extensional faults having offset greater than 150 feet typically have relatively thin fault cores (less than 2 feet), and in some areas have displacement that exceeds the potential for clay smearing. Of the 20 high-displacement extensional fault cores that Bastesen and Braathen (2010) examined, more than half (56%) were composed of permeable carbonate breccia. They also pointed out that fault relays and bends (in map view) can significantly increase the occurrence and size of damage zones and fault windows.

Groundwater flow through fractures is primarily controlled by density, unfilled aperture, roughness, geometry, and connectivity of the fracture system (Singhal and Gupta, 2010). A well-connected and dense fracture network having many open apertures will be more conducive to fluid flow than a sparse, poorly connected network of filled and closed fractures.

Fracture density, as outlined above, is related to fault offset and lithology. The primary units of interest for this study are carbonates and possibly sandstones. Both of these rock types are generally highly competent and therefore will have relatively higher fracture densities than fine-grained rock or unconsolidated materials.

Fracture aperture and geometry are functions of the regional stresses that create the structures associated with the fractures. The two types of fracture sets generally associated with faults and folds are oblique conjugate shear fractures and orthogonal extensional fractures. The shear fractures are generally considered not conducive to groundwater flow, owing to smaller and tighter apertures. Shear fractures generally do not form parallel to the dominant structure axis, and they form in sets separated by an angle of approximately 60 degrees. Extensional fractures are generally parallel or perpendicular to the main structure axis, have open apertures relative to shear fractures, and form in sets separated by an angle of approximately 90 degrees. Mineralization, infilling by fine-grained sediments, and heat expansion of the fractured rock can decrease the effective fault aperture, in turn reducing permeability. Hydraulic fracture connectivity is a function of the geometric distribution of fracture-forming faults and folds and the permeability structure of the fault (figure 24).

Methods

For this study, we attempted to detect linear features in several different remotely sensed data sets. We also examined the structure of the Hurricane fault and attempted to approximate the size of the damage zone.

Structural Trends Methods

Fault and fold traces: We collected fold-axis and fault strikes from measurements on the St. George (Biek and others, 2009) and Kanab (Doelling, 2008) 1:100,000-scale geologic maps. We used ArcGIS (ESRI, 2010) to accurately measure the orientation of major faults and folds in the vicinity of the I-15 corridor region. We parsed the shapefiles of the structures into individual line segments and used the coordinates of the endpoints of the line segments to determine the attitude of each line segment. We compiled the attitudes into rose diagrams and computed circular statistics of the features using the computer software Oriana (Kovach Computing Services, 2011).

Manually recognized lineaments: We also manually traced lineaments (figures 25 and 26) in some areas using ArcGIS (ESRI, 2010). We created a shapefile of smaller-scale lines by tracing observable natural linear features from 1-foot resolution aerial photographs. We created a similar regional-scale lineament shapefile by tracing observable lineaments from DEMs, side-looking radar imagery, and Landsat
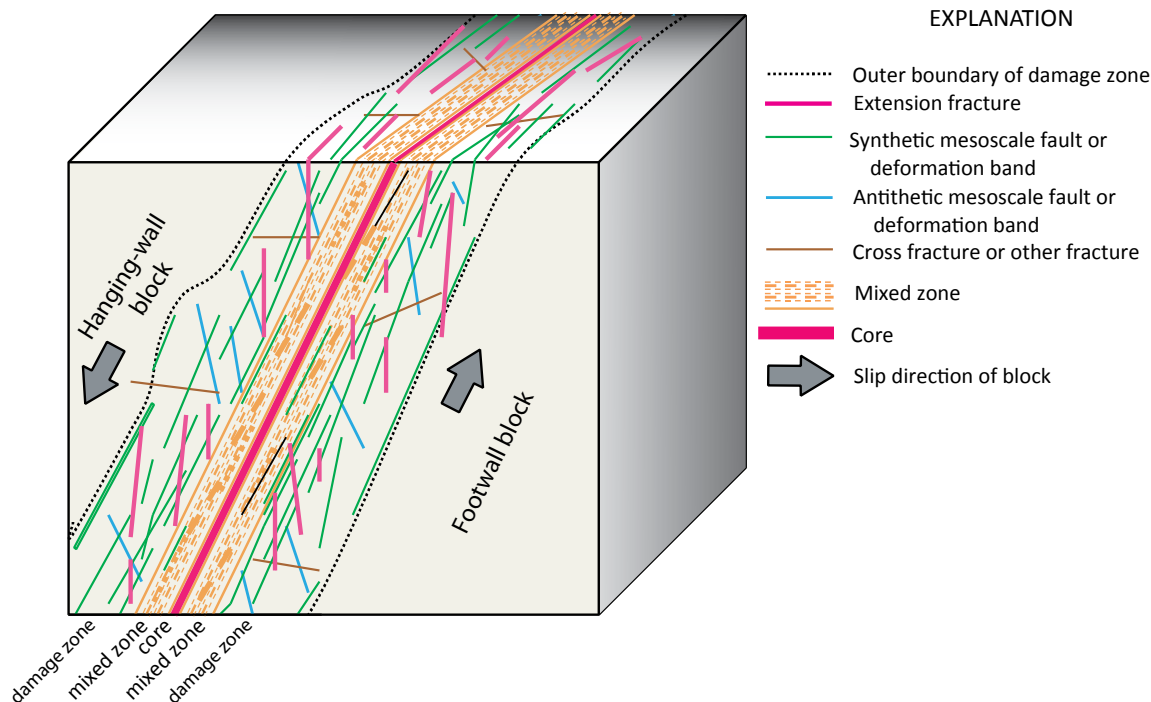
Figure 24. *Generalized extensional fault structure, modified from Minor and Hudson (2006). The fault structure is made up of the core, a mixed zone of gouge and fractured material, and the damage zone.*

thematic mapper imagery. We then determined the attitude of each line in the shapefiles and created rose diagrams of the line orientations.

Automatically recognized lineaments: In an attempt to avoid possible bias created from manual lineament tracing, we also tried to detect lineaments using automated techniques. The methods to automatically detect lineaments for this study are similar to the methodology outlined by Gettings and Bultman (2005). Lineaments follow areas of high contrast, which are areas where the gradient in a surface is high. Gettings and Bultman (2005) detected edges using the first and second derivatives of the surface to find local regions of the maximum gradient. We used Canny and Sobel image filters (Abarca, 2006) to approximate the first and second derivatives of images to find local maximums of image gradients. A Hough transform then analyzed the filtered image by applying lines to the traces of the regions of high gradient. We created a shapefile of automatically recognized regional lineaments using elevation imagery (DEM derived lineaments), side-looking radar imagery (SLR derived lineaments), and Landsat thematic mapper imagery (TM derived lineaments), as well as rose diagrams of the line orientations and density maps of the fractures (figure 27).

Damage Zone Approximation Methods

We applied the power law equation (equation 1) to estimate fracture density and distribution. We tested the sensitivity of equation 1 by varying the fault constant and the decay exponent over the range of values provided by Savage and Brodsky

(2011) that are appropriate for a fault having greater than 1000 feet of displacement. We determined that fracture distribution changed most drastically in response to changes in the fault constant.

The appropriate range for the decay exponent for a fault having 300 to 2000 meters of displacement is 0.2 to 0.6. However, based on Savage and Brodsky's (2011) table 1, most faults having similar displacements and lithologies have a decay exponent of approximately 0.45 to 0.65. For our approximation, we used 0.55.

The fault constant is the most poorly constrained variable by Savage and Brodsky (2011), as it is primarily a function of lithology. The constant can range between about 10 and 100 for a fault having greater than 150 meters of displacement. Savage and Brodsky (2011) noted that displacement has little influence on the fault constant after 150 meters of displacement. Using higher fault constants results in increased fracture density, which in turn results in higher hydraulic conductivity. We applied fault constants of 10, 50, and 100 to the equation to better understand the range of possible fracture densities.

Structure and Fluid Flow Methods

Due to the scarcity of available aquifer property data for the deep fractured carbonates and sandstones in the I-15 corridor area, we estimated the range of possible hydraulic conductivities in the area. We used the empirical relationship between fracture density, fracture aperture, and hydraulic conductivity
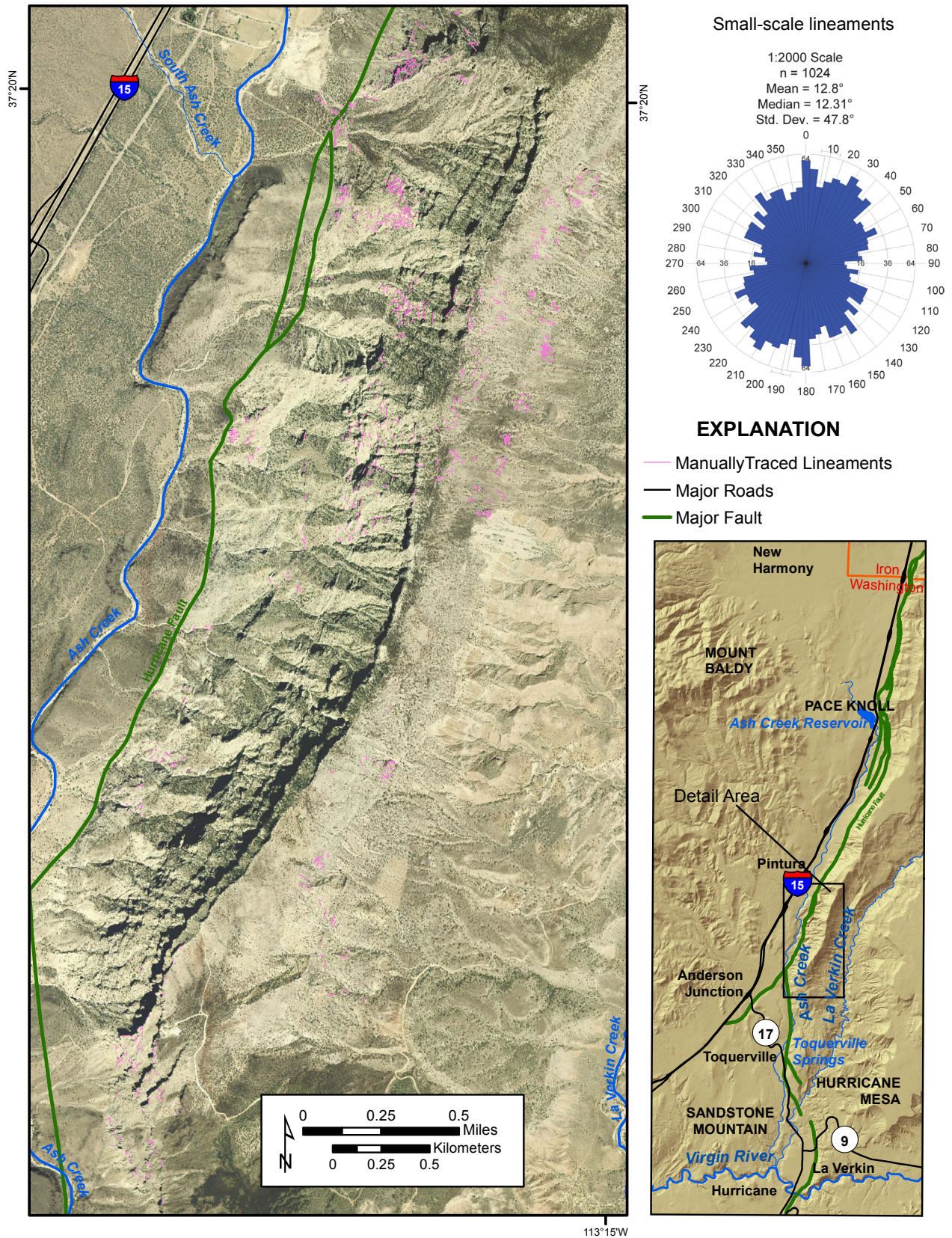
Figure 25. *Distribution of small-scale, manually traced lineaments in the I-15 corridor area.*
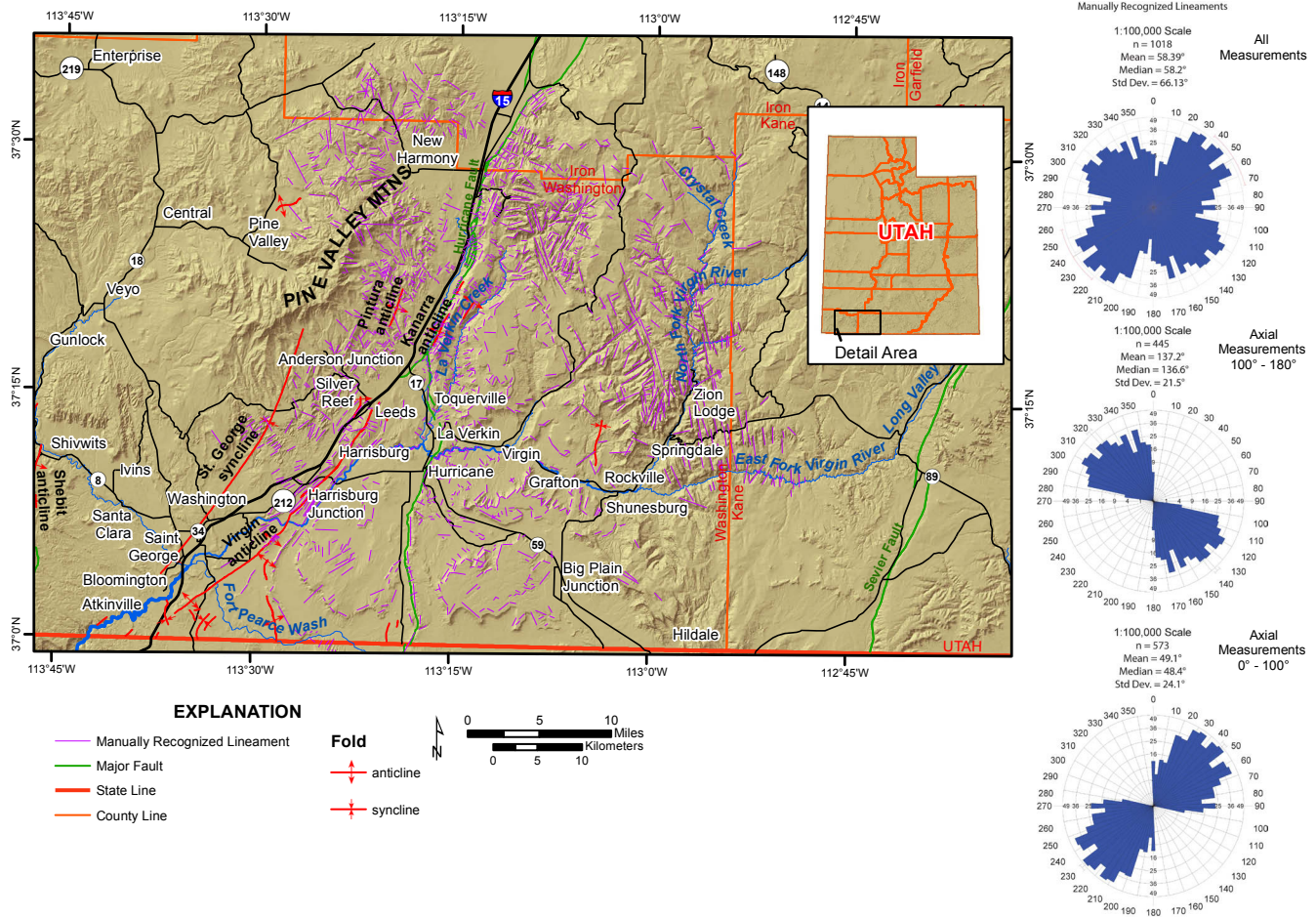
Figure 26. *Manually recognized regional lineaments in the Virgin River basin.*

that Hurlow (1998) determined for the Navajo Sandstone in the central Virgin River basin. We then checked our estimates from the Hurlow (1998) technique against a method applied by Stearns and Friedman (1972). Hurlow (1998) derived the following relationship between fracture spacing, average fracture aperture, and hydraulic conductivity of fractures:

$$K_f = (f_d \times a_a \times 1000)^{0.801 \pm 0.107} \qquad (2)$$

where:

$K_f =$ hydraulic conductivity of fractures (meters per day)

$f_d =$ fracture spacing (count per meter)

$a_a =$ average fracture aperture (millimeters)

We used the fracture density distribution estimated above and data from Dutson (2005) to estimate fracture density and aperture. Based on measurements from Dutson (2005) of the Toroweap Formation, average fracture aperture at ground surface is 1.81 mm. Estimates of average fracture aperture from Dutson (2005) are based on surface measurements where the Virgin River intersects the Hurricane fault, so the actual subsurface apertures will likely be smaller than those used in the Hurlow (1998) equation. Also, Dutson (2005) noted that frac-

ture densities may be higher than the power relationship estimate predicts for some areas along the Hurricane fault. The deviation from estimated fracture density may be due to the presence of Sevier-age fracture sets that predate the Hurricane fault.

Results and Discussion

Structural Trends

The mean of the fold-axis directions of the folds derived from the St. George 30' x 60' geologic map (Biek and others, 2009) is 22 degrees east of north. The mean strike direction of the extensional faults shown on the St. George 30' x 60' map (Biek and others, 2009) is 6 degrees east of north, having a standard deviation of ±31 degrees. Although the strikes of the faults and folds in the area are similar, the differences in their means are great enough to suggest that they would make two distinct sets of lineaments offset by approximately 16 degrees. In terms of groundwater flow, because the folds are significantly older than the extensional faults, the fold-related fractures parallel to the fold axes may have undergone more pore-filling mineralization than the fractures associated with the extensional faults.
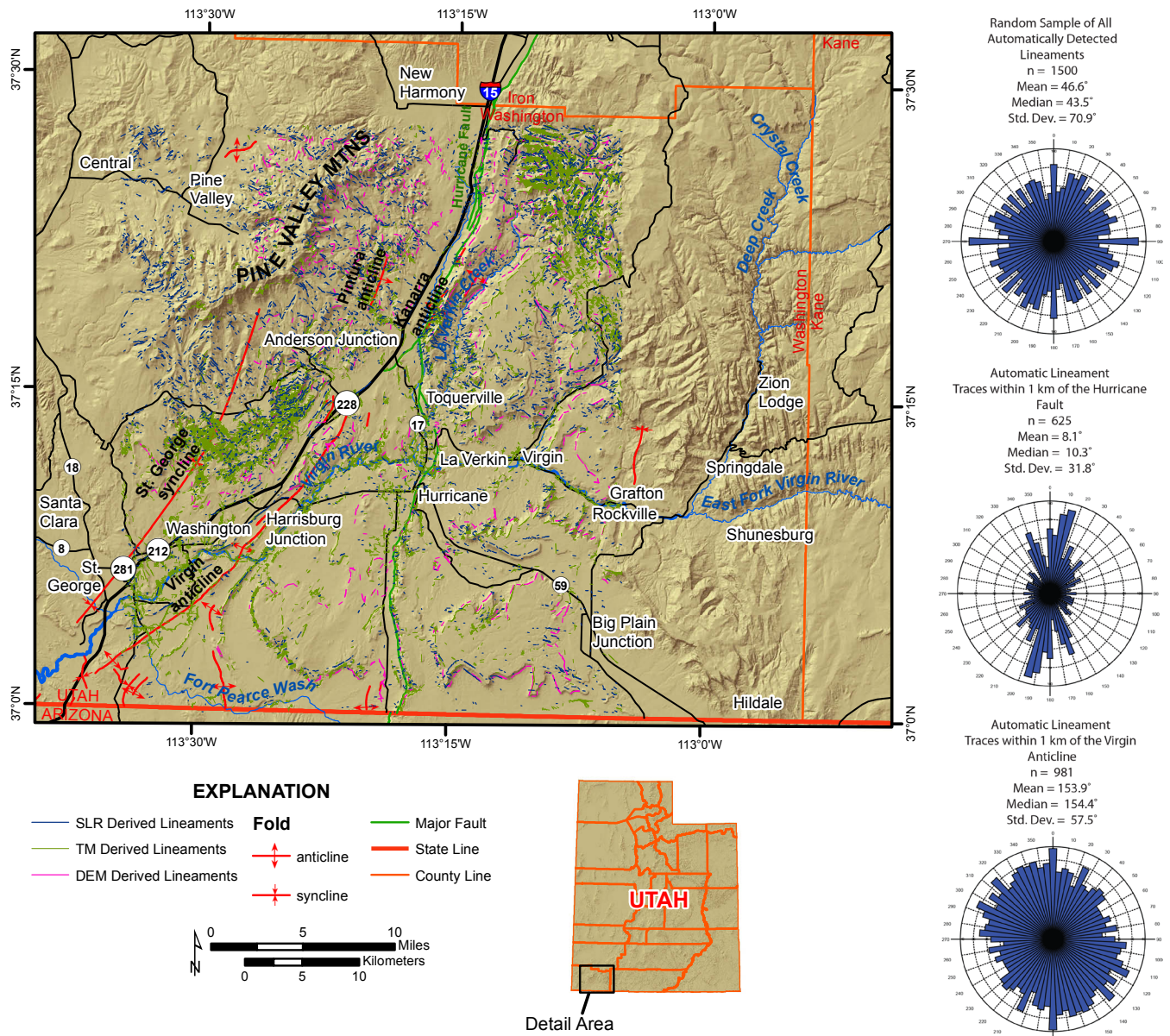
Figure 27. *Distribution of automatically recognized regional lineaments in the Virgin River basin.*

The small-scale, manually recognized lineaments (figure 25) appear to show a mixture of fault and fold influenced lineaments. The greatest number of lineaments have an axial orientation of 0 degrees. The next greatest number of lineaments are found from 15 to 45 degrees, and another large grouping appears at approximately 145 degrees. The lineament orientations likely reflect the stresses associated with both the Kanarra anticline and, dominantly, the Hurricane fault. We examined lineaments over a relatively small geographic extent (near the Hurricane Cliffs), and at a fairly focused scale (1:2000). Based on the current limited data sets examined, manually detected lineaments are dependent on scale in this area (figures 25 and 26), as the regional trends differ from the small scale trends. As observed by Hurlow (1998), dominant lineament directions vary depending on the area of measurement.

Hurlow (1998) used field measurements and examination of aerial photographs to map fracture distribution in the Navajo Sandstone, and noted alternating zones of high and low fracture density in the Navajo Sandstone. Hurlow (1998) noted lineaments in the Navajo Sandstone in the hanging wall of the Hurricane fault lacking apparent vertical movement, and that the fractures in some areas may have formed predominantly due to extensional forces perpendicular to the fracture planes. Hurlow's (1998) rose diagrams display lineament orientations expected for fractures related to the Hurricane fault and Sevier folds in the area. Major peaks in his rose diagrams include 20 degrees, 40 to 60 degrees, and 110 to 120 degrees. The 20-degree peaks approximately align with orientations of the major folds in the area. The other two sets may be conjugate sets associated with the folding.

The 40-to-60 degree and 110-to-120 degree ranges from Hurlow (1998) partly coincide with the ranges observed in the large-scale manual lineament traces from this study (figure 26). The manually recognized lineaments display a bimodal distribution in the rose diagrams (figure 26), having smaller occurrences of lineament directions from 0 to 10 degrees and 80 to 100 degrees. The peaks of the rose diagrams are approximately 30, 50, 60, 120, and 140 degrees. Although some recognizable patterns in these data exist, significant variance is still present, which we attribute to the large geographic extent of the data.

We found that automatic lineament detection produced highly variable trends that were not useful in our investigation of groundwater flow. The automatic techniques may have also inadvertently introduced bias in the eight main ordinal directions, as artifacts of collection technique and linament enhancement methods.

The significant relief in the area may contribute to the poor results seen in the automatic detection methodology. Steep slopes can produce significant shadows that mask important detail. These slopes also harbor large amounts of talus, whose arrangement could add variance to lineament detection. High-relief terrain can also cause two-dimensional images to appear distorted, which may add variance to lineament measurements.

Damage Zone Approximation

Estimates of damage zone thickness vary from about 330 to 16,400 feet (3 miles), depending on the fault constant value. More brittle/competent rocks, such as the carbonates in the field area, accommodate stress by fractures, whereas more pliable rocks, such as clay-, silt-, and gypsum- bearing rocks also ductily deform to accommodate stress. Based on the power-law relationship, we would expect the carbonates in the area to display a larger zone of deformation than the overlying siliciclastic and gypsiferous units. We should expect a wide zone of increased fracture permeability extending as far as 16,400 feet (3 miles) from the main Hurricane fault.

Dutson (2005) measured fracture density of the Permian-age carbonates in the footwall of the Hurricane fault, where it intersects the Virgin River. Dutson (2005) noted that the fracture density did not decrease exponentially as expected by the power relationship. Dutson (2005) attributed the unexpectedly high fracture density to the pre-fault deformation associated with the Virgin and Kanarra anticlines. Another possible explanation is that there are splays of the Hurricane fault that Dutson (2005) did not account for in her fracture density examination, as Savage and Brodsky (2011) observed that fault splays will increase fracture density where present. However, independent of the validity of either hypothesis, fracturing in the more competent Permian units is likely as great or greater than estimated by the power relationship specified by Savage and Brodsky (2011).

Dutson (2005) only examined the fracture density of the footwall of the Hurricane fault. Fracture density in the footwall may differ from that in the hanging wall (Bernard and others, 2002) due to differences in response to extensional deformation, differences in lithology, and differences in the distribution of stress.

Fracture density may decrease with depth due to an increase in the ductility of rocks with depth and increases in lithostatic pressure; however, the units in which we are interested are not deep enough for dominantly ductile deformation, so fractures are present.

Structure and Fluid Flow

Based on fracture density estimates (Savage and Brodsky, 2011) and Hurlow's (1998) approximation of conductivity from fracture density (equation 2), if a driller completed and screened a well within 500 feet of the main Hurricane fault damage zone, the probable hydraulic conductivity would range from approximately 0.6 to 6 feet per day, which falls within an adequate range for a production well (figure 28).

The alignment of fractures parallel to the extensional faults and the Sevier folds in the region would indicate a regional north-to-south or south-to-north flow. However, multiple lineaments in a large variety of directions, as observed in the manual and automatic lineament detections, are indicative of good connectivity of the north-south trending fracture sets.

Extensional fractures in the area are conducive to flow, and examination of the fractures in Arizona (Ross, 2005) supports that their apertures have undergone dissolution enlargement in the carbonate units. High fracture densities associated with extensional fault damage zones and Sevier folding allow for interconnection of fracture sets from different stress events, increasing probability of high hydraulic interconnection.

The Hurricane fault has significant offset, and numerous relays and bends, which are conducive to creating an expansive network of fractures and fault windows throughout the area (Bastesen and Braathen, 2010; Savage and Brodsky, 2011). In many places along the Hurricane fault, especially in areas where the fault bends (in map view), significant thicknesses of competent rock are present, and the probability for hydraulic connection between the footwall and hanging wall is high. However, several areas along the fault have low-conductivity units juxtaposed against relatively higher-conductivity units, creating an effective barrier in those areas. One such area is where the Virgin River crosses the Hurricane fault; low-permeability Triassic units are juxtaposed against higher-permeability Permian units.

The hydraulic conductivities of the fractured carbonates and sandstones less than approximately 20 feet from the fault are likely lower due to the presence of low-conductivity fault core.
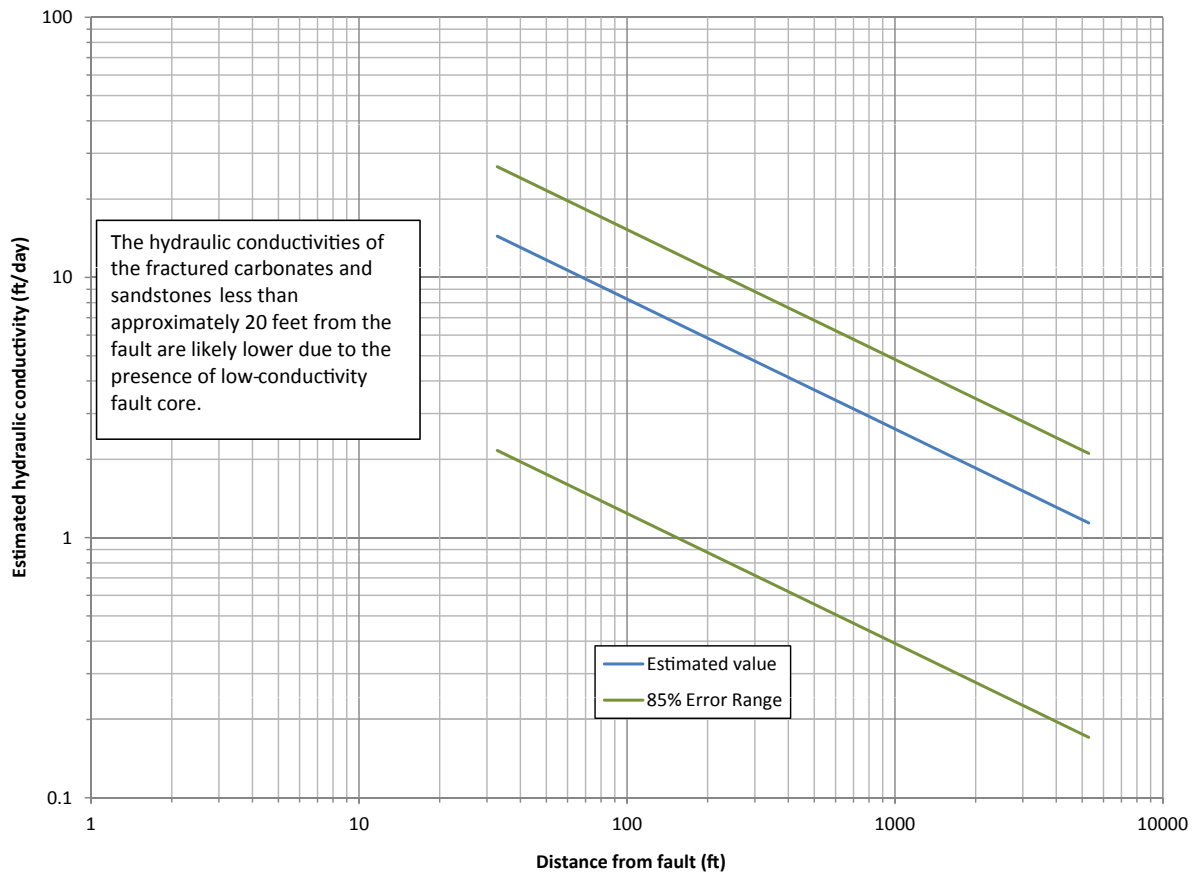
Figure 28. *Range of estimates of hydraulic conductivity as a function of distance from the Hurricane fault.*

GROUNDWATER QUALITY CHARACTERIZATION

Introduction

Hierarchical cluster analysis (HCA) of hydrochemical samples separates data into statistically distinct facies or groups and describes ranges of variation in multivariate data. Although cluster analyses do not provide statistical proof of samples' relationships, they allow for a better understanding of those relationships, and when plotted spatially, can give insight into potential flow paths. Statistical software packages, like the free software R (R Development Core Team, 2011), can efficiently apply cluster analyses to large datasets. When examined with hydrostratigraphic information, characterization of water chemistry also allows for an understanding of general quality of each aquifer. Many workers have applied cluster analyses to help understand groundwater flow and distribution (Thyne and others, 2004; Güler and Thyne, 2006; Templ and others, 2008; Suvedha and others, 2009; Belkhiri and others, 2010; Hershey and others, 2010).

Methods

We analyzed chemical variations in terms of (1) statistical analysis of all water samples and (2) a separate analysis based on source aquifers. We assigned aquifers to wells having water chemistry data based on methods outlined above in the Potentiometric Surface and Unit Identification section. We then applied statistical cluster analyses to available chemistry data and examined available oil well log chemistry data.

Cluster Analysis Methods

To conduct the cluster analysis, we first compiled water-quality samples. We queried the USGS NWIS database in the greater region of the field area (figure 1). We selected samples containing the following constituents: temperature, pH, total dissolved solids (TDS), silica, calcium, magnesium, sodium, potassium, chloride, fluoride, and sulfate. We also chose samples containing alkalinity data and/or bicarbonate and carbonate values. Data compiled by Wilkowske and others (1998) were also incorporated into the compilation.

Compiled data required quality assurance. We discarded samples missing the required constituents listed above. We used Aquachem 2010.1.83 (Schlumberger, 2010) water chemistry analysis software to calculate missing bicarbonate and carbonate values using alkalinity and pH values. We balanced ion charges for each sample and eliminated samples above or below 10% electroneutrality. We also ensured that there was only one sample per station, and if there were duplicates, we used the most recent sample.

After filtering the data, we were left with 217 samples for the Virgin River basin area. We used the free statistical software, R (R Development Core Team, 2011), to conduct cluster analyses and plotted cluster results in ArcMap (ESRI, 2010). For the cluster analysis, we applied the Ward, Euclidean distance technique of four clusters. The statistical clustering was based on relative concentrations between samples of total dissolved solids (TDS), silica, calcium, magnesium, sodium, potassium, chloride, fluoride, sulfate, and bicarbonate. We tried from 3 to 10 different cluster groups. Using five cluster groups produced two very similar groups that should be merged together, and using three cluster groups did not split up the various samples sufficiently. We created box plots and trilinear diagrams to better understand relationships between samples. We were able to assign an aquifer of origin to 102 of the 217 samples

(figure 29). A Piper diagram (figure 30) and box plot (figure 31) illustrate the chemistry results.

Oil Well Water Chemistry Compilation Methods

We reviewed 284 oil well drillers' records and noted any relevant water quality data provided. Only 17 records contained water information, and five contained water-quality analyses. Although drilling fluids likely contaminated all of the quality samples from oil wells, the oil well samples were still considered because they are the only chemical analyses available for the R and C aquifers.

To better understand the distribution of qualitative oil well water salinity, we organized the qualitative descriptions into three categories: drinking-water quality, limited use, and saline (figure 32). For the five samples having TDS data, "drinking-water quality" water refers to samples having TDS values less than 3000 mg/L, "limited use" water refers to samples having TDS from 3000 to 10,000 mg/L, and "saline" water has TDS higher than 10,000 mg/L. However, the converse is not true. For example, water lacking TDS data but described as "drinking-water quality" by the driller may not necessarily have TDS less than 3000 mg/L.

Discussion and Results

Our cluster analyses produced four statistically distinct groups of samples. Waters from different aquifer groups also show some similarities. Water chemistry can show seasonality and fluctuate significantly for a single sample site.
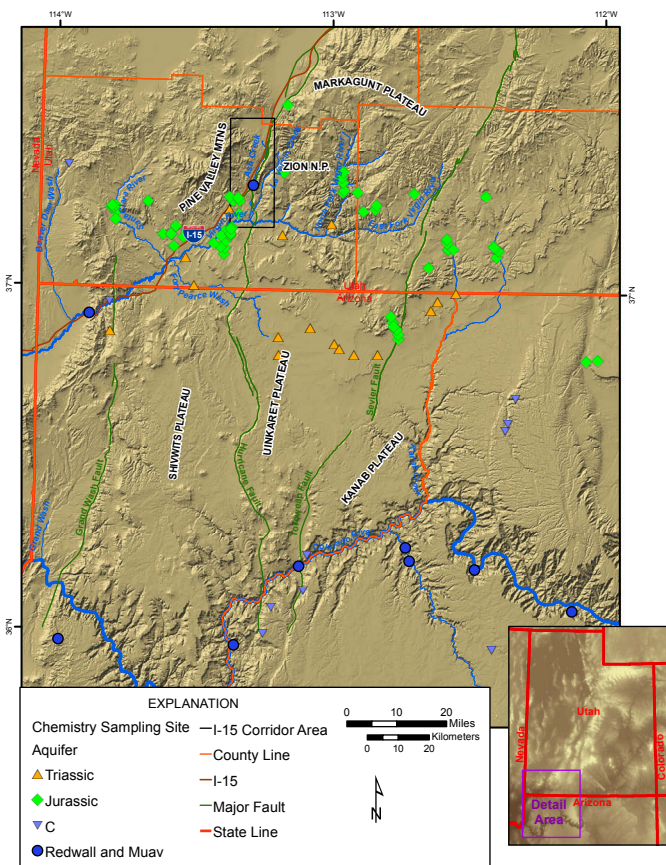
Figure 29. *Distribution of chemistry samples assigned to aquifer units.*
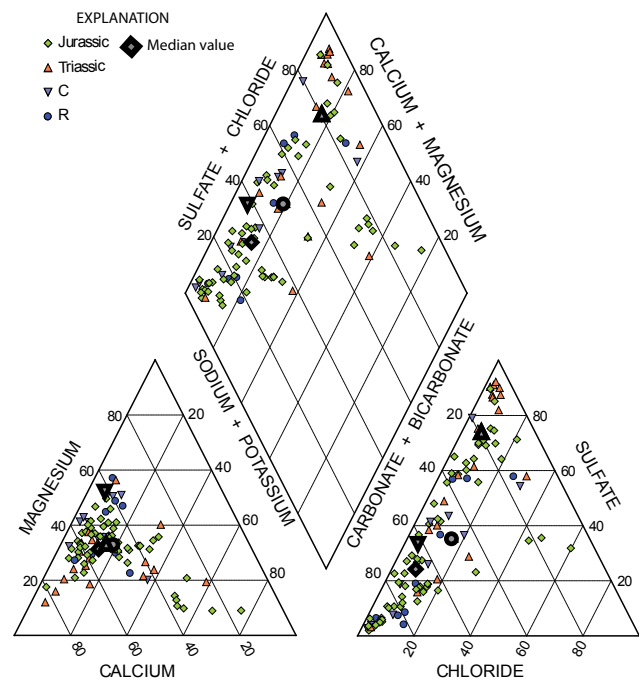
Figure 30. *Piper diagram of water chemistry samples symbolized by aquifer type.*
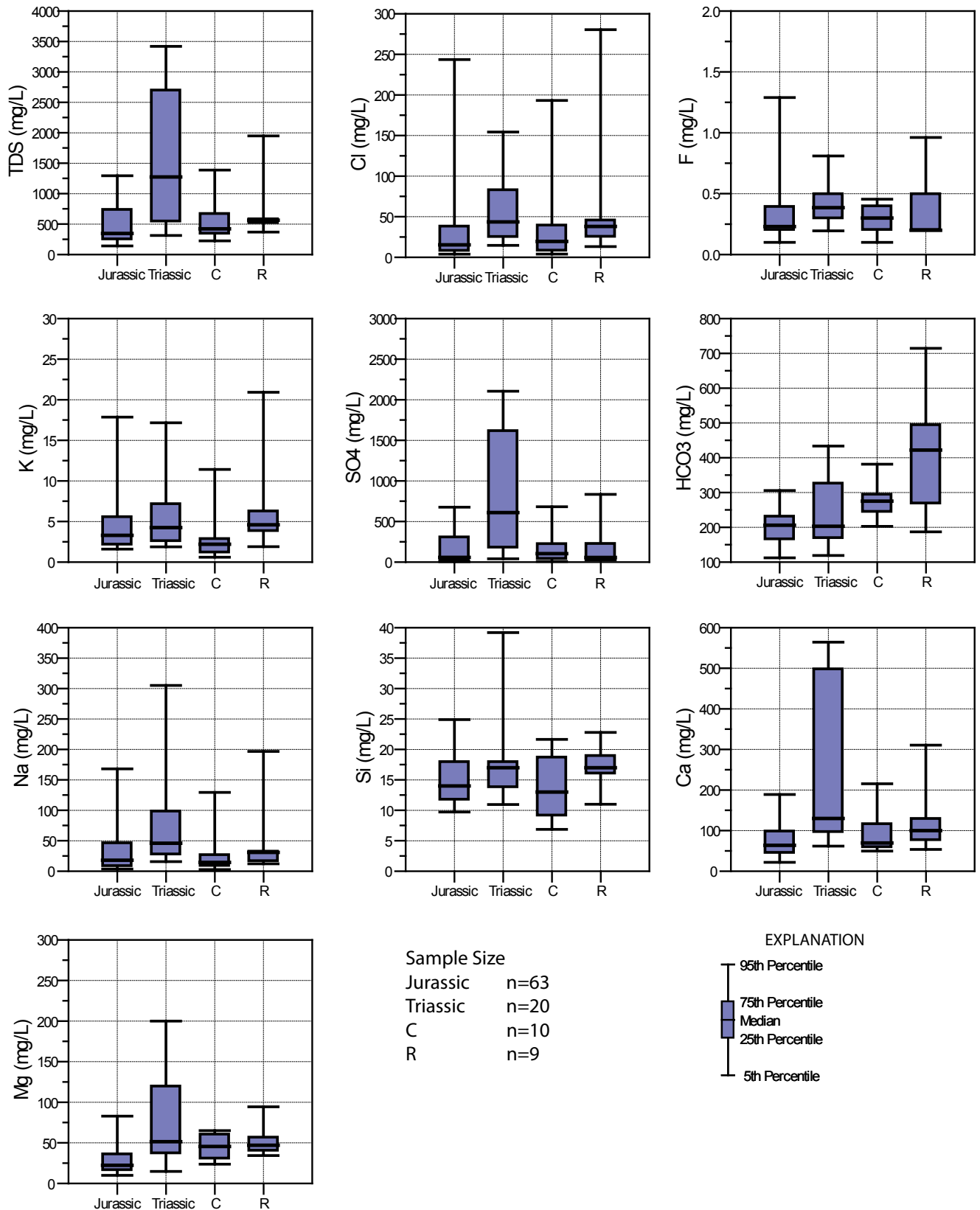
Figure 31. Box and whisker plots of chemical concentrations found in various aquifer groups.
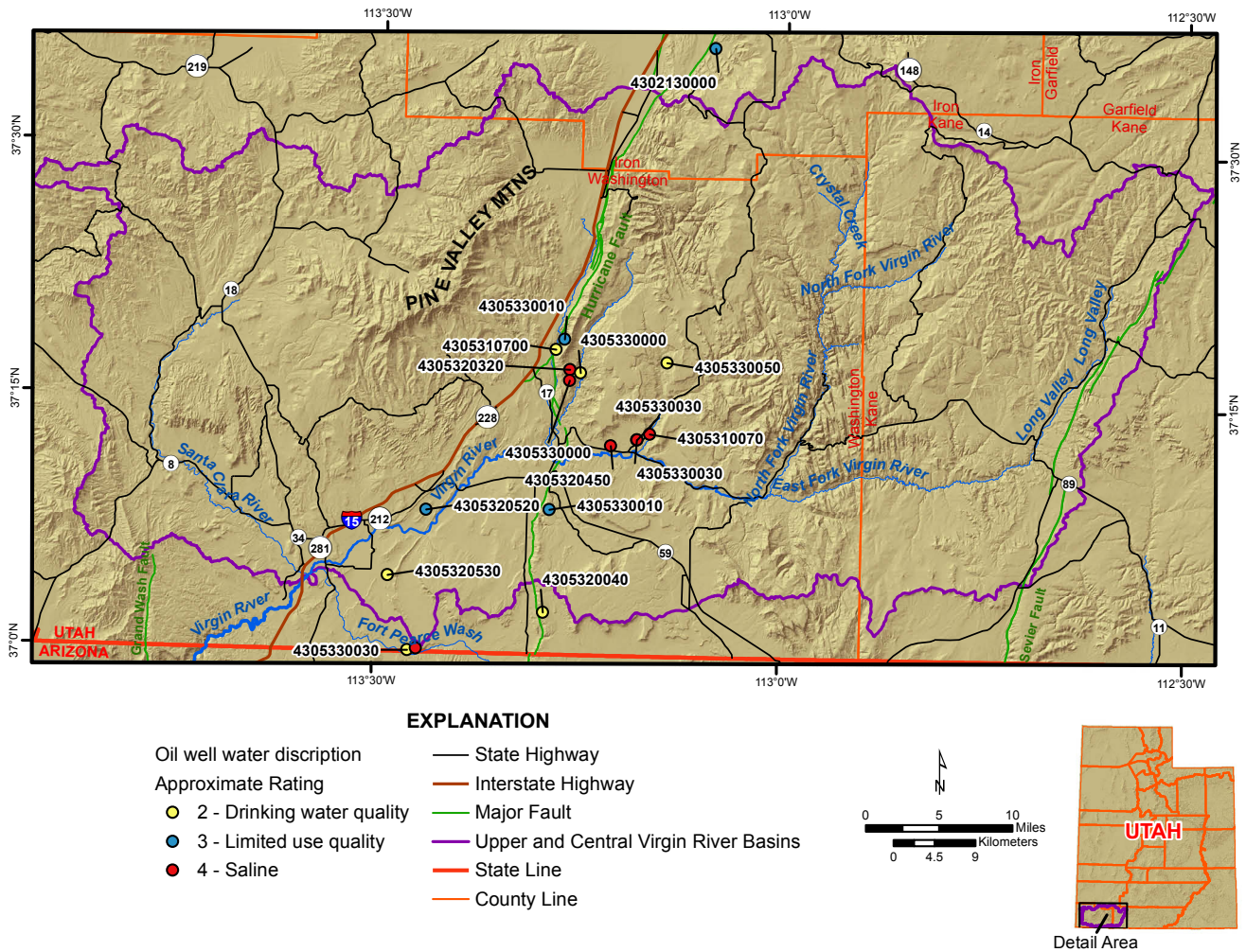
Figure 32. *Distribution of oil well water quality based on descriptions from oil well logs. Wells are identified by their American Petroleum Institute (API) number.*

Cluster Analyses

The four groups resulting from the cluster analyses, when plotted on a Piper diagram (figure 33), show similar trends as those presented by Heilweil and others (2002) (figure 34). More "mature," groundwater discharge-related samples plot in groups D and C (figure 35). These samples have significantly higher TDS values than those of groups A and B (figure 36). High TDS values are likely related to the dissolution of gypsum, which would lend to higher sulfate (SO_4) and calcium levels. Group D also shows relatively high concentrations of sodium (Na), potassium (K), and chloride (Cl) ions, implying the dissolution of halite, sylvite, or another evaporite commonly associated with gypsum.

The differences in concentrations of the various constituents presented on the box-and-whisker plots (figures 31 and 36) are good indication that the cluster analysis separated the samples into statistically significant groups. Although groups A and B, groups B and C, and groups C and D appear similar on a trilinear (Piper) diagram (figure 34), they do have notable differences. Group B has significantly higher median Si, Na, Cl, and K values than group A (figure 36). Group D has much
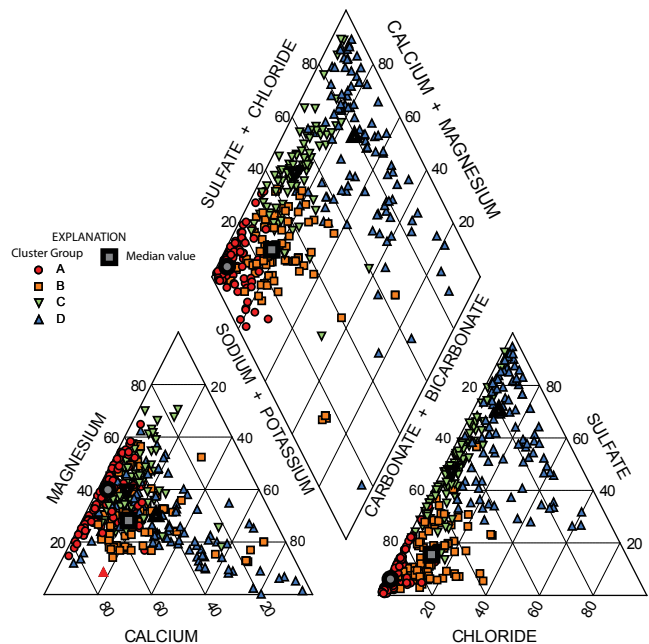
Figure 33. *Piper diagram of chemical samples from the Virgin River basin grouped into statistical clusters. See figure 35 for the geographical distribution of these data.*
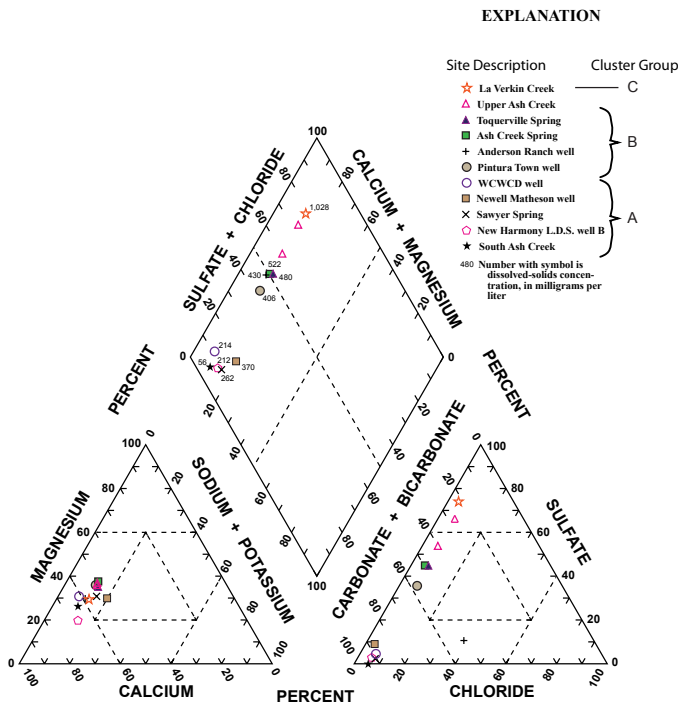
Figure 34. *Piper diagram of various groundwater sources (modified from Heilweil and others, 2000). The sources on this diagram were included in the samples that we analyzed using cluster analysis.*

higher Ca, Na, TDS, and K concentrations than group C, and group C has significantly higher TDS, SO_4, and Mg concentrations than group B (figure 36).

The variation in TDS among the groups likely represents chemical evolution from recharge areas to discharge areas (figure 35). Many of the points in the Pine Valley Mountains and upper regions of the Virgin River fit into the A group, while samples from deeper sources, such as Pah Tempe (Toquerville) springs fall into group D. We did not model the progression from A to D, so it is unknown if our assumptions are correct and how the progression proceeds.

Lithologic Influences

Lithology influences variations in water chemistry. Samples from the Triassic aquifers show distinctly higher TDS, sulfate, and calcium values than the other aquifer groups. When plotted on a trilinear diagram (figure 30), groundwater chemistry from Triassic aquifers aligns with the high TDS values observed in the statistically clustered groups C and D (figure 33). Samples from the C and R aquifers have significantly
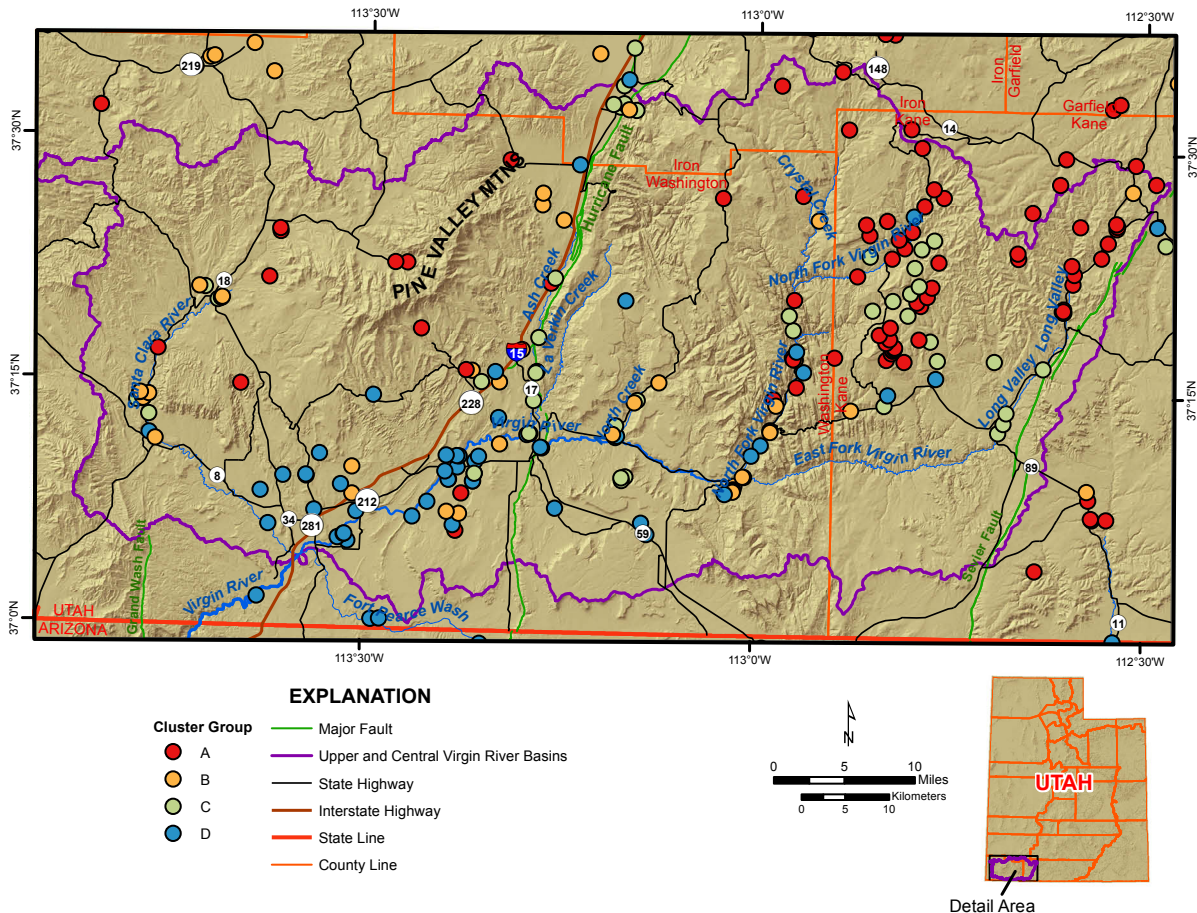
Figure 35. *Distribution of statistically clustered groundwater samples from the Virgin River basin. The samples were clustered based on general chemistry using a Ward Euclidean hierarchical cluster technique. These data are also presented in figures 33 and 36.*
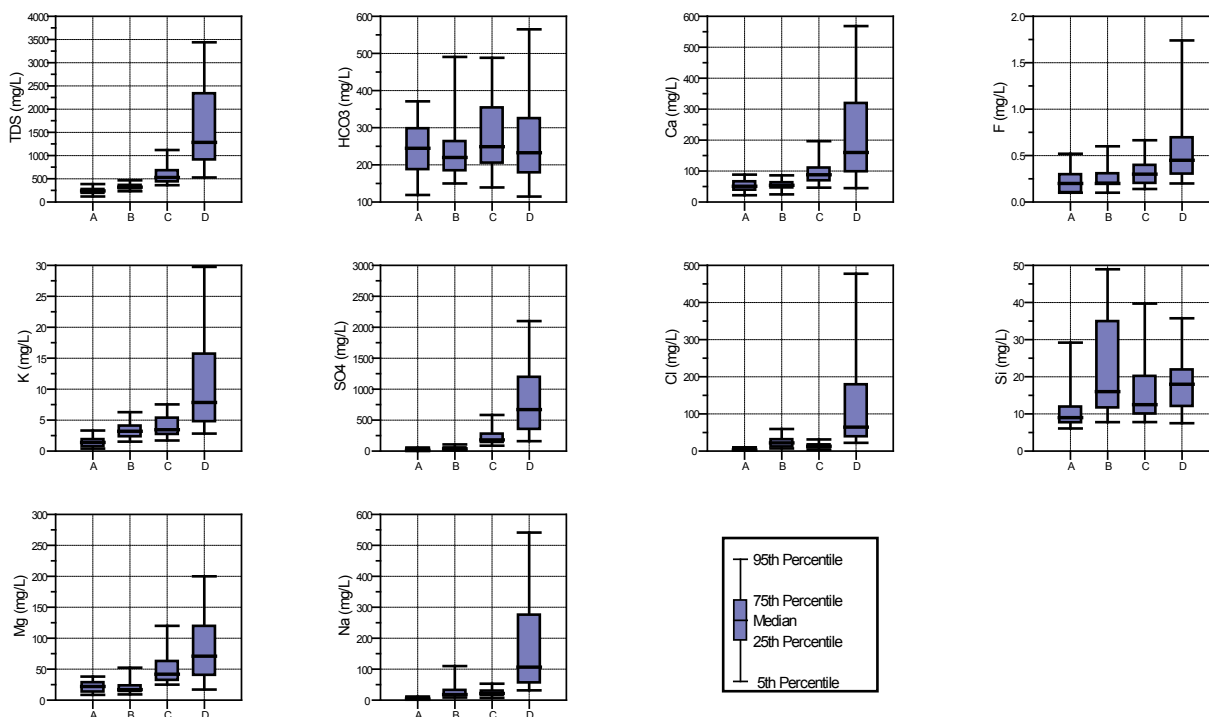
Figure 36. *Box and whisker plots of clustered chemistry samples.*

lower sulfate and calcium concentrations than samples from the Triassic aquifers. However, water samples collected from deep wells that have elevated temperatures and are related to areas of seepage from deeper formations generally have elevated TDS (Heilweil and others, 2000). Dutson (2005) proposed that the quality of water seeping up along the fractured zone of the Hurricane fault may be negatively impacted by dissolution of gypsum and other evaporites in the Triassic and upper C aquifers (Toroweap and Kaibab). Examination of our data supports this hypothesis. Conversely, the quality of water infiltrating into the deeper C and R aquifers may also be impacted by chemical interactions with the Tertiary units. Areas that do not have significant thickness of the Tertiary units appear to have lower TDS values.

Although we compiled several hundred samples, sample group sizes are relatively small; only 10 samples are from the C aquifer and nine samples from the R aquifer. Water chemistry can vary over space and time for the same aquifer, and the relationships we show are preliminary.

Oil Wells

Oil wells along the crests of the Virgin and Kanarra anticlines show relatively higher water quality based on qualitative groundwater chemistry descriptions than do other areas, which may be associated with the lack of evaporite-rich Triassic deposits in the area.

DISCUSSION AND CONCLUSIONS

Groundwater Flow

In the I-15 corridor, groundwater flows principally through basin-fill material, fractured basalt, and Navajo Sandstone. Groundwater in these units moves from the New Harmony basin and the Pine Valley Mountains and follows the I-15 corridor south. Groundwater may be moving into the basin-fill sediments in the I-15 corridor via westward flow from the fractured carbonates in the footwall of the Hurricane fault (Hurlow, 1998). Some groundwater may flow into and out of the Jurassic aquifer units, especially the Navajo Sandstone, in the area of the I-15 corridor, where the Jurassic formations are buried and in contact with footwall strata, as suggested by Hurlow (1998). In most cases, even in the deeper aquifers, groundwater generally follows the surface topography and flows towards the Virgin River.

The Hurricane fault may create a groundwater boundary between the upper (eastern) and central Virgin River basins. The offset of the fault of 3470 to 7450 feet is significant enough to ensure even the thickest aquifer systems are no longer adjacent. Exposure of Paleozoic rocks in the footwall along the Hurricane fault in Utah indicates that overlying Triassic and Jurassic units are discontinuous across the fault, meaning that Triassic and Jurassic aquifers are truncated at the fault in this area. Although the Hurricane fault truncates the major aquifer systems, they still may be hydrologically connected to each other through extensive fractures sur-

rounding the fault, thus allowing flow both along and across the fault.

Fine-grained sediment and gypsum mineralization of the Triassic Formations likely seal the Hurricane fault from groundwater flow where the units are present. In some instances, significant amounts of fault offset may negate the sealing effects of clay smearing (Bastesen and Braathen, 2010). In the southern part of the area, near the Colorado River, the potentiometric surface of the C aquifer is perched above the underlying R aquifer potentiometric surface, due to the low-conductivity Supai Group between the two units. Near the I-15 corridor, Lower Permian strata (Queantoweap Sandstone and Pakoon Formation) contain more transmissive facies than correlative Permian strata (Supai Group) in Arizona, and fractures related to the Hurricane fault and Sevier folds may provide hydrologic connection between the two aquifers.

For the C and R aquifers in the hanging-wall block of the Hurricane fault, there appears to be a groundwater divide in northern Arizona, north of the Grand Canyon. A low point in potentiometric surface near the Virgin River could indicate a zone of discharge from the R aquifer into overlying hydrologic units, as suggested by Heilweil and others (2000). Fractures associated with the Virgin anticline and extensional faults in the area could enhance discharge from the deeper aquifers into the overlying systems.

In the footwall of the Hurricane fault, the C aquifer is closest to the surface in Utah at the base of the Hurricane Cliffs. On the hanging wall, high points are near the crest of the Virgin anticline and the extreme southwestern part of the map (figure 17).

Based on fold attitude measurements, the mean direction of fold traces in the Virgin River basin is about 22 degrees east of north. The mean strike direction of the extensional faults is 6 degrees east of north. Although the strikes of the faults and folds in the area are similar, the differences in their means are significant enough to create two distinct, open fracture sets differing by approximately 16 degrees. However, in terms of groundwater flow, the fractures parallel to the fold trends may have undergone more pore-filling mineralization than the fractures parallel to the extensional faults.

The alignment of fractures parallel to extensional faults and Sevier folds in the region may enhance the north-south regional flow. Fault, fold, and lineament patterns indicate flow is likely in the axial direction of approximately 6–20 degrees east of north. Extensional fractures that are conducive to groundwater flow are most likely parallel to the traces of the major structures in the region. The large number of lineaments that have other axial trends increases the probability that the main fracture network is well connected, which is essential if one is developing the fractured material as a groundwater supply.

Although facture alignment implies a south-north flow, available potentiometric-surface contours do not reflect this flow pattern. However, very little potentiometric-surface data exist near the Hurricane fault, and, due to enhanced fracture permeability, water flow near the fault may differ from regional flow patterns.

Groundwater Chemistry

The four groups (A, B, C, and D) resulting from the cluster analyses show a progression of TDS from recharge areas to discharge areas. Many of the points in the Pine Valley Mountains and upper regions of the Virgin River fall into group A, while samples from deeper sources, such as Pah Tempe springs, fall into group D. The chemistry of C and D samples indicates more-evolved, discharge-related water. Groups C and D generally have significantly higher TDS concentrations than those of groups A and B (figure 36), which are likely caused by the dissolution of gypsum, which is prominent in the Triassic aquifer system and upper part of the C aquifer system.

When the constituent chemistry concentrations were grouped solely by lithology, samples from the Triassic aquifers show distinctly higher TDS, sulfate, and calcium values than the other aquifer groups. The quality of water seeping up along the fractured zone in discharge zones and infiltrating through the Triassic system in recharge zones may be negatively impacted by dissolution of gypsum and other evaporites in the Triassic aquifers.

High TDS concentrations are present in the R aquifer in southwestern Utah. The Government Wolf 1 well (API 4305310704) appears to have produced small quantities of potable drinking water from the C and R aquifers in the region, however pumping water from a depth of 400 feet (or greater, which is likely near this location) may amount to significant pumping costs. Based on water chemistry samples from the Federal 30-B3X well (API 4305330001), salinity increases with depth.

RECOMMENDATIONS

Potential exists for previously unidentified additional sources of water from regional groundwater flow systems. Identification of a new source requires installation of a monitoring well to explore the potential for a water source of adequate quantity and quality and to gather water-quality data to define the aquifer's source and age. The ideal position of a monitoring well requires that (1) the C and R aquifers are near the land surface to minimize costs, (2) the saturated zone of the aquifers is sufficiently close to the ground surface to minimize pumping costs, (3) permeability is sufficient to maintain a water supply, and (4) water quality is adequate for domestic purposes. Based

on our investigation of the groundwater flow system in the Virgin River basin, we recommend three locations for monitoring wells (figure 37), in order of priority: (1) near the Hurricane fault zone (in the hanging wall) in the I-15 corridor area, (2) along the axis of the Virgin anticline, and (3) along the Hurricane fault zone (in the hanging wall) near the Utah-Arizona state line. For the monitoring well design estimates, we focused on the I-15 corridor location, as it is the priority location we designated for a monitoring well.

We also recommend a sampling program to better define the relation between the aquifer units identified in this study and the source of groundwater contained in the aquifers.

Potential Monitoring Well Sites

All of our proposed drill sites are located on the hanging-wall side the Hurricane fault. The fault dips 65 to 80 degrees west and is interpreted to be listric at depth (Biek and others, 2009). At the near-fault locations, drilling would penetrate through the damage zone of the hanging wall, into the fault core, and then through the damage zone of the footwall of the Hurricane fault, while at the Virgin anticline location, drilling would penetrate through the fractured core of the anticline. Locating the drilling site on the footwall side of the fault would allow for contact with the footwall damage

zone adjacent to the fault, but distance from the fault would increase with vertical depth of the well.

I-15 Corridor

The I-15 corridor area has several potential sites adequate for exploratory monitoring wells. Rocks in this area have high fracture densities due to a combination of deformation related to the Hurricane fault and Kanarra anticline. The area is also a conduit for water coming from the Pine Valley Mountains, the northwestern drainages of Zion National Park, the New Harmony basin, and the western slope of the Hurricane Cliffs.

Geologic conditions change along the I-15 corridor. The Kanarra anticline plunges to the north, meaning the units encountered by a monitoring well in the footwall of the Hurricane fault would be younger (Middle Permian) to the north and older (Pennsylvanian and Mississippian) to the south. The two major lithologies that a driller would encounter in the damage zone of the footwall are sandstone, mainly the Queantoweap Sandstone, and carbonates, mainly the Pakoon Formation and the Redwall Limestone. The Queantoweap Sandstone would likely have a dual-porosity system, which includes the primary porosity of the rock matrix and the secondary porosity created by fractures. The carbonates have minor primary effective porosity, but have the advantage of likely having undergone dissolution expansion of the secondary fracture porosity.
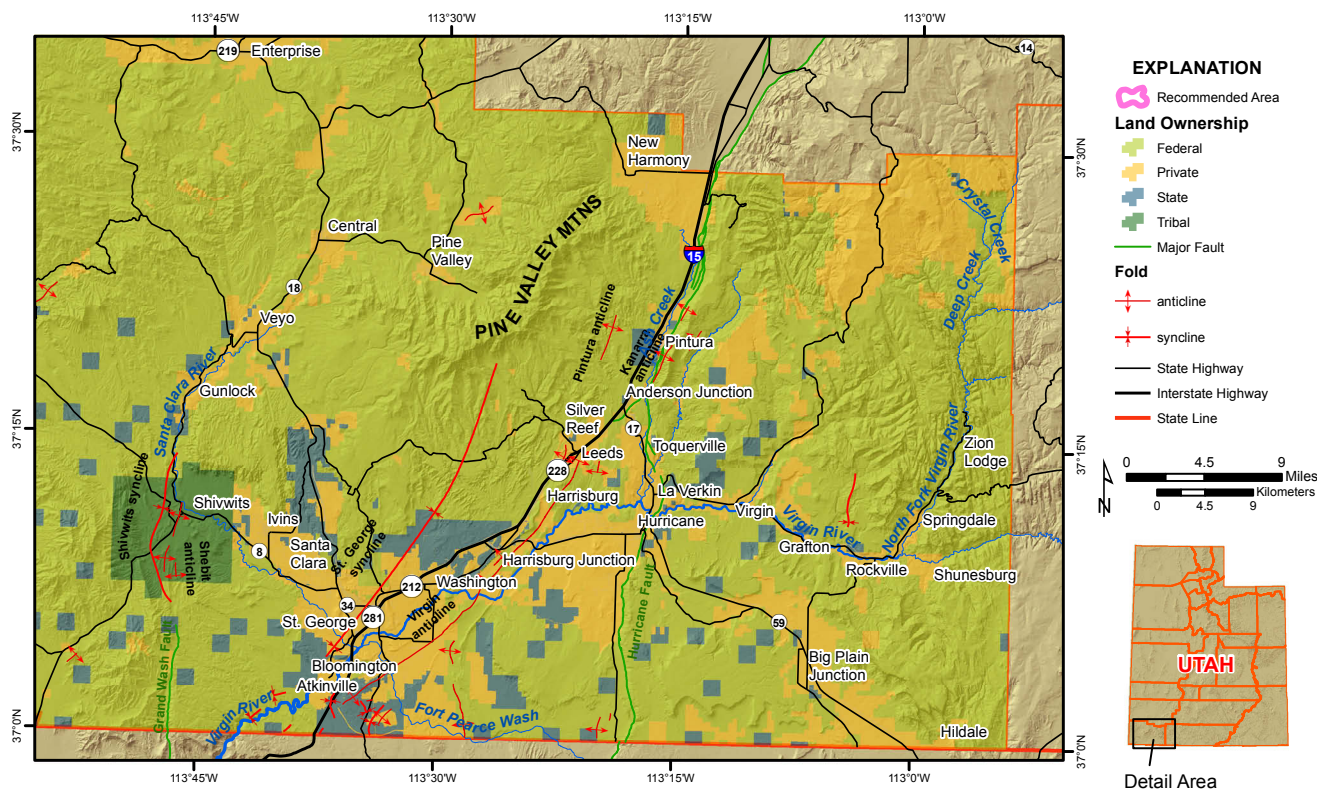

Figure 37. Recommended locations for a research and monitoring well that penetrates fractured C aquifer strata.

The I-15 corridor region is of greatest research interest relative to the other potential sites. We know very little about groundwater flow across the fault, the subsurface geology of the footwall, and the quality of water in the damage zone of the footwall. A monitoring well in this area could potentially greatly advance our knowledge of all of these interests.

Virgin Anticline Axis

The axis of the Virgin anticline exposes older Permian rocks, making the C and R aquifers accessible in this area. The axis of the Virgin anticline is highly fractured from folding of the strata. However, because the Virgin anticline is of Sevier age, mineralization may have filled some of the factures.

Potentiometric-surface maps indicate that the Virgin anticline is a potential discharge area for several aquifer systems. Relatively high groundwater temperatures and higher TDS values also indicate that groundwater is moving through the Triassic strata from the C and R aquifers (Heilweil and others, 2000). We think the high TDS values are a result of dissolution of gypsum as the water travels through Triassic and Upper Permian strata, and the currently available chemistry data support this, but the water in the C and R aquifers may also contain high TDS.

The I-15 corridor is a better location to drill than the Virgin anticline axis, because the Virgin anticline axis has undergone less fracture-induced deformation and some data suggest that the water from this area may be warm and have high TDS.

Near the Utah Border

This area is advantageous because Permian units are at the surface in the footwall and the hanging wall of the Hurricane fault. Fracturing associated with the Hurricane fault is present in this area. There are also several folds mapped in this area (Biek and others, 2009) that may contribute open fractures. Qualitative descriptions of water from oil well 4305320040 indicate water may be of drinking water quality.

This site is not ideal because we have very little information about the subsurface geology in the area and it is fairly remote. Also, the fracture density in this area is likely less than that of the I-15 corridor region.

Monitoring Well Design

Depth to water in a well penetrating to the Hurricane fault footwall from the hanging wall at the I-15 corridor location would likely be between 500 and 800 feet below ground surface, which would require at least a 4-inch diameter well to accommodate a pump that has enough lift to recover water for water-quality sampling. The Utah Division of Water Rights requires at least an 8-inch diameter borehole to accommodate a 4-inch diameter well and the required 2-inch annular seal. This configuration would allow for the minimums to control explora-

tion costs. However, our recommended configuration would be to expand the initial pilot borehole to 12 inches in diameter to accommodate a steel-cased, 8-inch diameter well. The advantages to this configuration would be that the well could possibly be used as a supply well in the future, and a pump adequately sized for sampling and aquifer tests could be placed in the well.

Expected lithologic units overlying the fault in the hanging wall are relatively thin unconsolidated sand and gravel, basalt lava flows as much as 200 feet thick, and possibly some quartz monzonite porphyry. The footwall of the fault contains Mesozoic and Paleozoic shale, conglomerate, sandstone and/or limestone. The basalt may be cavernous and the sedimentary bedrock likely would be fractured. Oil and gas exploration holes in the area were drilled with air and encountered zones of minor lost circulation in the sedimentary bedrock.

Air is the preferred drilling fluid to allow for collection of maximum hydrologic information during drilling. There may be a perched zone in the basalt, but the target water zone is in the damage zone of the footwall. We anticipate the deep water table to be between 500 and 800 feet deep. Preliminary hydrologic testing should be conducted during drilling, such as halting the drilling and blowing with air to determine if water has been encountered; below saturation, conducting blow tests while monitoring air pressure to gauge the amount of water entering the hole; and measuring water level in the hole through the drill pipe at the start of the day or during idle drilling periods.

Before the casing is set we recommend downhole geophysical logging of the well. A geophysical log is a key piece of information in understanding the stratigraphy and correlating it to surrounding wells. If the borehole is too unstable to risk loss of the equipment, a reduced suite of geophysical logs can be obtained after the well is completed.

Total depth of the monitoring well will depend on the quantity and quality of groundwater encountered and the cost and duration of the drilling operation, but will likely range between 1400 and 1800 feet. We recommend the well consist of an 8-inch diameter steel casing and a 100-foot long wire wrap screen, positioned at the most promising aquifer intervals (projected to be between 1000 feet and 1700 feet depth). The well design should include an annular sand pack surrounding the well screen and an annular grout seal. Air lifting is the recommended development method.

Chemical Sampling

We recommend sampling for general chemistry, nutrients, temperature, stable isotopes, dissolved gasses, and tritium from at least five of the sites previously sampled by Heilweil and others (2000). We also recommend sampling carbon isotopes at three to six of the previously sampled sites. Comparison of the results of general chemistry samples can provide insight into the lithologies that contained the groundwater and allow

for comparison to other groundwater samples collected in the past. Temperature provides an estimate of source depth of the water and the current ambient temperature of the aquifer. Stable isotope values can indicate infiltration temperature and/or elevation and the probable amount of evaporation before recharge (Clark and Fritz, 1997). Carbon isotopes and tritium results will allow us to better constrain the ages and recharge setting of water in the area.

We also recommend that a suite of water-quality samples be collected from the proposed monitoring well. The anticipated deep water table will pose specific challenges in sampling. In order for the water samples to be representative of the different water-bearing intervals, the sampling interval will have to be hydraulically isolated from the rest of the borehole. Initial samples collected during drilling can be collected with air lift drilling, as long as sampling intervals are isolated using gaskets or packers. Once the well is complete, samples should be extracted using a pump and analyzed for general chemistry, temperature, stable isotopes, carbon isotopes, tritium, and dissolved gasses.

Aquifer Test

Aquifer tests can provide a significant amount of information about a groundwater system. In the case of faults, an aquifer test could indicate the presence and location of a groundwater barrier, and even provide some indication of how much that barrier inhibits the flow of water. We recommend that an aquifer test lasting at least 48 hours take place, and that the pumping rate during the test be sufficient to cause measurable drawdown in the pumping well and, ideally, surrounding wells. The well should be at least 8 inches in diameter to fit a pump that would properly stress the aquifer.

Groundwater levels should be measured prior to, during, and after the aquifer test takes place. We recommend measuring at intervals appropriate to the assumed rates of groundwater-level change during and after pumping, and at hourly intervals prior to pumping.

The aquifer test should take place after the well is completed. Well discharge rates should be measured during the test and discharge water should be diverted away from the well site. Sampling can also be completed during this process.

SUMMARY

- Groundwater-level information indicates that depth to water in wells screened to the R and C aquifers may be greater than 500 feet below ground surface in the I-15 corridor area. A groundwater divide for the R and C aquifers likely exists south of the Utah-Arizona state line. Groundwater discharges near the Virgin River.

- Lineament and structural data suggest that open fracture systems are parallel to the traces of the extensional faults and Sevier folds in the area, having mean axial orientations of approximately 6 and 22 degrees, respectively. Regional groundwater fracture flow likely preferentially follows these trends.

- Fracture hydraulic conductivity is highest in the area nearest to the fault adjacent to the fault core (about 30 feet from the fault) and decreases with distance from the fault. The estimated values of fracture hydraulic conductivity range from as great as 20 feet per day at 30 feet from the fault to as little as 0.2 feet per day at a distance of 4000 feet from the fault.

- Groundwater quality in the area seems to be highly influenced by the dissolution of evaporites, most of which are found in the Triassic units in the area. Groundwater quality of the R and C aquifers in selected regions near the Kanarra anticline may be sufficient for public use, but there are some oil wells in the vicinity in which drillers qualitatively described the water as "salty."

- We recommend the placement of a deep monitoring well near the Hurricane fault in the I-15 corridor area, preferably near the town of Pintura. This well should be sampled for general chemistry, temperature, stable isotopes, carbon isotopes, and tritium.

- We recommend sampling six sites, including the monitoring well, for groundwater sources previously sampled by Heilweil and others (2000) for tritium, general chemistry, and dissolved gas, and recommend sampling three to six sites, including the monitoring well, for carbon isotopes.

ACKNOWLEDGMENTS

REFERENCES

Abarca, M.A.A., 2006, Lineament extraction from digital terrain models: Enschede, Netherlands, International Institute of Geo-information Science and Earth Observation, M.S. thesis, 86 p.

Alpine, A.E., ed., 2010, Hydrological, geological, and biological site characterization of breccia pipe uranium deposits in northern Arizona: U.S. Geological Survey Scientific Investigations Report 2010–5025, 353 p., 1 pl., scale 1:375,000.

Anderson, R.E., and Christenson, G.E., 1989, Quaternary faults, folds, and selected volcanic features in the Cedar City 1°x2° quadrangle, Utah: Utah Geological and Mineral Survey Miscellaneous Publication 89-6, 29 p.

Arizona Department of Water Resources, 2011a, Arizona well registry: Online, http://www.azwater.gov/AzDWR/GIS/documents/GWSI.zip, accessed May 2011.

Arizona Department of Water Resources, 2011b, Groundwater site inventory database: Online, https://gisweb.azwater.gov/waterresourcedata/WellRegistry.aspx, accessed May 2011.

Bastesen, E., and Braathen, A., 2010, Extensional faults in fine grained carbonates—analysis of fault core lithology and thickness-displacement relationships: Journal of Structural Geology, v. 32, no. 11, p. 1609–1628.

Bastesen, E., Braathen, A., Nøttveit, H., Gabrielsen, R.H., and Skar, T., 2009, Extensional fault cores in micritic carbonate—case studies from the Gulf of Corinth, Greece: Journal of Structural Geology, v. 31, no. 4, p. 403–420.

Belkhiri, L., Boudoukha, A., Mouni, L., and Baouz, T., 2010, Application of multivariate statistical methods and inverse geochemical modeling for characterization of groundwater—a case study—Ain Azel plain (Algeria): Geoderma, v. 159, no. 3-4, p. 390–398.

Bernard, D.X., Labaume, P., Darcel, C., Davy, P., and Bour, O., 2002, Cataclastic slip band distribution in normal fault damage zones, Nubian sandstones, Suez rift: Journal of Geophysical Research, v. 107, no. B7, p. 1–12.

Biek, R.F., 2003a, Geologic map of the Hurricane 7.5' quadrangle, Washington County, Utah: Utah Geologic Survey Map 187, scale 1:24,000.

Biek, R.F., 2003b, Geologic map of the Harrisburg Junction 7.5' quadrangle Washington County, Utah: Utah Geological Survey Map 191, scale 1:24,000.

Biek, R.F., 2007, Geologic map of the Kolob Arch quadrangle and part of the Kanarraville quadrangle, Washington and Iron Counties, Utah: Utah Geological Survey Map 217, scale 1:24,000.

Biek, R.F., Maldonado, F., Moore, D.W., Anderson, J.J., Rowley, P.D., Williams, V.S., Nealey, L.D., and Sable, E.G., 2011, Interim geologic map of the Panguitch 30' x 60' quadrangle, Garfield, Iron, and Kane Counties, Utah: Utah Geological Survey Open-File Report 585, scale 1:100,000.

Biek, R.F., Rowley, P.D., Hayden, J.M., Hacker, D.B., Willis, G.C., Hintze, L.F., Anderson, R.E., and Brown, K.D., 2009, Geologic map of the St. George and east part of the Clover Mountains 30' x 60' quadrangles, Washington and Iron Counties, Utah: Utah Geological Survey Map 242, scale, 1:100,000.

Billingsley, G.H., 2000, Geologic map of the Grand Canyon 30' x 60' quadrangle, Coconino and Mohave Counties, northwestern Arizona: U.S. Geological Survey Geologic Investigations Series I-2688, scale 1:100,000.

Billingsley, G.H., Block, D.L., and Dyer, H.C., 2006, Geologic map of the Peach Springs 30' X 60' quadrangle, Mohave and Coconino Counties, northern Arizona: U.S. Geological Survey Scientific Investigations Map 2900, scale 1:100,000.

Billingsley, G.H., Priest, S.S., and Felger, T.J., 2008, Geologic map of the Fredonia 30' X 60' quadrangle, Mohave and Coconino Counties, northern Arizona: U.S. Geological Survey Scientific Investigations Map 3035, scale 1:100,000.

Billingsley, G.H., and Wellmeyer, J.L., 2003, Geologic map of the Mount Trumbull 30' x 60' quadrangle, Mohave and Coconino Counties, northwestern Arizona: U.S. Geological Survey Geologic Investigations Series I-2766, scale 1:100,000.

Billingsley, G.H., and Workman, J.B., 2000, Geologic map of the Littlefield 30' x 60' quadrangle, Mohave County, northwestern Arizona: U.S. Geological Survey Geologic Investigations Series I-2628, scale 1:100,000.

Blank, H.R., and Kucks, R.P., 1989, Preliminary aeromagnetic, gravity, and generalized geologic maps of the USGS Basin and Range-Colorado Plateau transition zone study area in southwestern Utah, southeastern Nevada, and northwestern Arizona—the "BARCO" project: U.S. Geological Survey Open-File Report 89-432, 18 p.

Braathen, A., Tveranger, J., Fossen, H., Skar, T., Cardozo, N., Semshaug, S.E., Bastesen, E., and Sverdrup, E., 2009, Fault facies and its application to sandstone reservoirs: AAPG Bulletin, v. 93, no. 7, p. 891–917.

Caine, J.S., Evans, J.P., and Forster, C.B., 1996, Fault zone architecture and permeability structure: Geology, v. 24, no. 11, p. 1025–1028.

Cary, R.S., 1963, Pintura anticline, Washington County, Utah, *in* Heylmun, E.B., editor, Guidebook to the geology of southwestern Utah: Intermountain Association of Petroleum Geologists, 232 p.

Christensen, P.K., Hughes, J.C., and Hansen, W.R., 2005, Groundwater discharge from the Navajo Sandstone to the streamflow of the Virgin River in the Zion National Park area: National Park Service Technical Report 2005/343, 58 p.

Christiansen, H.K., 2009, Central Virgin River area, *in* Burden, C.B., editor, Groundwater conditions of Utah: Utah Division of Water Resources Cooperative Investigations Report No. 50, p. 84–88.

Clark, I.D., and Fritz, P., 1997, Environmental isotopes in hydrogeology: New York, CRC Press, Lewis Publishers, 328 p.

Clyde, C.G., 1987, Groundwater resources of the Virgin River basin: Utah Division of Water Resources Misc. Publication, 104 p.

Cook, K.L., and Hardman, E., 1967, Regional gravity survey of the Hurricane fault area and Iron Springs district, Utah: Geological Society of America Bulletin, v. 78, no. 9, p. 1063–1076.

Cordova, R.M., 1978, Groundwater conditions in the Navajo Sandstone in the central Virgin River basin, Utah: Utah Department of Natural Resources Technical Publication No. 61, 72 p.

Cordova, R.M., 1981, Groundwater conditions in the upper Virgin River and Kanab Creek basins area, Utah, with emphasis on the Navajo Sandstone: Utah Department of Natural Resources Technical Publication No. 70, 98 p.

Cordova, R.M., Sandberg, G.W., and McConkie, W., 1972, Groundwater conditions in the central Virgin River basin, Utah: Utah Department of Natural Resources Technical Publication No. 40, 74 p.

Crossey, L.J., Fischer, T.P., Patchett, P.J., Karlstrom, K.E., Hilton, D.R., Newell, D.L., Huntoon, P., Reynolds, A.C., and de Leeuw, G.A.M., 2006, Dissected hydrologic system at the Grand Canyon—interaction between deeply derived fluids and plateau aquifer waters in modern springs and travertine: Geology, v. 34, no. 1, p. 25–28.

Doelling, H.H., 2008, Geologic map of the Kanab 30' x 60' quadrangle, Kane and Washington Counties, Utah, and Coconino and Mohave Counties, Arizona: Utah Geological Survey Miscellaneous Publication 08-2DM, scale 1:100,000.

Dutson, S.J., 2005, Effects of Hurricane fault architecture on groundwater flow in the Timpoweap Canyon of southwestern Utah: Provo, Utah, Brigham Young University, M.S. thesis, 66 p.

ESRI (Environmental Systems Resource Institute), 2010, ArcMap 10.0: ESRI, Redlands, California.

Everitt, B. and Einert, M., 1994, The 1985 slug test of Pah Tempe Springs, Washington County, Utah, *in* Blackett, R.E., and Moore, J.N., editors, Cenozoic geology and geothermal systems of southwestern Utah: Utah Geological Association Publication 23, p. 189–194.

Faulkner, D.R., Mitchell, T.M., Jensen, E., and Cembrano, J., 2011, Scaling of fault damage zones with displacement and the implications for fault growth processes: Journal of Geophysical Research, v. 116, B05403, 11 p.

Gates, J.S., 1965, Groundwater in the Navajo Sandstone at the east entrance of Zion National Park, in Guidebook to the geology of Utah: Utah Geological Society and Inter-

mountain Association of Petroleum Geologists, no. 19, p. 151–159.

Geosoft Inc., 2001, Oasis montaj: Toronto, Ontario.

Gesch, D.B., 2007, The national elevation dataset, *in* Maune, D., editor, Digital elevation model technologies and applications—the DEM users manual, 2nd edition: Bethesda, Maryland, American Society for Photogrammetry and Remote Sensing, p. 99–118.

Gettings, M.E., and Bultman, M.W., 2005, Candidate-penetrative-fracture mapping of the Grand Canyon area, Arizona, from spatial correlation of deep geophysical features and surficial lineaments: U.S. Geological Survey Digital Series 121, 26 p.

Giardina, S., Jr., 1979, Geologic review of northwestern Arizona for petroleum exploration investigators: Arizona Geological Survey Special Publication 4, 72 p.

Grand Canyon Wildlands Council, 2001, An inventory, assessment, and development of recovery priorities for arizona strip springs, seeps and natural ponds—a synthesis of information: Flagstaff, Arizona, unpublished consultant's report for Arizona Water Protection Fund, 49 p.

Grant, S.K., 1995, Geologic map of the New Harmony quadrangle: Utah Geological Survey Miscellaneous Publication 95-2, scale 1:24,000.

Güler, C., and Thyne, G.D., 2006, Statistical clustering of major solutes—use as a tracer for evaluating interbasin groundwater flow into Indian Wells Valley, California: Environmental and Engineering Geoscience, v. 12, no. 1, p. 53–65.

Hayden, J.M., 2004, Geologic map of The Divide quadrangle, Washington County, Utah: Utah Geological Survey Map 197, scale 1:24,000.

Heilweil, V.M., and Freethey, G.W., 1992, Simulation of groundwater flow and water-level declines that could be caused by proposed withdrawals, Navajo Sandstone, southwestern Utah and northwestern Arizona: U.S. Geological Survey Water-Resources Investigations Report 90-4105, 60 p.

Heilweil, V.M., Freethey, G.W., Wilkowske, C.D., Stolp, B.J., and Wilberg, D.E., 2000, Geohydrology and numerical simulation of groundwater flow in the central Virgin River basin of Iron and Washington Counties, Utah: Utah Department of Natural Resources Technical Publication No. 116, 206 p.

Heilweil, V.M., Watt, D.E., Solomon, D.K., and Goddard, K.E., 2002, The Navajo aquifer system of southwestern Utah, *in* Lund, W.R., editor, Field guide to geologic excursions in southwestern Utah and adjacent areas of Arizona and Nevada: U.S. Geological Survey Open-File Report 02-172, p. 105–130.

Herbert, L.R., 1995, Seepage study of the Virgin River from Ash Creek to Harrisburg Dome, Washington County,

Utah: Utah Department of Natural Resources Technical Publication No. 106, 8 p.

Hershey, R., Mizell, S., and Earman, S., 2010, Chemical and physical characteristics of springs discharging from regional flow systems of the carbonate-rock province of the Great Basin, western United States: Hydrogeology Journal, v. 18, no. 4, p. 1007–1026.

Hintze, L.F., and Kowallis, B.J., 2009, Geologic history of Utah—a field guide to Utah's Rocks: Brigham Young University Geologic Studies Special Publication No. 9, 225 p.

Hintze, L.F., Willis, G.C., Laes, D. Y. M., Sprinkel, D.A., and Brown, K.D., 2000, Digital geologic map of Utah: Utah Geological Survey Map 179DM, scale 1:500,000.

Huntoon, P.W., 1970, The hydro-mechanics of the ground water system in the southern portion of the Kaibab Plateau, Arizona: Tucson, University of Arizona, Ph.D. dissertation, 393 p.

Huntoon, P.W., 1981, Fault controlled groundwater circulation under the Colorado River, Marble Canyon, Arizona: Ground Water, v. 19, no. 1, p. 20–27.

Hurlow, H.A., 1998, The geology of the central Virgin River basin, southwestern Utah, and its relation to groundwater conditions: Utah Geological Survey Water-Resources Bulletin No. 26, 65 p.

Hurlow, H.A., and Biek, R.F., 2003, Geologic map of the Pintura quadrangle, Washington County, Utah: Utah Geological Survey Map 196, scale 1:24,000.

Johnson, P.W., and Sanderson, R.B., 1968, Spring flow into the Colorado River, Lees Ferry to Lake Mead, Arizona: Arizona State Land Department Water-Resources Report No. 24, 31 p.

Karlstrom, K.E., Crow, R.S., Peters, L., McIntosh, W., Raucci, J., Crossey, L.J., Umhoefer, P., and Dunbar, N., 2007, ^{40}Ar/^{39}Ar and field studies of Quaternary basalts in Grand Canyon and model for carving Grand Canyon—quantifying the interaction of river incision and normal faulting across the western edge of the Colorado Plateau: Geological Society of America Bulletin, v. 199, no. 11/12, p. 1283–1312.

Kovach Computing Services, 2011, Oriana v. 3.2.1: Anglesey, Wales.

Langenheim, R.L., Jr., 1963, Mississippian stratigraphy in southwestern Utah and adjacent parts of Nevada and Arizona: Association of Petroleum Geologists Annual Field Conference Guidebook no. 12, p. 30–41.

Loughlin, W.D., 1983, The hydrogeologic controls on water quality, ground water circulation, and collapse breccia pipe formation in the western part of the Black Mesa hydrologic basin, Coconino County, Arizona: Laramie, University of Wyoming, M.S. thesis, 139 p.

Lund, W.R., Hozik, M.J., and Hatfield, S.C., 2007, Paleoseismic investigation and long-term slip history of the Hurricane fault in southwestern Utah: Utah Geological Survey Special Study 119, 87 p.

Lund, W.R., Taylor, W.J., Pearthree, P.A., Stenner, H.D., Amoroso, L., and Hurlow, H.A., 2002, Structural development and paleoseismicity of the Hurricane fault, southwestern Utah and northwestern Arizona *in* Lund, W.R., editor, Field guide to geologic excursions in southwestern Utah and adjacent areas of Arizona and Nevada: U.S. Geological Survey Open-File Report 02-172, p. 1–84.

McGavock, E.H., Anderson, T.W., Moosburner, O., and Mann, L.J., 1986, Water resources of southern Coconino County, Arizona: Arizona Department of Water Resources Bulletin No. 4, 53 p.

Milsom, J., 1996, Field geophysics: New York, John Wiley and Sons, 187 p.

Minor, S.A., and Hudson, M.R., 2006, Regional survey of structural properties and cementation patterns of fault zones in the northern part of the Albuquerque basin, New Mexico—implications for groundwater flow: U.S. Geological Survey Professional Paper 1719, 34 p.

Montgomery, S.B., 1992, Study of McCulloch Oil Corporation test well, Wolf No. 1, in Wahlquist, M.C. (Letter to Toquerville Mayor): Bountiful, Utah, 8 p.

Nelson, S.T., Mayo, A.L., Gilfillan, S., Dutson, S.J., Harris, R.A., Shipton, Z.K., and Tingey, D.G., 2009, Enhanced fracture permeability and accompanying fluid flow in the footwall of a normal fault—The Hurricane fault at Pah Tempe hot springs, Washington County, Utah: Geological Society of America Bulletin, v. 121, no. 1-2, p. 236–246.

Parasnis, D.S., 1997, Principles of applied geophysics: New York, Chapman and Hall, 429 p.

Pederson, J., Karlstrom, K., Sharp, W., and McIntosh, W., 2002, Differential incision of the Grand Canyon related to Quaternary faulting—constraints from U-series and Ar/Ar dating: Geology, v. 30, no. 8, p. 739–742.

Poehls, D.J., and Smith, G.J., 2009, Encyclopedic dictionary of hydrogeology: Boston, Elsevier, 527 p.

R Development Core Team, 2011, R—a language and environment for statistical computing: R Foundation for Statistical Computing, Vienna, Austria, ISBN 3-900051-07-0, URL http://www.R-project.org.

Reber, S.J., 2003, Hydrological evaluation of the groundwater potential relative to the Conde property: St. George, unpublished consultant's report, 7 p.

Ross, L.E.V., 2005, Interpretive three-dimensional numerical groundwater flow modeling, Roaring Springs, Grand Canyon, Arizona: Flagstaff, Northern Arizona University, M.S. thesis, 148 p.

Rowley, P.D., and Dixon, G.L., 2010, Geology and hydrogeology of Anderson Junction reservoir, Anderson Junction well field, and Cottam well field, Washington County,

Utah: Washington County Water Conservancy District Report WCWCD-03, 22 p., 2 plates.

Rowley, P.D., Williams, V.S., Vice, G.S., Maxwell, D.J., Hacker, D.B., Snee, L.W., and Mackin J.H., 2006, Interim geologic map of the Cedar City 30' x 60' quadrangle, Iron and Washington Counties, Utah: Utah Geological Survey Open-File Report 476DM, scale 1:100,000.

Sandberg, G.W., and Sultz, L.G., 1985, Reconnaissance of the quality of surface water in the upper Virgin River basin, Utah, Arizona, and Nevada, 1981–82: Utah Department of Natural Resources Technical Publication No. 83, 79 p.

Savage, H.M., and Brodsky, E.E., 2011, Collateral damage—evolution with displacement of fracture distribution and secondary fault strands in fault damage zones: Journal of Geophysical Research, v. 116, B03405, 14 p.

Schlumberger, 2010, Aquachem v. 2010.1.83: Reno, Nevada.

Scholz, C.H., and Cowie, P.A., 1990, Determination of total strain from faulting using slip measurements: Nature, v. 346, p. 837–839.

Shipton, Z.K., and Cowie, P.A., 2001, Damage zone and slip-surface evolution over μm to km scales in high-porosity Navajo sandstone, Utah: Journal of Structural Geology, v. 23, p. 1825–1844.

Singhal, B.B.S., and Gupta, R.P., 2010, Applied hydrogeology of fractured rocks: New York, Springer, 408 p.

Stearns, D.W. and Friedman, M., 1972, Reservoirs in fractured rock: American Association of Petroleum Geologists Memoir 16, Stratigraphic Oil and Gas Fields, p. 82–106.

Stewart, M.E., and Taylor, W.J., 1996, Structural analysis and fault segment boundary identification along the Hurricane fault in southwestern Utah: Journal of Structural Geology, v. 18, no. 8, p. 1017–1029.

Suvedha, M., Gurugnanam, B., Suganya, M., and Vasudevan, S., 2009, Multivariate statistical analysis of geochemical data of groundwater in Veeranam catchment area, Tamil Nadu: Journal of the Geological Society of India, v. 74, no. 5, p. 573–578.

Telford, W.M., Geldart, L.P., Sheriff, R.E., and Keys, D.A., 1976, Applied geophysics: New York, Cambridge University Press, 860 p.

Templ, M., Filzmoser, P., and Reimann, C., 2008, Cluster analysis applied to regional geochemical data—problems and possibilities: Applied Geochemistry, v. 23, no. 8, p. 2198–2213.

Tetra Tech, 2004, TMDL water quality study of the Virgin River watershed: Salt Lake City, unpublished consultant's report for the Utah Division of Water Quality, 178 p.

Thyne, G., Güler, C., and Poeter, E., 2004, Sequential analysis of hydrochemical data for watershed characterization: Ground Water, v. 42, no. 5, p. 711–723.

Turner, C.E., 1990, Toroweap Formation, *in* Beus, S.S., and Morales, M., editors, Grand Canyon Geology: Oxford University Press, New York, p. 203–223.

U.S. Environmental Protection Agency, 2011, National hydrography dataset plus: Online, http://www.horizon-systems.com/NHDPlus, accessed May 2011.

U.S. Geological Survey, 2011, National water information system: Online, http://waterdata.usgs.gov/nwis, accessed May 2011.

Utah Division of Drinking Water, 2011, Municipal well and spring locations and chemistry data: Digital file obtained from GRAMA request, obtained March 2011.

Utah Division of Oil, Gas, and Mining, 2011, Oil and gas well locations: Online, http://gis.utah.gov/sgid-vector-download/utah-sgid-vector-gis-data-layer-download-index?fc=DNROilGasWells, accessed May 2011.

Utah Division of Water Quality, 2011, Utah Ground Water Quality Protection Program: Online, http://www.water-quality.utah.gov/GroundWater/gwclasses.htm, accessed May 2011.

Utah Division of Water Rights, 2011, Water rights points of diversion: Online, http://maps.waterrights.utah.gov/Downloads/wrpod.zip, accessed May 2011.

Wilkowske, C.D., Heilweil, V.M., and Wilberg, D.E., 1998, Selected hydrologic data for the central Virgin River basin area, Washington and Iron Counties, Utah, 1915-97: U.S. Geological Survey Open-File Report 98-389, 57 p.

APPENDIX A–GRAVITY SURVEY STATIONS AND DATA

APPENDIX A

GRAVITY DATA-COLLECTION AND REDUCTION PROCEDURES

Instrument: Scintrex CG-5, owned by UGS.

Base Stations: For absolute gravity, St. George base station established by USGS, 979,596.611 mGals; field base station at Anderson Junction, gravity value established at 979,517.280 ±0.004 mGals during study, tied to St. George USGS gravity base.

Measurement Time: 3 minutes, resulting in typical precision of 0.03 ± 0.02 mGal.

Elevation and Location (UTM-NAD83): Measured using Trimble R8 GNSS differential GPS survey equipment, with a typical vertical resolution of 1–2 cm.

Data Reduction Sequence (Geosoft Inc., 2001):

    A. Earth-tide correction

    B. Instrument drift

    C. Latitude correction

    D. Free Air Anomaly = absolute gravity (corrected for instrument drift and earth tide) – latitude correction + 0.308596 x station elevation in meters.

    E. Bouguer Anomaly – $g_{ba} = g_{fa} - 0.0419088$ x $[\rho h_s + (\rho_w - \rho)h_w + (\rho_i - \rho_w)h_i] + g_{curv,}$

where

        g_{ba} = Bouguer anomaly in milligals

        g_{fa} = free air anomaly in milligals

        ρ = Bouguer density of rock, assumed in this study to be 2.67 g/cm3

        ρ_w = density of water in g/cm3

        ρ_i = density of ice in g/cm3

        h_s = station elevation in meters

        h_w = water depth in meters – does not apply to this study

        h_i = ice depth in meters – does not apply to this study

        g_{curv} = earth-curvature correction

    F. Terrain correction, calculated using the algorithm of Geosoft Inc. (2001), with a 5-meter resolution digital elevation model for the local corrections and a 90-meter resolution digital elevation model for the regional corrections.

    G. Complete Bouguer anomaly = gba + terrain correction

The uncertainty of individual Bouguer anomaly values from this study is likely about 0.01 to 0.10 mGal. The largest sources of uncertainty in Bouguer anomaly values are uncertainty in elevation, deviation of the Bouguer reduction density from the true density of the rocks, and inaccuracy of the terrain correction. The uncertainty due to errors in elevation is less than 0.008 mGal. Errors of up to several tenths of a milligal in the terrain correction may arise in mountainous areas with significant topography that is not accounted for by the digital elevation model used to compute the reduction.

Table A1. Gravity data for I-15 corridor area, between New Harmony and Leeds.

Station	Easting (NAD83) (m)	Northing (NAD83) (m)	Elevation (m)	Gravity (mGal)	Free Air Anomaly (mGal)	Terrain Correction (mGal)	Complete Bouguer Anomaly (mGal)
ajgb	295689.4	4128863.7	1164.019	979517.280	-53.922	0.125	-182.82
acg1	301938.9	4146311.1	1500.482	979454.235	-26.958	0.053	-193.40
acg2	301272.7	4144421.1	1455.538	979461.089	-32.476	0.071	-193.89
acg3	301870.4	4144713.0	1470.466	979458.799	-30.401	0.095	-193.46
acg4	302076.6	4145409.2	1483.755	979456.947	-28.703	0.081	-193.25
acg5	302329.6	4146329.2	1507.636	979453.457	-25.551	0.101	-192.74
acg6	302256.8	4147153.0	1522.365	979450.709	-24.399	0.034	-193.30
acg7	301973.2	4147192.3	1527.663	979449.158	-24.342	0.063	-193.81
acg8	301536.9	4146323.3	1505.831	979452.485	-27.060	0.086	-194.07
acg9	300932.1	4145553.6	1470.737	979458.951	-30.808	0.195	-193.79
acg10	300954.3	4146298.1	1495.821	979454.088	-28.515	0.117	-194.38
acg11	300461.7	4146211.3	1482.530	979456.513	-30.115	0.060	-194.55
acg12	300041.5	4146098.5	1497.912	979452.884	-28.901	0.073	-195.04
acg13	300574.1	4144372.9	1473.075	979457.445	-30.658	0.268	-193.83
acg14	300444.3	4144746.3	1501.036	979451.946	-27.819	0.227	-194.15
acg15	299750.6	4145989.9	1498.182	979452.446	-29.164	0.180	-195.22
acg16	298600.2	4147229.4	1539.889	979443.608	-26.085	0.343	-196.63
acg17	299054.7	4146848.3	1515.361	979448.807	-28.163	0.269	-196.05
acg18	300825.4	4142506.3	1506.670	979451.382	-24.891	0.165	-191.91
acg19	299573.7	4143207.4	1592.403	979434.593	-15.751	0.063	-192.44
acg20	298596.8	4143338.9	1611.287	979430.162	-14.438	0.392	-192.90
acg21	301849.0	4142705.4	1492.356	979455.303	-25.563	0.314	-190.84
acg22	301809.7	4142144.2	1473.170	979457.656	-28.689	0.274	-191.87
acg23	301933.5	4143837.0	1447.656	979463.099	-32.453	0.251	-192.81
acg24	301099.9	4143818.3	1440.833	979464.616	-33.010	0.235	-192.62
acg25	300534.5	4141633.8	1529.752	979446.133	-22.325	0.056	-192.03
acg26	300018.5	4141486.1	1533.477	979445.695	-21.489	0.039	-191.63
acg27	299072.2	4141042.1	1563.050	979439.370	-18.321	0.167	-191.63
acg28	298407.3	4141097.1	1601.726	979431.270	-14.516	0.560	-191.74
acg29	301537.6	4141415.4	1458.135	979458.933	-31.474	0.533	-192.72
acg30	295836.3	4129385.9	1185.694	979512.751	-52.175	0.131	-183.48
acg31	296243.7	4129966.8	1181.984	979513.672	-52.863	0.142	-183.74
acg32	296399.2	4130747.4	1169.441	979515.988	-55.033	0.191	-184.47
acg33	296727.3	4131111.2	1187.186	979513.999	-51.838	0.254	-183.19
acg34	296666.9	4131439.2	1278.427	979493.295	-44.641	2.248	-184.15
acg35	296882.6	4131913.3	1225.521	979505.817	-48.823	0.109	-184.58
acg36	296964.4	4132205.2	1232.761	979504.032	-48.604	0.093	-185.18
acg37	297320.5	4132969.7	1244.490	979501.757	-47.866	0.093	-185.75
acg38	297424.5	4132811.3	1244.172	979501.996	-47.603	0.076	-185.47

Station	Easting (NAD83) (m)	Northing (NAD83) (m)	Elevation (m)	Gravity (mGal)	Free Air Anomaly (mGal)	Terrain Correction (mGal)	Complete Bouguer Anomaly (mGal)
acg39	297797.3	4132077.3	1247.722	979502.730	-45.205	0.324	-183.22
acg40	298181.6	4132699.9	1194.134	979513.203	-51.764	0.990	-183.15
acg41	297552.8	4131533.5	1207.628	979510.473	-49.403	0.470	-182.81
acg42	297091.0	4131041.1	1175.940	979516.345	-52.914	0.340	-182.92
acg43	297171.6	4130199.3	1129.937	979525.696	-57.100	0.438	-181.90
acg44	297203.8	4133801.3	1289.539	979492.513	-43.859	0.193	-186.66
acg45	296564.9	4134063.1	1328.849	979484.152	-40.282	0.121	-187.53
acg46	296010.8	4134714.9	1378.078	979473.541	-36.203	0.444	-188.61
acg47	297852.4	4135533.0	1311.118	979487.482	-43.603	0.255	-188.74
acg48	298117.7	4136340.5	1361.090	979476.734	-39.569	0.462	-190.07
acg49	298430.5	4137203.6	1406.643	979467.362	-35.568	0.288	-191.32
acg50	298564.5	4137943.5	1417.887	979465.368	-34.676	0.322	-191.64
acg51	296869.2	4133922.5	1314.407	979487.133	-41.653	0.175	-187.24
acg52	296320.0	4134400.7	1344.824	979481.488	-38.277	0.171	-187.26
acg53	295757.1	4134786.1	1415.221	979465.367	-32.966	0.376	-189.58
acg54	295475.1	4135302.0	1454.730	979457.521	-29.019	0.308	-190.11
acg55	294190.0	4136143.0	1593.359	979427.040	-17.356	1.568	-192.64
acg56	294386.5	4135527.7	1537.222	979440.624	-20.616	0.647	-190.56
acg57	295003.8	4135364.2	1482.253	979452.201	-25.886	0.209	-190.14
acg58	297511.4	4133212.0	1239.014	979503.052	-48.455	0.115	-185.71
acg59	297808.8	4133689.2	1239.037	979503.184	-48.696	0.118	-185.95
acg60	299092.2	4136078.7	1251.100	979497.944	-52.114	0.445	-190.38
acg61	298916.4	4135781.8	1246.889	979498.939	-52.183	0.385	-190.04
acg62	298654.2	4135386.2	1244.225	979499.794	-51.834	0.219	-189.56
acg63	298378.1	4135216.5	1251.789	979498.808	-50.347	0.170	-188.97
acg64	298222.6	4134660.1	1255.317	979499.003	-48.624	0.077	-187.73
acg65	298035.7	4134052.4	1243.905	979502.110	-48.558	0.117	-186.35
acg66	299526.2	4136637.4	1271.387	979494.260	-49.985	0.325	-190.63
acg67	299549.2	4136881.8	1280.467	979492.457	-49.179	0.253	-190.91
acg68	298363.6	4132454.5	1206.449	979511.413	-49.565	1.588	-181.72
acg69	298508.1	4132407.1	1228.918	979507.221	-46.789	2.604	-180.43
acg70	299692.2	4137261.9	1285.706	979491.180	-49.139	0.185	-191.52
acg71	300212.9	4138457.0	1321.773	979483.080	-47.058	0.624	-193.02
acg72	299792.4	4137962.4	1288.064	979489.994	-50.151	0.510	-192.47
acg73	295254.0	4128663.0	1165.837	979517.622	-52.853	0.133	-181.95
acg74	294956.6	4129357.2	1225.059	979504.808	-47.930	0.172	-183.57
acg76	294860.4	4128131.6	1154.073	979520.167	-53.514	0.086	-181.34
acg77	294636.3	4128454.0	1174.322	979515.618	-52.062	0.137	-182.09
acg78	294414.9	4128917.4	1200.634	979509.617	-50.303	0.268	-183.13
acg79	294523.1	4127723.2	1143.012	979522.405	-54.362	0.096	-180.95
acg80	294702.9	4129919.7	1262.496	979496.455	-45.167	0.228	-184.92
acg81	294405.3	4130397.6	1327.899	979480.882	-40.926	0.396	-187.80
acg82	294115.3	4130590.8	1361.166	979473.264	-38.424	0.748	-188.65
acg83	296834.3	4129628.4	1142.178	979521.084	-57.479	0.099	-183.97
acg84	295607.4	4129696.0	1212.467	979507.167	-49.736	0.157	-183.99
acg85	295200.4	4130076.6	1251.899	979498.920	-46.105	0.180	-184.73
acg86	297445.7	4136165.5	1364.680	979476.703	-38.342	0.320	-189.38

Station	Easting (NAD83) (m)	Northing (NAD83) (m)	Elevation (m)	Gravity (mGal)	Free Air Anomaly (mGal)	Terrain Correction (mGal)	Complete Bouguer Anomaly (mGal)
acg87	294169.1	4127046.0	1133.197	979524.582	-54.675	0.032	-180.24
acg88	294648.2	4126204.5	1100.368	979531.882	-56.856	0.195	-178.61
acg89	296211.8	4127808.3	1132.230	979520.975	-59.218	0.487	-184.22
acg90	295548.8	4128093.0	1134.404	979523.419	-56.315	0.241	-181.80
acg91	298350.9	4127377.8	1136.038	979522.019	-56.702	3.095	-179.52
acg92	296391.8	4128246.9	1204.929	979506.237	-51.870	0.193	-185.25
acg93	296992.8	4128629.4	1192.044	979509.665	-52.729	0.134	-184.74
acg94	297233.1	4128247.0	1192.585	979509.483	-52.449	0.269	-184.38
acg95	293593.9	4126354.3	1123.189	979526.840	-54.952	0.055	-179.38
acg96	292934.0	4125746.7	1113.597	979530.759	-53.503	0.058	-176.86
acg97	292217.5	4125188.5	1086.913	979537.355	-54.691	0.051	-175.09
acg98	291554.8	4124460.2	1097.569	979536.539	-51.634	0.187	-173.08
acg99	302924.7	4146317.1	1526.743	979451.019	-22.094	1.035	-190.48
acg100	303176.0	4146066.3	1583.368	979439.650	-15.796	3.556	-187.98
acg101	300910.0	4138748.0	1306.784	979485.962	-49.044	1.629	-192.33
acg102	301105.1	4139071.2	1314.106	979484.517	-48.487	1.995	-192.22
acg103	291221.1	4133279.9	1639.647	979414.148	-13.658	0.262	-195.41
acg104	292132.2	4132510.9	1565.346	979429.990	-20.158	0.531	-193.36
acg105	292747.4	4131984.3	1499.602	979444.462	-25.573	0.530	-191.44
acg106	293153.3	4131410.8	1446.624	979454.667	-31.274	0.519	-191.25
acg107	293664.8	4130886.8	1402.502	979464.196	-34.960	0.683	-189.85